

IDENTIFYING OPTIMUM PARAMETERS OF HOT EXTRUSIONS

by

R. W. Rice and J. G. Hunt

GPO PRICE \$ _____

CFSTI PRICE(S) \$ _____

Hard copy (HC) 4.00

Microfiche (MF) .75

Prepared for

653 July 65

National Aeronautics and Space Administration

Contract NAS 7-276

N66 29910

FACILITY FORM 602	ACQUISITION NUMBER	DATE
	<u>115</u>	<u>1</u>
	CR-76057	<u>15</u>

THE BOEING COMPANY
Aerospace Group
and
NUCLEAR METALS, INC.

NOTICE

This report was prepared as an account of Government sponsored work. Neither the United States, nor the National Aeronautics and Space Administration (NASA), nor any person acting on behalf of NASA:

- A.) Makes any warranty or representation, expressed or implied, with respect to the accuracy, completeness, or usefulness of the information contained in this report, or that the use of any information, apparatus, method, or process disclosed in this report may not infringe privately owned rights; or
- B.) Assumes any liabilities with respect to the use of, or for damages resulting from the use of any information, apparatus, method or process disclosed in this report.

As used above, "persons acting on behalf of NASA" includes any employee or contractor of NASA, or employee of such contractor, to the extent that such employee or contractor of NASA, or employee of such contractor prepares, disseminates, or provides access to, any information pursuant to his employment or contract with NASA, or his employment with such contractor.

Requests for copies of this report should be referred to:

National Aeronautics and Space Administration
Office of Scientific and Technical Information
Attention: AFSS-A
Washington, D.C. 20546

IDENTIFYING OPTIMUM PARAMETERS OF HOT EXTRUSIONS

by

R. W. Rice and J. G. Hunt

Prepared for

National Aeronautics and Space Administration

Contract NAS 7-276

THE BOEING COMPANY
Aerospace Group
and
NUCLEAR METALS, INC.

NOTICE

This report was prepared as an account of Government sponsored work. Neither the United States, nor the National Aeronautics and Space Administration (NASA), nor any person acting on behalf of NASA:

- A.) Makes any warranty or representation, expressed or implied, with respect to the accuracy, completeness, or usefulness of the information contained in this report, or that the use of any information, apparatus, method, or process disclosed in this report may not infringe privately owned rights; or
- B.) Assumes any liabilities with respect to the use of, or for damages resulting from the use of any information, apparatus, method or process disclosed in this report.

As used above, "persons acting on behalf of NASA" includes any employee or contractor of NASA, or employee of such contractor, to the extent that such employee or contractor of NASA, or employee of such contractor prepares, disseminates, or provides access to, any information pursuant to his employment or contract with NASA, or his employment with such contractor.

Requests for copies of this report should be referred to:

National Aeronautics and Space Administration
Office of Scientific and Technical Information
Attention: AFSS-A
Washington, D.C. 20546

INTERIM REPORT II
IDENTIFYING OPTIMUM PARAMETERS OF HOT EXTRUSIONS

by
R. W. Rice and J. G. Hunt

Prepared for
National Aeronautics and Space Administration

May 3, 1966

Contract NAS 7-276

Technical Management
NASA Headquarters
Washington, D.C.
Materials Office
James Gangler

THE BOEING COMPANY
Aerospace Group
Seattle, Washington
and
NUCLEAR METALS, INC.
Concord, Massachusetts

IDENTIFYING OPTIMUM PARAMETERS OF HOT EXTRUSIONS

Contract NAS 7-276

This program was conducted jointly by The Boeing Company and Nuclear Metals, Inc. Boeing selected and prepared ceramic materials which were supplied to Nuclear Metals, who performed the extrusions; selection of extrusion parameters and evaluation of extrusion results were joint efforts. Boeing analyzed the extruded ceramics.

Mr. Roy Rice, the principal Boeing investigator wishes to acknowledge the following assistance: specimen preparation, A. Donovan; electron probe analysis, R. Racus; electron microscopy, C. Smith; and x-ray analysis, I. Brower. Particular recognition is due A. Jenkins for his patience and skill in optical analyses and specimen preparation.

Mr. James Hunt was the principal Nuclear Metals investigator.

CONTENTS

	<u>PAGE</u>
SUMMARY	1
INTRODUCTION	2
Background	2
Summary of 1964-1965 Work	2
BILLET FABRICATION	4
General Technique	4
Fabrication Development	4
Materials	4
EXTRUSION	5
Equipment	6
Technique	6
Description and Results	7
MATERIALS ANALYSIS	9
Technique	9
Extrusion Uniformity and Can Interaction	9
Density	10
Cracking	10
Microstructure	11
Annealing	12
STRENGTH AND FRACTURE ANALYSIS	13
Microhardness Testing	13
Mechanical Preparation and Testing	13
Strength and Fracture Results	14
DISCUSSION	17
Extrusion	17
Cracking	17
Strength and Fracture	18
Annealing	21

CONTENTS (Cont'd)

	<u>PAGE</u>
CONCLUSIONS	22
FUTURE WORK	24
Fabrication	24
Extrusion	24
Analysis	25
REFERENCES	26
APPENDIX 1 - Vacuum Hot Pressing Procedure A	75
APPENDIX 2 - Vacuum Hot Pressing Procedure B	76
APPENDIX 3 - Firing Schedule A	77
APPENDIX 4 - Billet Heat Loss Estimate	78
APPENDIX 5 - Strength of Hot Pressed MgO	79
APPENDIX 6 - Calcining Procedure A	87

LIST OF FIGURES

<u>FIGURE NO.</u>		<u>PAGE</u>
1	RANDOM AND LINEAR CRACKING IN TRANSVERSE SECTIONS	28
2	EXTRUDED BILLET CROSS SECTION SAMPLES	29
3	HEATED CATCH TUBE	30
4	EXTRUSION BREAKDOWN AND REDUCTION	31
5	MULTIDIAMETER CERAMIC EXTRUSION	32
6	MULTIDIAMETER EXTRUSION MgO-11	33
7	EXTRUSION MgO-12	34
8	EXTRUSION MgO-14	35
9	EXTRUSION MgO-14 COOLING	36
10	SPECIAL CAN CONFIGURATIONS	37
11	FRACTURE IN CUTTING UNCRACKED EXTRUSIONS	38
12	CRACKING IN EXTRUSION MgO-10 (UNEXTRUDED)	39
13	EXTRUDED ZrO_2	40
14	TYPICAL MICROSTRUCTURES	41
15	GRAIN STRUCTURE OF EXTRUDED ZrO_2	43
16	ZrO_2 ANALYSIS	44
17	MgO-5 w/o Al_2O_3 ANALYSIS	45
18	ANALYSIS OF SURFACE PROTRUSIONS	47
19	MgO HARDNESS INDENTATIONS	48
20	EXTRUDED MgO STRENGTH-GRAIN SIZE DATA	49
21	SAMPLE HOT PRESSED AND EXTRUDED MgO FRACTURE	50
22	SAMPLE FUSED (CRYSTAL) AND EXTRUDED MgO FRACTURE	52
23	PROBABLE FLAW INDUCED FRACTURE IN EXTRUDED MgO	54

LIST OF FIGURES (CONT'D)

<u>FIGURE NO.</u>		<u>PAGE</u>
24	SELECTED EXTRUDED MgO STRENGTH-GRAIN SIZE DATA	55
25	PETCH PLOT OF HOT PRESSED AND EXTRUDED MgO	56
26	FRACTURE OF SPECIMEN FROM EXTRUDED BILLET M-f-4	57
27	MATCHING FRACTURE HALVES OF SPECIMEN FROM EXTRUDED BILLET M-f-1	59
28	MATCHING FRACTURE HALVES OF SPECIMEN FROM EXTRUDED BILLET M-f-2	60
29	MATCHING FRACTURE HALVES OF SPECIMENS FROM EXTRUDED BILLETS M-f-2 AND M-1-11	61
30	SAMPLE DISLOCATION DENSITY IN SURFACE GRAINS OF MgO TEST SPECIMENS	62

LIST OF TABLES

<u>TABLE NO.</u>		<u>PAGE</u>
I	BILLET FABRICATION	63
II	RAW MATERIALS	66
III	EXTRUSION PARAMETERS	67
IV	EXTRUDED BILLET DATA	68
V	EXTRUSION ANNEALING	71
VI	COMPARISON OF EXTRUDED MgO STRENGTHS ON DIFFERENT SPANS	72
VII	FRACTURE STATISTICS	73
VIII	INTERNAL FRACTURE DATA	74

SUMMARY

The purpose of this program is to develop a technique for hot extruding MgO and to determine the effect of hot extrusion on MgO. Preliminary evaluations of the effects of extrusion will be made on other oxide bodies.

Crack free MgO extrusions were obtained from 1"-diameter billets in a 1"-thick-wall tungsten can, while extrusion of 1.5" diameter billets in a 0.75"-thick-wall can were cracked. Extrusion into a catch tube heated to 2000°C (3635°F) reduced, but did not eliminate cracking. The mechanism of cracking appears to be either excessive shear or thermal stress of the ceramic, with the latter favored.

Testing of extruded MgO showed that its strength is 50%, or more, greater than hot pressed MgO of equivalent grain size. The increase in strength was shown to be due to decreased misorientation of grains by the $\langle 100 \rangle$ axial texturing. The extruded material obeyed the Petch relationship. Fracture texture of the extruded MgO allowed fracture origins to be detected, which, along with strength analysis, showed that crack nucleation by dislocation pile-up at grain boundaries occurs in extruded MgO, and is probably the controlling factor in the strength of all dense MgO of adequate purity and flaw content.

Extruded bodies, especially those without cracks, were found to have residual stresses. This apparently was the cause of weakening of the bodies by chemical polishing. Annealing for 1 hour at 2200°F (1205°C) relieved these stresses.

In addition, this work confirmed results of the first year's study. These include substantial grain elongation during extrusion; nearly, though not fully, complete recrystallization during cooling; slower grain growth and the same or greater orientation on annealing; that the least porous and finest grain size starting billets generally give the least porous and finest grain size extrusions; and that extrusion improves alloy homogeneity.

INTRODUCTION

Background

Hot extrusion of refractory oxides⁽¹⁻³⁾ in this program is primarily intended to improve mechanical properties of these materials and increase knowledge of their high temperature deformation characteristics. In brittle ceramics, mechanical failure initiates with crack nucleation and subsequent rapid propagation. In several, and possibly all refractory oxides, cracks are nucleated at lower temperatures due to grain boundary constraints on microscopic plastic deformation; while at higher temperatures, failure frequently occurs due to grain boundary sliding. Both of these mechanisms increase with increasing grain misorientation. Hot extrusion was, therefore, proposed to improve mechanical properties because it should develop a preferred texture, reducing this grain misorientation.

Ceramic alloying was proposed in conjunction with the extrusion because it should reduce grain boundary crack nucleation and sliding, as well as inhibit crack propagation⁽¹⁻⁴⁾, and because extrusion provides an excellent means of preparing many possible alloys.

That hot extrusion of ceramics was indeed feasible was shown by the pioneering work of Hunt and co-workers on reactor fuel rods⁽⁵⁾, subsequent cursory work⁽²⁾, and then an exploratory study of MgO by Rice and Hunt⁽²⁾. The technique was generally to co-extrude the ceramic in a metal can of suitably matching stiffness. It was also suggested that some ceramics would have adequate plasticity to allow extrusion without cans.

Summary of 1964-1965 Work

Work in 1964-1965 under NASA contract NAS 7-276, "Identifying Optimum Parameters of Hot Extrusions"^(6,7), showed that ZrO₂, CaO, and a CaO-MgO alloy were extrudable in molybdenum alloy (TZM) cans after heating to temperatures of approximately 2000°C (3530°F)*. Both showed distinct discoloration part way into the extruded ceramic indicating reaction with or contamination by the can. CaO showed $\langle 100 \rangle$ texture along the extrusion axis similar to MgO^(2,6,7). Separate single trials of extruding NiO and CeO₂ in molybdenum alloy (TZM) cans apparently resulted in decomposition of these oxides. A trial of MgAl₂O₄ was thwarted by what appeared to be rapid reaction with a CaO billet in contact with it in the same can.

Attempts to extrude MgO with only a thin metal shell were unsuccessful - possibly due to the sacrifice in billet quality needed to obtain the necessary large billets (2.4"-2.9" diameter by 5" to 7" long).

*Throughout this report, the first temperature indicates the scale in which the equipment was calibrated.

MgO and MgO alloys containing NiO, Al₂O₃, CaO, or ZrO₂ were successfully extruded in the several experiments using 3" OD, 1.5" ID sintered tungsten cans. Solid billets made by sintering (usually hot pressing and firing) or fusion generally produced denser extrusions than the extrusion of powder. MgO, MgO-NiO, and MgO-1 w/o Al₂O₃ all extruded similarly, generally requiring heating to over 2100°C (3810°F) and extrusion pressures of about 60-70 tons/in². MgO-CaO, MgO-ZrO₂, and MgO-5 w/o Al₂O₃ extruded similarly, but required heating to temperatures of over 2300°C (4170°F), the same or greater extrusion pressures, and underwent less reduction than MgO and similar materials. Alloy homogeneity was generally improved, though some grain boundary accumulation of the second phase was present after extrusion (apparently due to re-precipitation).

Lowest density bodies usually underwent the greatest densification, but the least porous starting bodies of the same composition were generally the least porous after extrusion. Similarly, the largest grain size bodies usually underwent the greatest reduction in grain size, but the finer starting grain size generally gave the finer extruded grain size. MgO bodies with second phases (due to CaO, ZrO₂ or Al₂O₃) had the finest grain sizes.

All extruded MgO and CaO bodies were found to be mostly but not completely recrystallized. MgO, MgO-NiO, and MgO-1 w/o Al₂O₃ bodies had a very strong $\langle 100 \rangle$ texture parallel to the extrusion axis and MgO-CaO, MgO-ZrO₂, and MgO-5 w/o Al₂O₃ had a somewhat less pronounced texture. Annealing at temperatures up to 3000°F (1650°C) appeared to increase orientation, but produced slower than usual grain growth.

Reduction ratios of 9 and 13 to 1 were readily achieved with higher reductions seen feasible. Higher reductions appeared to increase orientation and reduce grain size.

The major problem was cracking. This could generally be classified as either random or linear depending on whether the intersection of cracks with planes either through or perpendicular to the extrusion axis are approximately random or straight lines (see Figures 1 and 2 for examples). Random cracks were generally more dense and generally associated with second phases (precipitates or pores) and less textured specimens. Some cracking appeared to be due to irregularities of the extruded ceramic allowing the tungsten can to mechanically constrain ceramic shrinkage on cooling. Radial cracks appeared to start at the center in both extruded and unextruded (stalled) billets. Use of cans with slots down the side so the can broke open upon cooling may have reduced this (and facilitated removal of the ceramic), but were not always well controlled upon exit from the die in the limited tests performed. Extrusion into an insulated tube tripled time for loss of red heat to about 3 minutes, but made no noticeable change in cracking.

The program was continued, emphasizing use of solid billets of various compositions or parameters in tandem in thick wall cans, with the major emphasis on reducing cracking and obtaining data on mechanical effects of extrusion on MgO and its alloys. Some work on other oxides was planned, with particular interest in study of an anisotropic oxide such as Al₂O₃ (8) because even greater strengthening effects by texturing an anisotropic material was predicted. Fabrication of better billets and further evaluation of uncanned extrusions were also considered, but in a secondary role depending on need and opportunity for development without dilution of the main program effort.

BILLET FABRICATION

General Technique

Billet fabrication continued to be based on Vacuum Hot Pressing Procedure B (Appendix 2) except for modifying the temperatures at which pressure is applied and held. These modifications, particularly in applying pressure, were made to avoid problems of excessive gas entrapment⁽⁶⁾. Modification of the pressing temperature also reflects correction of thermocouple errors. (The Appendix Procedure B has also been corrected). Earlier work at temperatures in the order of 1000°C(1835°F) had appeared satisfactory with fine gauge chromel-alumel thermocouples. Later, a much heavier gauge was used for longer life and higher temperatures. Subsequent testing showed these to read about 50°C(90°F) low at 950°C(1745°F) and about 100°C(180°F) low at 1300°C(2375°F) when compared with Pt-Pt 10% Rh thermocouples. The latter were found to exhibit some inconsistencies with themselves and die surface optical readings even though the couple was protected in an Al₂O₃ tube inside a molybdenum tube. The presence of induction power was found to explain a small percent of the difference, however use of the die as its own susceptor or with a separate susceptor made no change. Subsequent checking of platinum couple and optical readings against melting points observed independently inside a hot pressing die, showed optical pyrometer reading to be the most accurate and consistent. Inside and outside die readings were also found to rapidly equilibrate at constant induction power (tests performed using a separate susceptor). Optical hot press readings are therefore used and are shown in Table I along with other data for the billets fabricated.

All hot pressed billets were subsequently fired on Firing Schedule A (Appendix 3) to remove residual volatile impurities and improve alloy homogeneity. Maximum temperatures (see Table I) were reduced to limit grain growth.

Fabrication Development

Previous hot pressed, dense billets had typically been 1.5" in diameter and 1" long. Parameters for an experiment on can wall thickness called for additional billets of the same length but of 1.0" and 2.0" diameter. The smaller size presented no basic problems. However, when just a single die, instead of a stack of 3 dies, was used to load powder in the die, repeated cold pressing was required. Even though cold pressed surfaces were cleaned and roughened, patches of trace laminations were seen at the original powder interfaces. Two-inch-diameter billets were readily fabricated to about the same quality as 1.5"-diameter billets using Procedure B and a stack of 3 dies for powder loading.

Longer billets are also desired for both more efficient fabrication and extrusion. Other Boeing studies had shown that MgO can be hot pressed at lower temperatures to high but not full density (typically 85-95% of theoretical density), then re-hot pressed to full density. Thus it was considered that such separate pre-hot pressing of two billets could provide two spacers between which to hot press MgO powder. The latter pressing could be carried out at normal conditions to fully densify both the powder and pre-hot-pressed pieces in one continuous billet approximately three times the normal length feasible. Initial experiments showed this was indeed feasible, with good densification being obtained in all three sections and only limited remnants of the original interfaces remaining.

Isostatic pressing of powder, then dry machining a slug to fit the hot press die was seen as another method to get more powder in a die and hence a longer billet. This also proved successful (see M-3-31 in Table I). Loose powder added on either end of the pressed and machined slug hot pressed well and bonded to the slug, though the joint is readily seen at the surface in the as-hot-pressed body.

Fisher Electronic grade MgO was "dead burned" at approximately 2400°F(1315°C) for 20 hours in order to remove volatile contaminants, then screened through 28 mesh for "powder billets". Such powder billets are designated with a small "m".

For comparison with both powder and hot pressed billets, several bodies were isostatically or unidirectionally cold pressed and fired as shown in Table I.

Materials

Dies for 1" and 1.5" billets were Graph-i-tite G*, and dies for 2" billets were ATJ**.

Raw materials used in billet fabrication are shown in Table II.

Mixing, where necessary, was by ball milling 2 hours using Al₂O₃ cylinders and cyclohexane as a fluid.

MgO-Al₂O₃ bodies were made with Alon C; MgO-1/2, 2, and 5 w/o ZrO₂ with Colloidal ZrO₂; and MgO-6 w/o ZrO₂ with fused ZrO₂. Fisher Electronic grade MgO was used in the Al₂O₃-1/2 w/o MgO bodies.

In addition to previous unused billets⁽⁶⁾ and those shown in Table I, billets were machined from:

- (1) A piece of fused MgAl₂O₄*** (Sma-1-4).
- (2) A custom fused ingot**** of Al₂O₃-45 w/o MgO (A45M_e-1-1, -2)
- (3) Zircoa C***** rod (Z-1-3, -4).
- (4) Coors AD-99 Al₂O₃ rod***** (A-1-2 1.0" diameter x 2" long).
- (5) Fused MgO crystals*****.

The fused MgO crystals were approximately cubes .8" to 1" on a side and consisted mostly or completely of a single crystal. They and their respective approximate orientation perpendicular to their cube faces are M-f-10, <100>; M-f-11, <110>; and M-f-12, <111> .

*Basic Carbon Division of Carborundum, Sanborn, New York.

**National Carbon Corporation, New York, New York.

***Through the courtesy of J. Ardis of Muscle Shoals Electrochemical Corporation, Tuscumbia, Alabama.

****Tennessee Electro-Mineral Corporation

*****Zirconium Corporation, Solon, Ohio

*****Coors Porcelain Company, Golden, Colorado

*****The Norton Company, Worchester, Mass.

EXTRUSION

Equipment

All extrusions were performed on a Loewy 1400-ton horizontal press whose present tooling ID is 3". The liner is heated to 400°C.

The previous ZrO₂ insulated induction billet heating furnace⁽⁶⁾ was not large enough for some of the longer billets this year. Therefore, an existing vertical furnace using a graphite susceptor was used.

Initially, ZrO₂ coated steel dies were again used. However, other work at Nuclear Metals had established greater reliability of solid ZrO₂ dies or die nibs, so these were subsequently used.

A heated catch tube to receive the extrusion on exit from the die and to subsequently control extrusion cooling was constructed as shown in Figure 3. The existence of a second 100KW, 3KC induction unit at Nuclear Metals was an important factor in selecting induction over resistance heating.

The catch tube (purged with argon) was found to heat to 2175°C(3950°F) in 6 minutes at 98KW. Holding at 20KW for 33 minutes maintained the temperature between 2080°C(3780°F) and 2130°C(3865°F). During this time, the transite shell became only slightly warm and the high silica cloth insulation between the coils only dull red, while cooling water through the coils remained cold. Subsequent natural cooling of the catch tube without power took 15 minutes to drop from 2100°C to 1620°C. Due to the location of the die, the distance from the die exit to start of the catch tube is about 50 inches. The hot zone is about another 10 inches further from the die.

Technique

The extrusion technique is basically the same as previously used. The ceramic billets are cleaned and loaded in the can, which then has a closing plug welded in the end. The can and billets are heated in the furnace vertically, then dropped down a chute, from which it rolls across glass lubricant onto the press loader. The time for transfer from furnace to the press is 3 to 7 seconds, and extrusion time is 2 to 5 seconds. Extrusion temperatures can be only roughly estimated (see Appendix 4: Billet Heat Loss Estimate), so "drop temperature", the billet temperatures just before dropping from the furnace, are listed.

Cans 2 to 3 inches longer (totalling about 12 inches) were used for extrusions into the heated catch tube so the longer tail could remain unextruded in order to stop the extrusion in heated zone of the catch tube. Thus, with present tooling and can lengths, about 60% of the extrusion is not in the catch tube hot zone.

A typical breakdown of billet and can arrangement is shown in Figure 4.

Description and Results

The first experiment planned was to check the effect of can wall thickness by a multidiameter extrusion as shown in Figure 5. This was delayed by cracking of the can during machining and during welding of the tail. These problems had been solved when an uranium fire at Nuclear Metals contaminated the MgO billets, rendering them unusable. These were replaced. However, the extrusion stalled (due apparently to excessive cooling resulting from loading difficulties) after the penetrator densified the "powder billet" (Figure 5). The can and MgO billets broke on removal from the liner. Another multidiameter ceramic extrusion was prepared and successfully extruded at 2300°C(4175°F), 9 to 1 reduction ratio, and 80 tons per square inch (with very important results as discussed later). The latter is shown in Figure 6.

The second experiment was to check the effect of the heated catch tube on extrusion cracking. On the first attempt (MgO-12), the ZrO₂ coating on the steel die spalled, broke or eroded off, resulting in an oversized extrusion which bent and failed to go into the catch tube. This resulted in the catch tube being dislodged and further bending of the extrusion (see Figure 7). It was at this stage that solid dies were replaced with the solid ZrO₂ nibs.

Extrusion MgO-13 was successfully extruded through a solid ZrO₂ die into the heated catch tube at 2000°C(3635°F) with the tail of the can unextruded as planned. However, the extrusion broke near the tail, allowing most of it to pass through the heated catch tube and fall onto the floor. It was quickly picked up with tongs and put back into the heated catch tube before it had cooled below an estimated 1300°C(2375°F).

Extrusion MgO-14 (Figure 8) was successfully extruded into and brought to rest in the heated catch tube as planned. Its cooling is shown in Figure 9.

To evaluate the effect of the heated catch tube on extruded MgO alloys, extrusion MgO-15 was planned. This was canned in a split tungsten can in a slotted TZM shell (see Figure 10A) in order to minimize mechanical gripping of the extruded ceramic by the can which was observed⁽⁶⁾ most in these alloys. In order to prevent reaction and melting due to the Mo-C eutectic (approximately 2200°C), the graphite susceptor and base were lined with tantalum foil. This did not prevent reaction and melting at about 2350°C(4260°F), so the extrusion was aborted. The split tungsten can was salvaged and the ceramic billets showed limited contamination and may be reuseable.

In order to limit cooling before, during and after extrusion, the self-insulating can concept of Figure 10B was devised. Limiting cooling before extrusion reduces heating required to obtain a given extrusion temperature. This is especially important for materials such as Al₂O₃ which may have to be extruded close to their melting point. It is also important in reducing grain growth before extrusion and hence grain size after extrusion. It was expected that cooling would be reduced by the ceramic shells and metal-ceramic interfaces; the shrinkage of the MgO shells away from the metal due to the greater MgO thermal contraction; and in extreme cases by shattering of the MgO shells. It was also felt such an experiment could lead to cheaper cans, and provide further information on ceramic extrusion by evaluating the extruded MgO shells as well as the core. MgO was chosen primarily because it was known to be compatible chemically and mechanically with tungsten in extrusion. Since the "drop-temperature" was to be 2200°C(3990°F) instead of 2400°C(4350°F) as above, it was felt the

Mo-C eutectic could be avoided. It was not. Some melting of the outer TZM shell occurred, causing sticking of the billet in the furnace and chute, and finally in deformation so it would not slide into the press liner.

A first attempt at extruding Al_2O_3 was made using a TZM can. Since it was felt that the TZM might be too soft for the Al_2O_3 , the ID of the can was made larger (2.0") and the space packed with dense tungsten powder. The billet was heated to an optical reading of 1950°C (3540°F), dropped and successfully extruded.

Parameters for extrusions are shown in Table III.

Table IV presents data on the billets in each extrusion.

MATERIALS ANALYSIS

Technique

Extrusions were removed from cans by grinding two diagonally opposed slots nearly through the can wall with a surface grinder, then breaking the can open by a slight wedging action in the slots. Since the maximum length that could be reasonably handled was about 18" (requiring 1-2 hours for slotting), the extrusion was cut in shorter pieces on a cutoff saw using radiographs of the extrusion to indicate the most desirable places to cut.

Subsequent to visual examination and preliminary photographing, extruded ceramic sections were cut on a diamond saw, and cut surfaces were dry sanded to a 600 grit finish. Etching all MgO rich bodies in concentrated boiling chromic acid (2.5 gm of CrO₃ to 10 cc H₂O) was used to reveal dislocations, sub-boundaries, and grain boundaries, as well as aid in revealing second phases. This technique was used for both optical and electron microscopy, with fracture surfaces being etched for 2 to 10 seconds and sanded surfaces 10 to 150 seconds.

Thin sections were prepared per standard petrographic techniques.

Specimens for electron probe and orientation analysis were generally processed through a 1 micron Al₂O₃ wet sanding on silk.

Orientation of MgO bodies was determined by evaluating the ratio of the peak x-ray intensity of an oriented plane in the transverse section to the same plane in a randomly or near randomly oriented body of the same or similar composition. All values were obtained using Cu K α radiation with a scintillation counter, after initial tests showed saturation problems in the available geiger counters. Cursory evaluation indicated that extensive abrading of the surface could reduce the intensity by as much as 20%.

Grain sizes were measured by counting boundary intersections along straight lines.

Extrusion Uniformity and Can Interaction

All completed MgO extrusions resulted in generally uniform rods. Again, there was often some variation in diameter in a given cross section (see Figure 2), which changed along the billet. Some extruded billets were separated, in which case they sometimes had bulbous noses, while others were jointed by smooth flow of the tail of one over the nose of the other (see Figures 6 and 7). These effects are reflected in reduction ratio data in Table IV. In jointed billets the interface between the two original billets was readily discernible as previously shown^(6,7). The extruded ZrO₂ billet (Z-1-3 - extrusion MgO-12) also extruded fairly uniformly, except for a bulbous nose (Figure 7).

MgO and MgO alloy specimens could be readily removed from the cans except many of those that were obviously porous after extrusion (due apparently to initial porosity or outgassing during heating). The difficulty appeared to be mechanical rather than chemical bonding.

The ZrO_2 was readily removed where its interface with the can was smooth, in which case both the ZrO_2 and tungsten can surfaces were glossy. Removal was difficult where the interface was rough due to extensive ZrO_2 cracking.

The Al_2O_3 , Al_2O_3 - MgO , and $MgAl_2O_4$ billets were all extremely irregular, and were not removed from the can. The front billets had diameters in the order of 0.1" and the rear ones approached 0.75" in places. No sign of reaction with the can was observed.

Density

Densities before and after extrusion are given for many billets in Table IV. Again, the more porous billets generally underwent the greatest densification, but the least porous before extrusion were generally the least porous after extrusion. One exception that has been noted is that "powder billets" will frequently have higher extruded densities than some solid billets starting with some porosity.

Cracking

The 1.0" diameter billets located in the front and rear of the multidiameter extrusion MgO -11 apparently extruded without cracks. No cracks could be found by visual, optical, or x-ray Vidicon examination in the resulting rods (approximately 0.33" diameter by 9" long). The 1.5" diameter billets gave 0.5" diameter rods with about normal longitudinal and transverse cracking, except one or two sections of 0.75" to over 1" in length were obtained which were free of transverse (but not longitudinal) cracks. The 2.0" diameter billet gave a rod about 0.7" in diameter which had about average or fewer than average transverse cracks, but more than average longitudinal cracks.

Diamond sawing of all extruded bodies has typically resulted in the specimen fracturing along the saw line for about the last 5 to 20% of the cut, especially in transverse cuts (perpendicular to the extrusion axis). However, in cutting the apparently uncracked extrusions this fracturing was up to 50-75% of the proposed cut as shown in Figure 11. Further, after longitudinal cutting (parallel to the extrusion axis), transverse linear cracks as shown in Figure 11B occurred with the same separation or closer than in other extrusions. Subsequent testing of the more transparent sound sections from cracked extrusions showed that some transverse cracks developed in them while cutting longitudinally. This transverse cracking was found to be reduced by annealing at 2000°F (1095°C) for one hour and to be eliminated by annealing for one hour at 2200°F (1205°C) prior to cutting. Most of the cracking in earlier extrusions was observed without any cutting, grinding, or other preparation. To check whether extrusion cracking frequency had been over estimated by including possible cracking from sawing, sections were annealed, then cut. No significant difference was observed. Further, the frequency with which cracking during sawing occurred in unannealed sound sections of cracked extrusions was much less than in the smaller, uncracked extrusions.

The stalled multidiameter extrusion billets were cracked as shown in Figure 12.

Extrusion MgO-12 which was oversized, bent, and failed to go into the heated catch tube showed linear cracking in the dense MgO bodies and showed random cracking in the more porous ones, especially those mechanically bonded to the can. The ZrO₂ in this extrusion had fine random cracking as shown in Figure 13. It also showed signs of cylindrical cracking just inside the surface black band (Figures 7, 13).

Extrusion MgO-13 which went through the catch tube, and was reloaded in the catch tube (at 2000°C) before the extrusion cooled below about 1300°C showed the usual linear cracking. In addition to this, the MgO-5 w/o Al₂O₃ billet at the back of the extrusion showed wider cracks going in a short distance from the surface. Many of the fractures in this extrusion showed signs of thermal etching, especially near the center of the extrusion.

Extrusion MgO-14 which was successfully extruded into and brought to rest in the catch tube at 2000°C(3635°F) appears to have significantly reduced cracking. Analysis is incomplete, but long solid-appearing lengths were obtained (see Figure 8). Cutting of several sections shows substantially less than average cracking.

MgO-CaO and MgO-ZrO₂ alloy billets recovered from the attempted extrusion MgO-15 (in a split tungsten can with a slotted TZM shell) showed only possible faint cracks.

All billets from the attempts to extrude in a "self-insulating" can (alternate tungsten and MgO cylindrical sleeves) were cracked. The two larger (1.5" diameter) and one smaller (approximately 1" diameter) billets that were less dense than the others showed both less cracking and less distinct cracking. Cracks were almost all longitudinal, except for a transverse crack approximately across the center (about 1/2" from either end) of the densest billet, which also had the most pronounced longitudinal cracking.

All billets of the Al₂O₃ extrusion were highly fractured.

Microstructure

Grain size data is shown in Table IV. The stalled extrusion (MgO-10) shows grain sizes resulting from billet heating prior to extrusion. MgO microstructures were the same as in earlier work^(2,6,7) (see Figure 14) with some variation in grain size and not completely equiaxial grains. Again, in many specimens, a complete or partial rim of grains about one-half the average grain size was observed with a typical thickness of a few to about 20 grains. One billet (M-3-19) had grains about twice the average size within the rest of the extrusion.

Again, frequent evidence of grain elongation and subsequent breaking up due to substantial recrystallization was observed, along with some residual sparse substructure, the latter mostly in large grains.

The extruded ZrO₂ grain size is somewhat smaller (30-40 microns), and is more equiaxial than grains of extruded MgO (see Figure 15).

Electron probe analysis shows that the purchased ZrO_2 billets have significant CaO accumulation over much of the grain boundary area (see Figure 16A). Net CaO accumulation was less in the extruded ZrO_2 , and this accumulation was frequently more intense along cracks than at grain boundaries (see Figure 16B, C). Iron and hafnium impurities were generally uniformly distributed both before and after extrusion. Tungsten was found only as scattered isolated particles averaging about 5 microns in size, located in cracks or voids, up to 1500 microns from the extrusion surface (see Figure 16D). No detectable Si was observed. No difference in the distribution of impurities, Ca, O, or Zr was found with the probe between the black exterior ring and the brown interior of the extruded ZrO_2 .

$MgO-5$ w/o Al_2O_3 bodies hot pressed from mechanically mixed MgO and Al_2O_3 powders result in apparently randomly distributed second phase particles. These particles are typically 1 to 4 microns in size after firing to $2200^\circ F(1205^\circ C)$. On firing to higher temperatures, the second phase particles tend to increase in mean size (eg. size range is about 1-9 microns at $2600^\circ F(1425^\circ C)$) and begin to show a cubic shape (see Figure 17A). Hot extrusion of this composition results in a more uniform distribution of the second phase. Rapid cooling using a split can and only an insulated catch tube gives a fine rod shaped structure (Figure 17B), though some signs of larger particles (Figure 17C) were seen. Cooling of these extruded bodies in the heated catch tube (the extrusion went through the tube and was reloaded in the $2000^\circ C(3635^\circ F)$ tube before cooling below about $1300^\circ C(2375^\circ F)$) resulted in a coarser second phase structure, showing considerable evidence of cubic shapes. More grain boundary accumulation of the second phase is also seen in the latter extrusion. A thin section (Figure 17D) shows "stringers" indicating grain elongation from extrusion.

Laue patterns from two of the more uniform sections from about the center of the Al_2O_3 extrusion showed no definite sign of orientation.

Annealing

As noted earlier, annealing for 1 hour at $2200^\circ F(1205^\circ C)$ eliminated cracking during cutting and grinding of extruded MgO .

Orientation measurements, though still complicated by considerable scatter and limited repeatability indicate increased orientation after annealing for 1 hour at $2400^\circ F(1315^\circ C)$ as shown in Table V.

A thin section of an annealed $MgO-2$ w/o NiO specimen was prepared so as to preserve the surface having rectangular protrusions like those previously noted on many other annealed surfaces of MgO and its alloys, especially $MgO-NiO$ and $MgO-Al_2O_3$. Analysis showed the protrusions to be optically anisotropic, and hence not consisting exclusively of MgO , NiO , or any solution thereof. A subsequent electron probe survey of part of this thin section showed the protrusions to consistently contain less Mg and Ni than the surface, but that they contained Si and Ca which were not detected in the surface. The Si content was estimated at 5-10 percent, and the Ca content at less than half that of the Si. Sample photographs are shown in Figure 18. The annealings were performed in silicon carbide resistance heated furnaces with the specimens setting on MgO single crystals in Al_2O_3 boats inside of large 99 percent pure MgO crucibles. Annealing was conducted at various temperatures from $1150^\circ C(2105^\circ F)$ to $1650^\circ C(3000^\circ F)$.

STRENGTH AND FRACTURE ANALYSIS

Microhardness Testing

Stoloff and Johnston⁽⁹⁾ have reported that hardness indentations are not a good measure of relative strengths in MgO single crystals with and without Mn, but that the inverse of the length of dislocation rosettes from Vickers indentations did give a reasonable comparison of relative strengths. Groves and Fine⁽¹⁰⁾ have also demonstrated this in crystals of the Mg-Fe-O system.

The reference work⁽⁹⁾ was done on $\{100\}$ cleaved surfaces of single crystals. Almost all fracture of extruded MgO is by $\{100\}$ cleavage of grains. Therefore, this technique was applied to fractures of extruded MgO bodies. To obtain experience with this technique, both Knoop and Vickers indentations in the 5 to 50 gm range were made on cleaved MgO single crystals. Etched dislocation rosettes from these indentations showed increasing variation with decreasing load for either technique. The more symmetric rosettes from the Vickers point were judged to be easier to measure; therefore, all further tests were with Vickers point as in the reference work. To determine possible effects of grain boundaries on resulting rosettes, series of indentations were made across a bi-crystal boundary. Although some difficulty in repeatability from series to series was encountered at low weights, the low angle boundary of Figure 19 had limited effect on the rosette lengths across the boundary in a given series. However, to eliminate questions of grain boundary effects, it was decided to use light loads which would limit rosettes to a single grain if each indentation was centrally located in the selected cleaved grain, even though the light load indentations gave less uniform results.

Figure 19B shows that such indentations could be made, at least in the larger grains of extruded MgO. However, measurement of rosettes was complicated by the high random etch pit density.

Further development was not undertaken because extrusion MgO-11 provided specimens for direct mechanical testing.

Mechanical Preparation and Testing

Specimens were sawed and ground from the longer, uncracked sections of extruded billets M-3-7, M-2-11, and M-3-8 with moderate breakage. Grinding was done on a surface grinder with water cooling using a 320 grit diamond wheel. When the edges and one side were flat each was dry sanded on 240, 400 and 600 grit silicon carbide sandpaper. Groups of specimens were then attached to a flat plate with double-back tape and similarly ground and sanded together. Edges were rounded by hand.

Chemical polishing of several unannealed specimens was done in boiling phosphoric acid for five minutes. The acid was diluted with water to a density of 1.3-1.4 gm/cc (which boils at approximately 150°C) based on earlier experience with MgO crystals. Single crystals of MgO were included in each batch to indicate adequate operation of the polishing bath. Some polycrystalline specimens obtained a glossy finish like the single crystals and some did not.

Numerous specimens were either annealed before or after cutting, grinding, and sanding, or both. Those annealed after cutting, etc. were tested as annealed.

Testing was by 3 point bending at ambient conditions on an adjustable jig with steel loading rams with diameters of 0.125". Spans of 0.5, 0.75, 1.0, 1.5 and 2.0" were used, though 0.75" was most common. Data in Table VI shows that test span has little or no effect on strength within this range for the same bar if only fractures at the center are accepted. (Fracture away from the center is often due to a flaw or some other fault since maximum stress is at the center.) This lack of span effects is in agreement with other testing of both hot pressed MgO and Al₂O₃ at Boeing. Specimens were typically about 0.25" wide and 0.12" thick; however, specimens as much as 50% smaller were used to provide larger populations.

Tests were made on numerous occasions over a period of several months, thus averaging effects of set up, weather, and time of specimen storage. All were with a head travel speed of 0.05 in/min.

Strength and Fracture Results

Modulus of rupture versus grain size for all specimens failing at the center of the test span are shown in Figure 20. Strength of Boeing's best vacuum hot pressed and fired MgO specimens tested in the as-fired condition are shown for comparison (see Appendix 5). Chemically polished extruded specimens were typically weaker than the as-sanded specimens. Specimens annealed at 2200°F(1205°C) for 1 hour prior to cutting and a few MgO-2 w/o NiO specimens are included for comparison.

Microscopic examination of the fracture surfaces frequently revealed that both fracture ridges or steps several grains wide, and microscopic cleavage steps on individual grains, all pointed to a single grain or area of a grain, as shown in Figures 21 and 22, indicating a probable origin of fracture*. While such origins were frequently several grains inside of the tensile surface of the specimen, others were at the surface or corners; often near possible flaws (see Figure 23A) or near the edge of flaws extending in from the tensile surface (see Figure 23B). The latter were seen most frequently in chemically polished specimens (see Table VII).

Grain size was measured by counting grains along straight lines near the origin on the fracture surface.

*Note: Adequate lighting for such photos could be obtained only at magnifications of 100X or more. Thus, many photos had to be taken to show a significant area of the specimen. Varying focus from photo to photo, required by the complex fracture topography, often makes the large ridges less distinct in the composite picture than in actual observation.

Selection of only those specimens appearing to have fracture origins away from corners or the tensile surface and hence minimizing possible surface effects on fracture substantially reduced the data scatter as shown in Figure 24. Such selection eliminated all but two of the chemically polished specimens. The few annealed specimens tested showed about the same distribution as unannealed specimens. The best hot pressed and fired MgO data is again included for comparison.

Figure 24 shows that the unextruded bodies have a strength versus grain size slope of about -0.44 . Most of the large grain extrusions are from extruded MgO crystals and hence pore free (they are very transparent) while all of the fine grain specimens are from hot pressed billets (except the one powder billet specimen) and have a fractional percent porosity and hence may be weakened slightly. Thus, the slope of the curve for all fully dense extruded specimens would be -0.44 or greater.

Since both the hot pressed (see Appendix 5) and extruded MgO bodies have strength versus grain size slopes of near -0.5 , a plot of strength versus the inverse square root of grain size (a Petch plot) can be made. Such a plot is shown in Figure 25 where it is seen that hot pressed and extruded bodies have distinctly different slopes, but both have intercepts at several thousand psi.

Fourteen specimens from MgO powder extrusion from previous work⁽⁷⁾ were also tested. Half were tested as sanded, and half as annealed at 2200°F (1205°C). All had some porosity, generally ranging from about 0.25% to about 2%. All, with the possible exception of one, failed at the surface or corner and this one may have failed at a flaw. Many of these were much weaker than the other denser extruded bodies. Some, mostly the ones with less than 1% porosity, approached the strength of the denser extruded bodies. The extruded powder body with the finest grain size (about 13 microns) was one of these and is shown in Figure 24 (with an arrow indicating a correction in strength for its porosity).

Limited testing of specimens annealed at temperatures of 2200 to 2800°F (1205 to 1540°C) after cutting and grinding indicates the same or greater strength, on an equivalent grain size basis, for specimens failing at the center of the test span and inside of the body. These specimens also indicate some increased tendency for intergranular failure with increasing anneal temperature, and structure suggestive of impurities on the exposed grain boundaries. The fractures are still predominately cleavage which indicates the same order of preferred orientation. Annealed specimens also show a possible increase in frequency of failure at the surface or corners (see Table VII).

Only about 10% of over one hundred specimens tested broke off center. Many specimens failing off center showed fracture initiation at the surface or corners, a few failed from internal flaws (extrusions cracks). However, numerous ones had internal origins such as those of Figures 21 and 22. The statistics on fractures which occurred at the center of the test span are shown in Table VII. Overall, about 75% of specimens failing at the center of the test span had internal origins. Survey data on the depth of origin of most specimens with internal origins is shown in Table VIII.

Fractures were almost exclusively cleavage as shown in Figures 21 and 22, with larger grain size specimens having rougher fractures (contrast Figure 21 and 22). Fractures propagated from either a grain boundary surface as in Figure 21, or a cleaved grain as in Figure 22. The latter were definitely the most predominant and typically showed river marks pointing back to an origin at the boundary between 2 or 3 cleaved grains as shown in Figure 22. Etching specimens of this type frequently revealed one or more slip bands indicating piled up dislocations at the point of apparent fracture origin. These were observed in both extruded hot pressed and extruded fused bodies, though more frequently in the latter probably because the large grain size facilitated observation by allowing lower magnifications and hence greater depth of focus. Examples of different combinations of slip band pile-ups are seen in Figures 26 - 29. The slip bands typically go from the boundary on one side of the grain to the boundary on the other side, usually at or near a triple point, and are parallel with cleavage steps on the grain.

Several cases of slip bands, which may or may not be associated with fracture (see Figure 29), were also observed passing through a boundary.

Although the fractures are much more regular than in unextruded MgO, more variation in angle from grain to grain between grains and the mean fracture plane exists than Figures 26-29 would suggest since care was taken to orient fracture surfaces for maximum clarity.

Roughness resulting from the angular variation, though limited, restricted detailed observations, especially around the specimen edges (away from the origin if it was at or near the edge). However, there are indications that many grains along the surface have a dense population of slip bands extending part way across them from the surface (see Figure 30).

DISCUSSION

Extrusion

The very irregular nature of the bodies in the Al_2O_3 extrusion, the apparent squeezing of material to the rear, and lack of apparent texture indicate that the Al_2O_3 may have been molten during extrusion.

The bending of MgO-12 indicates considerable MgO plasticity remains shortly after extrusion.

Numerous results indicating extensive grain elongation during extrusion, followed by nearly but not fully complete recrystallization, are in agreement with previous work^(6,7).

Cracking

The crack free extrusions from 1"-diameter starting billets demonstrate that cracking can be eliminated. However, by itself it does not identify the cause of cracking since (1) the thicker wall can could have absorbed more shear, thus preventing fracturing; (2) the thicker wall (can + sleeve) and the can-sleeve interface may have provided enough thermal insulation to eliminate cracking due to thermal stresses; and (3) the smaller diameter of the extruded rod would reduce any stresses in the rod which may depend on its radius such as thermal stress or possibly stresses due to its texture.

Cracking in the aborted extrusion attempts shows that cracked extrusions probably are not due to extrusion itself. The fact that similar cracks also occur in the unextruded powder billet indicates that cracking occurs after the billet is loaded in the press and the penetrator densifies it since it is believed that the powder billets are poorly densified until then. Since no cracks in these bodies appear to start from the outside, cracking cannot be due to radial flow of the billets with inadequate plasticity. (In which case, cracks start from the outside as consistently shown when hot pressing dies break.) Residual stresses might be introduced by the penetrator or ram since the one aborted extrusion which had little or no cracking was the only one which did not have ram or penetrator pressure on it. However, all those billets were also alloys which appear to have greater high temperature strength. Also, the greater thickness of the can plus shell and can-shell interface provided better insulation. Since longitudinal grain boundaries are preserved in extrusion⁽⁶⁾, longitudinal cracks occurring before the bodies enter the die might also be preserved. However, this would not explain transverse cracking, which does not appear to occur much in aborted extrusions.

Cracking in the self-insulating can does not prove the concept invalid, but does indicate it may be limited to extruded diameters of less than 1.5" if cracking is not due to ram or penetrator pressure. This does, however, show that cracking probably is not due to constraint of ceramic radial thermal expansion by the can wall since the can wall was only partially densified tungsten powder inside an MgO sleeve.

The presence of cracking in billets of the aborted extrusions indicates that orientation probably is not the cause of cracking since these bodies have little or no preferred orientation.

Much slower cooling in the heated catch tube appears to have considerably reduced but not eliminated cracking. Failure of the heated catch tube to eliminate cracking could be due to cooling from the die and the unheated space between the die and catch tube hot zone.

Thus, thermal stress still appears to be the most likely cause of cracking since:

- (1) The heated catch tube reduced cracking.
- (2) Improved insulation or smaller size were involved in all cases of reduced cracking and both reduce thermal stress.
- (3) It is unlikely that any ram or penetrator effects cause transverse cracking which normally accompanies longitudinal cracking.
- (4) Cracking due to excess shear is normally only transverse, and appears to start from the outside in and not the inside out.

When the MgO-5 w/o Al₂O₃ composition was the rear billet in an extrusion, some cracking starting from the outside was found. This indicates poorer plasticity due to cooling in agreement with previous results, since this composition has been extruded previously without such cracking when it was not the rear billet⁽⁶⁾. However, such cooling was not enough to crack the small MgO billet in the rear of the successful multidiameter extrusion.

Previous estimates⁽⁶⁾ based on thermal etching (again observed in several bodies) showed that cracking occurred above 1200°C (2195°F), and hence must be controlled above this temperature.

The reduction of cracking by cooling in the 2000°C (3635°F) catch tube, but not in the 1300°C (2375°F) cooling (extrusion first went through tube and was reloaded) is in agreement with these estimates.

Strength and Fracture

Selection of extruded test specimens with only internal fracture origins, though eliminating some good specimens, should eliminate any surface effects on fracture strength. Tests (see Appendix 5) show that surface finish has limited effect on the hot pressed MgO. Both hot pressed and extruded bodies have only small amounts of porosity. Therefore, since both the hot pressed MgO and extruded MgO were fabricated from the same materials and at the same range of conditions, the strength difference between the two types of bodies must be real and due to the only processing difference: hot extrusion.

The fracture surface of extruded specimens appears flatter than for hot pressed specimens, thus indicating that nucleation or growth of cracks below the critical Griffith size is the determining factor of strength and not crack propagation.

There is extensive data showing that the strength of MgO single and bi-crystals is dependent on slip and related phenomena. Johnston, et al⁽¹¹⁾ have shown that the probability of crack nucleation by dislocation pile-ups at grain boundaries in bi-crystals increases rapidly with increasing misorientation between the grains. Ku and Johnston⁽¹²⁾ confirmed this and have shown that this crack nucleation by dislocations in MgO bi-crystals of approximately $\langle 100 \rangle$ misorientation is described by the Petch equation:

$$\text{Fracture Stress: } \sigma_f = \sigma_o + K G^{-1/2}$$

where σ_o = stress to multiply dislocations,

K = a constant providing a qualitative measure of cohesive strength at the tip of a crack nucleating glide band, and

G = distance of dislocation source from the boundary.

Since the grain size is the upper limit of G , it should be approximately the grain size as is commonly found in metals. Copley⁽¹³⁾ has shown that sub-boundaries in MgO crystals apparently act as sources of mobile dislocations at elevated temperatures. In the present work slip bands associated with fracture origins traversed the grain, indicating possible origin from the boundary and showing G and grain size to be essentially the same. Wilson and Chapman⁽¹⁴⁾ showed that in metals, preferred orientation can change both σ_o and K in the Petch equation and that K can vary independently of σ_o if there is an alteration or orientation relationships of adjacent grains. They also noted that these effects became more pronounced as the number of slip systems decreases. Since the extruded bodies have a 100 texture similar to Ku and Johnston's bi-crystals, σ_o should not be affected unless there is residual work in the bodies.

The Petch plot of the data (Figure 25) clearly show that K is substantially changed and that there is little or no change in σ_o . Thus strengthening is primarily due to the preferred orientation as predicted^(1,2,6,7). This is in agreement with results which indicate the same or greater strength after annealing since annealing would reduce residual work. It should also follow that strength across the extrusion should not be reduced, but should be about the same as for hot pressed bodies since the orientations in that direction are approximately random.

The intercept of the extruded MgO data on the Petch plot (Figure 25) is approximately the stress to multiply dislocations in MgO, and not too far from Ku and Johnston's⁽¹²⁾ bi-crystal result of about 7800 psi. (Their value could be higher due to a possibly greater impurity content within the fused grains of their bi-crystals. The hot pressed and extruded material, though having about the same level of impurities, may have purer grains due to greater grain boundary surface area for accumulation of impurities.)

The observed slip bands associated with fracture origins do not appear to be due to edge components of the $\{110\} \langle 110 \rangle$ slip systems. First, there would be limited macroscopic resolved shear stress on these cleaved surfaces because of their trend toward perpendicularity with the tensile axis. Second, the observed slip bands are parallel to what appear to be $\{100\}$ cleavage steps. Edge components of the $\{100\} \langle 110 \rangle$ system have this orientation; however, this system is not known to operate at room temperature because it

requires stresses of the order of 1,000,000 psi⁽¹⁵⁾. Thus the slip bands appear to be screw components of the $\{110\} \langle 110 \rangle$ slip system since they are the only other components known to operate and have the indicated orientation.

Pile-up of edge dislocation components at grain boundaries in bi-crystals is observed to nucleate cracks, but not of screw components^(12,16,17). (It should, however, be noted that most bi-crystal tests have been such that screw components have low angles with the boundaries.) The orientation of the extruded bodies may be the fundamental factor in this apparent change in mechanisms. The $\langle 100 \rangle$ axial texture means that grain boundaries approximately parallel to the extrusion axis will be predominately of a tilt character while those approximately perpendicular to the axis will have a net predominately twist character. However, most of the latter may have limited twist misorientation or even only small tilt character since they are apparently formed by recrystallization of the elongated grains into several shorter grains. Hence, boundaries perpendicular to the extrusion axis with large misorientations (predominately twist) probably exist only as a remnant or result of the original boundaries between tandem elongated grains if there is no correlation in twist orientation between such elongated grains. Therefore, such boundaries would be in the minority.

A tentative concept of fracture of extruded MgO is thus offered as follows. Dislocation sources (probably from or near grain boundaries) are activated. The resulting edge components may reach a boundary perpendicular to the extrusion axis. If there is enough misorientation (predominately twist) and stress, fracture should occur due to pile-up; however, such boundaries are expected to be in the minority. Fracture origins from grain boundary surfaces which may have resulted from such edge dislocation pile-ups were not frequently observed. This would agree with the expected possible frequency of boundaries perpendicular to the extrusion axis with greater than average misorientation.

Screw components from the activated dislocation source may reach a grain boundary if the edge components of the dislocations have not yet met a boundary or have met a boundary of sufficiently low misorientation so as not to nucleate a crack. Failure of edge components to nucleate cracks can then allow higher than normally observed stresses to be applied to the screw dislocation pile-ups which then results in crack nucleation. The exact mechanism by which screw components would nucleate cracks is not yet clearly understood; however, two factors may be of importance in this suggested mechanism. First, the boundaries that screw components will most likely meet, due to the $\langle 100 \rangle$ texture of the body and their 100 motion, are mostly parallel to the extrusion axis (in agreement with observation) and hence mostly likely to be of high misorientation and predominately of tilt character. Second, the observed dislocation bands are commonly associated with crack nucleation from or near a triple point. Triple points could greatly change local stress concentrations to aid crack nucleation.

All the data and evaluations in this study indicate that crack nucleation by dislocation pile-up at grain boundaries is the determining factor in strength of extruded MgO unless substantial flaws are present. Further, since hot pressed MgO whose strength is not determined by impurities or substantial flaws (see Appendix 5) also obeys the Petch relationship and also extrapolates to about the stress to multiply dislocations in MgO crystals as the extruded MgO does, it is therefore concluded that crack nucleation by dislocation pile-up at grain boundaries is the determining factor in the strength of dense hot pressed MgO.

The reason that extruded MgO frequently fractures internally may be due to one or both of the following factors:

- (1) The statistical chance of finding the combination of a grain of the most favorable orientation with an adequately operable and located dislocation source may not commonly be found in the surface.
- (2) Sanding of the surface grains may introduce many mutually blocking slip bands similar to Alden's⁽¹⁸⁾ cyclical strengthening of MgO crystals since the chance of such slip bands nucleating cracks is reduced by orientation. Frequent high slip band densities in surface grains, and the apparent increase of surface failures in annealed specimens, would agree with this suggestion.

The degradation of strength of extruded MgO but not hot pressed MgO (see Appendix 5) by chemical polishing could be due to any one or a combination of:

- (1) Thermal shock of the bodies (taken from boiling phosphoric acid at approximately 150°C to hot water at approximately 60°C) enhanced by residual stress in unannealed extrusions. (The fact that annealing reduces cracking during cutting, shows residual stress exists in unannealed bodies.)
- (2) Stress-corrosion by the acid, most likely at grain boundaries, due to residual stress and possibly aided by impurities.
- (3) Stress-corrosion by the acid, most likely at grain boundaries, due to local stresses from possible work hardening of surface grains (from sanding) and possibly aided by impurities or residual extrusion stress.

The consistent failure of extruded powder MgO at surfaces and corners, particularly since this commonly occurs at substantially lower stresses than for denser extruded bodies of the same or larger grain size, shows the marked effect of porosity on strength and fracture.

Annealing

Orientation and fracture data both indicate that annealing results in the same or greater grain orientation than in the as-extruded body.

Strength and fracture studies, indicating increasing grain boundary failure and possible grain boundary impurity content, suggest agglomeration or precipitation of impurities during annealing.

Results suggest slower grain growth of extruded MgO during annealing in agreement with earlier results on both MgO and CaO⁽⁶⁾. This could be due to the limited amount of residual sub-structure which may be very slow to anneal⁽¹⁹⁾, or to reduced misorientation.

Since stalled extrusion billets show little or no increase in orientation, orientation must be due to extrusion. However, whether the orientation is caused directly by extrusion, or indirectly by extrusion effects on annealing (during cooling) cannot be determined.

CONCLUSIONS

From the foregoing work it is concluded that:

- (1) Crack free extrusions can be obtained.
- (2) Extrusion of MgO increases its strength 50 to 100% with a $\langle 100 \rangle$ rod texture.
- (3) Extruded MgO obeys the Petch relationship.
- (4) The increase in strength of extruded MgO is due to the preferred orientation, and not to residual work.
- (5) Crack nucleation by dislocation pile-up at grain boundaries is the source of fracture in extruded MgO and governs the strength of all dense MgO adequately free of flaws and impurities.
- (6) Extruded bodies have residual stress which is relieved by annealing at 2200°F(1205°C) for 1 hour.

This work has also shown that:

- (1) Billets of high density can be fabricated with both greater lengths and diameters than were obtained during the first year.
- (2) Extrusion into a heated catch tube, bringing the extrusion to rest in the hot zone, and subsequently controlling its cooling can be done.
- (3) Extrusion into a hot catch tube reduces cracking.
- (4) Chemical polishing of unannealed extruded MgO weakens it.

It has been reconfirmed that:

- (1) The densest starting billets give the densest extruded billets.
- (2) The finest grain starting billets give the finest grain extruded billets.
- (3) Substantial grain elongation occurs during extrusion, but nearly (though not fully) complete recrystallization occurs during cooling.
- (4) Extrusion improves alloy homogeneity.
- (5) Annealing results in the same or greater grain orientation than in the as-extruded bodies.
- (6) Grain growth during annealing of extruded MgO is apparently slower than in unextruded MgO.

This work also indicates that:

- (1) Thermal stress is most likely the main cause of extrusion cracking.
- (2) Screw dislocation bands can nucleate cracks, at least at or near triple points involving high angle tilt boundaries.
- (3) Extruded MgO may have a work hardened surface as a result of sanding.
- (4) Weakening of unannealed extruded MgO by chemical polishing is due to either residual stress from extrusion or surface finishing effects.

FUTURE WORK

Fabrication

Efforts to improve both size and quality of all billets and reduce grain size will continue. Hot pressed and fired bodies will continue to be the main source of billets, but experiments with both powder and fused billets will continue to be considered. Higher purity materials will be sought, particularly if they will allow achievement of finer grain sizes. All fabrication efforts will be limited by need or opportunity so as not to dilute the main effort on extrusion.

Extrusion

Extrusion using thick wall cans will continue to be the primary technique because experience with it should allow the greatest amount of information on extrusion effects to be gained in the coming year (though hot fluid to fluid extrusion appears feasible and indicates solution to several problems).

Evaluation of the heated catch tube to control extrusion cooling will be continued.

Further testing of the self-insulating can concept will be continued to lower heating requirements (thus limiting high temperature reactions, grain growth and chances of melting), by control of heat loss before and during, as well as after extrusion. Evaluation of ceramic shells in the cans will be done since this may also provide more information on extrusion (of tubes, wall thickness, cooling, etc.).

Extrusion of alloys and other oxides by tandem extrusion of appropriate compositions will be continued. Alloys are of prime interest because extrusion provides an excellent method of processing them, and they may provide much greater strength while also yielding further information on extrusion. Other oxides are of interest to understand the interaction of extrusion, deformation, and orientation, and because other oxides especially anisotropic ones should be strengthened even more than MgO by extrusion. This would result from orientation by extrusion not only reducing crack nucleation by dislocations (or twinning) phenomena, but also by reduction of internal stresses due to anisotropic elastic relationships and thermal contraction of grains.

Extrusion of single crystals of different orientation and of different shapes are of particular interest to learn more of extrusion texturing mechanisms. Extrusion of round billets through square dies is planned since this should either give some $\langle 100 \rangle$ texture perpendicular to the square face as well as along the axis, or change the texture along the axis. In either case, specimens with tensile stresses at measurable angles to the $\langle 100 \rangle$ direction could be obtained (preferably with tension along $\langle 111 \rangle$ directions.) This should result in substantially more strengthening of MgO than texturing in the $\langle 100 \rangle$ direction which offers the easiest mode of slip operation.

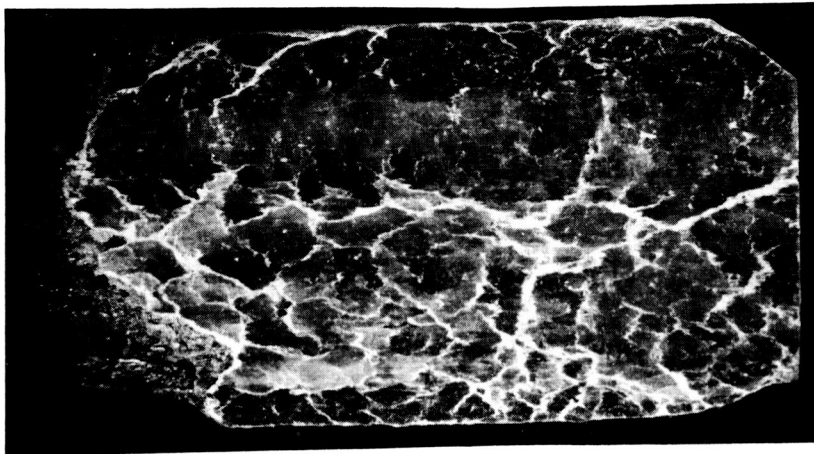
Analysis

Continued improvements in analysis techniques, such as orientation measurements, will be sought as warranted. Further evaluation of the effects of treatment such as chemical polishing, and annealing on extruded bodies will be conducted. Special effort will be made to study strength and fracture of extruded MgO at elevated temperatures since the preferred orientation in the extruded material should also reduce grain boundary sliding^(1,2,3) thus improving high temperature properties.

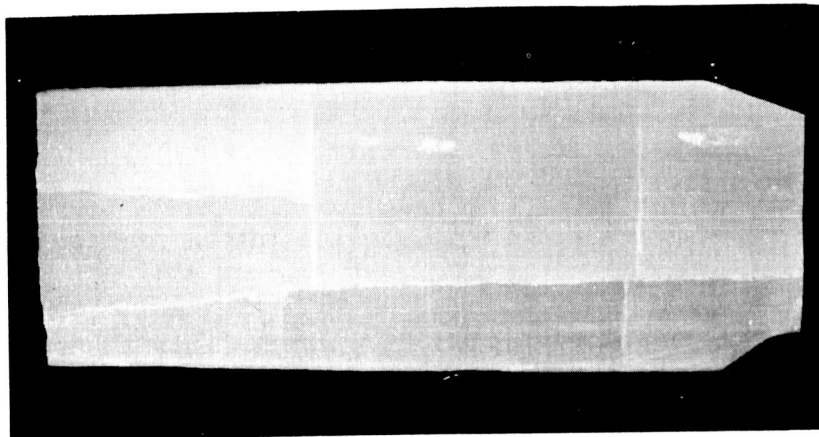
REFERENCES

1. "Technical and Management Proposal for a Study of Hot Extrusion of Refractory Oxides, D2-90517", submitted to Headquarters, National Aeronautics and Space Administration, January, 1964.
2. R.W. Rice and J.G. Hunt, "Hot Extrusion of MgO", presented at the 66th Annual American Ceramic Society Meeting at Chicago, Ill., April, 1964 (Abstract: Am. Ceram. Soc. Bulletin 43 (4), 279, April 1964).
3. R.W. Rice, "Internal Surfaces in MgO", presented at the Conference on the Role of Grain Boundaries and Surfaces in Ceramics at Raleigh, N.C., in November, 1964. (Proceedings to be published by Plenum Press, New York, N.Y.)
4. R.W. Rice, "Ceramic Alloying", presented at the 66th Annual American Ceramic Society Meeting at Chicago, Ill., April, 1964 (Abstract: Am. Ceram. Soc. Bul. 43(4), 265, April, 1964).
5. J.G. Hunt, P. Lowenstein, "Hot Extrusion of UO₂ Fuel Elements", Ceramic Bulletin 43 (8), 562-65, August, 1964.
6. R.W. Rice, J.G. Hunt, "Identifying Optimum Parameters of Hot Extrusions - Interim Report", NASA Contract NAS 7-276, May, 1965.
7. R.W. Rice, J.G. Hunt, "Hot Extrusion of Cubic Oxides", presented at the 67th Annual Ceramic Society Meeting in Philadelphia, Penn., May, 1965.
8. "Technical and Management Proposal for a Study of Hot Extrusion of Refractory Oxides - a continuation of Contract NAS 7-276", submitted to Headquarters, National Aeronautics and Space Administration, October, 1964.
9. N.S. Stoloff and T.L. Johnston, "Formation and Structure of Alloy Layers in the MgO-Mn Systems", presented at the 66th Annual American Ceramic Society Meeting, April, 1964 (Abstract: Am. Ceram. Soc. Bul. 43 (3), p. 339, 1964).
10. G.W. Groves and M.E. Fine, "Solid Solution and Precipitate Hardening in Mg-Fe-O Alloys", J. Appl. Phy. 35 (12), p. 3587-3593, December, 1964.
11. T.L. Johnston, R.J. Stokes, and C.H. Li, "Crack Nucleation in MgO Bi-Crystals Under Compression", Phil. Mag. 7, p. 29 (January, 1962).
12. R.C. Ku, T.L. Johnston, "Fracture Strength of MgO Bicrystals", Phil. Mag. 9 (98) p. 231-47 (February, 1964).
13. S.M. Copley Ph.D. Thesis - see S.M. Copley, J.A. Pask, "Deformation of Polycrystalline MgO at Elevated Temperatures", J. Am. Ceram. Soc. 48 (12) p. 636-42 (December, 1965).
14. D.V. Wilson, J.A. Chapman, "Effects of Preferred Orientations on the Grain Size Dependence of Yield Strength in Metals", Phil. Mag. 8 (93) p. 1543-51 (Sept., 1963).

15. C. Hulse, S. Copley, J. Pask, "Effects of Crystal Orientation on Plastic Deformation of MgO", J. Am. Ceram. Soc. 46 (7), p. 317 (July, 1963).
16. R.W. Rice, "Some Consideration in the Study of Mechanical Effects of Grain Boundaries in Ceramics", presented at the 15th Pacific Coast Regional American Ceramic Society Meeting in Seattle, Washington, October, 1962.
17. R.J. Stokes, C.H. Li, "Dislocations and Strength of Polycrystalline Ceramics", Materials Science Research Vol. 1 (ed. by H.H. Stadelmaier and W.W. Austin), Plenum Press, New York, N.Y. (1963).
18. T. Alden, "High Strength MgO", Appl. Phy. Letters 2 (6), p. 107 (March, 1963).
19. D.H. Bowen, F.J.P. Clarke, "The Growth of Neutron Irradiated MgO", Phil. Mag. 9 (99), p. 413-21 (March, 1964).

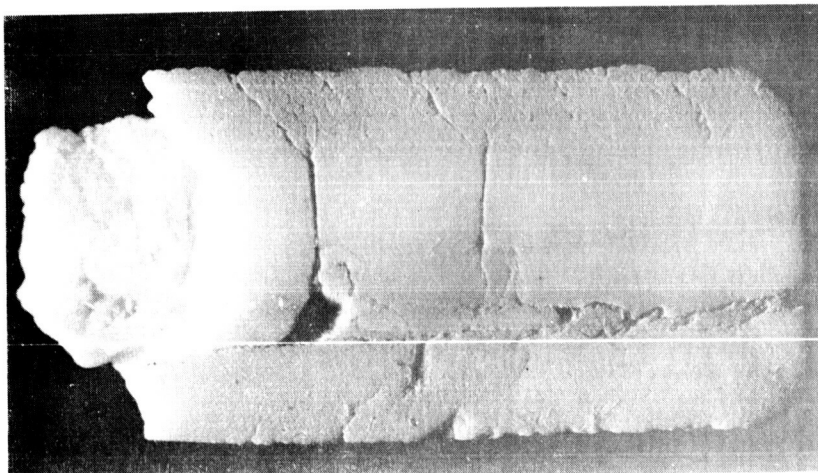


A



B

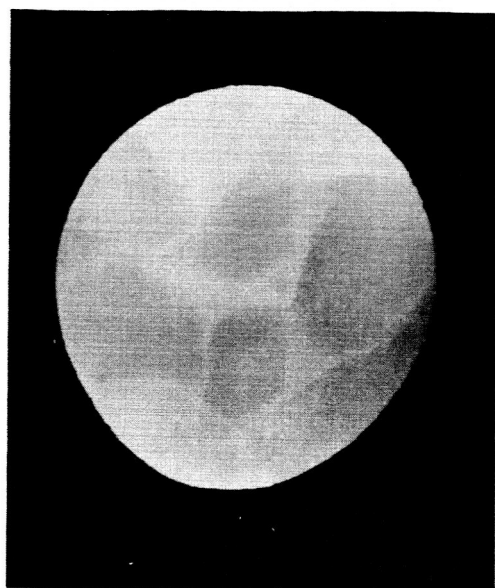
EXTRUSION
DIRECTION



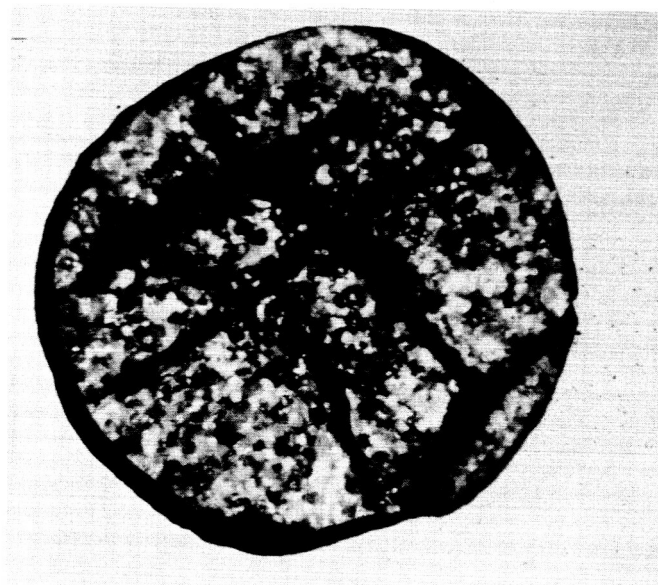
C

NOTE: ALL SPECIMENS ARE APPROXIMATELY 0.5" IN DIA.

FIGURE 1 RANDOM AND LINEAR CRACKING IN TRANSVERSE SECTIONS
(A) RANDOM CRACKING IN MION-1-1 (MgO-2)
(B) LINEAR CRACKING IN M-1-11 (MgO-5)
(C) INTERMEDIATE, M4C-1-4 (MgO-4)

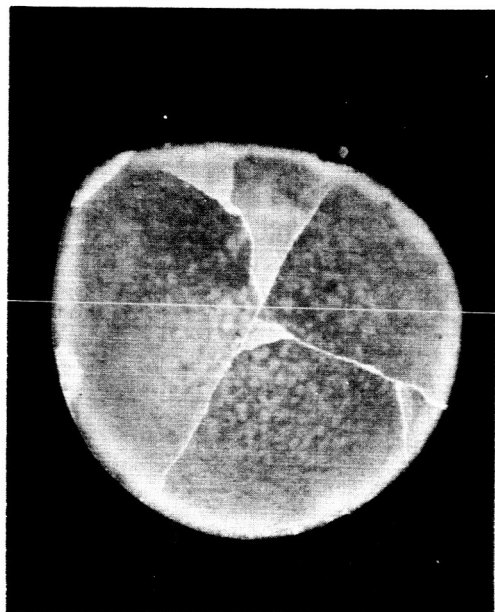


A



B

C



D

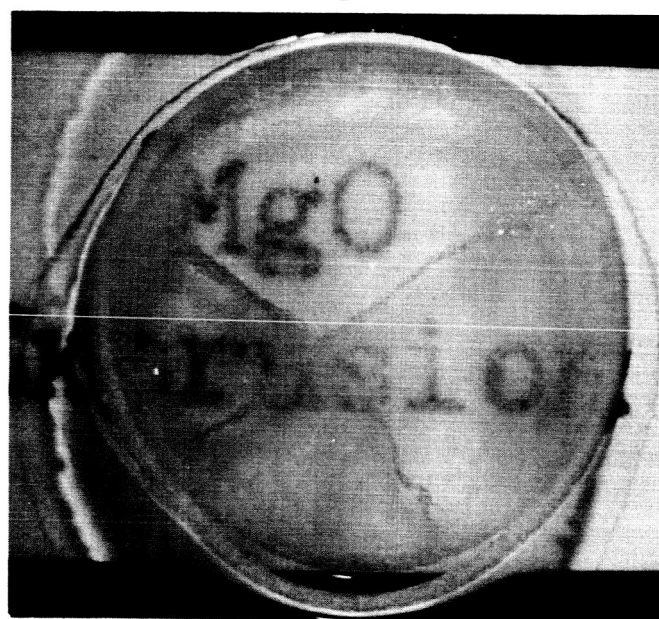


FIGURE 2 EXTRUDED BILLET CROSS SECTION SAMPLES

A) BILLET M1A-1-2 (MgO-3)

B) M-f-3 (MgO-3)

C) M2N-1-3 (MgO-2)

D) M-1-7 (MgO-5) - THIS SPECIMEN IS
SETTING IN A POOL OF GLYCERINE
TO SHOW TRANSPARENCY. ALL
SPECIMENS ARE APPROXIMATELY
0.5" IN DIAMETER.

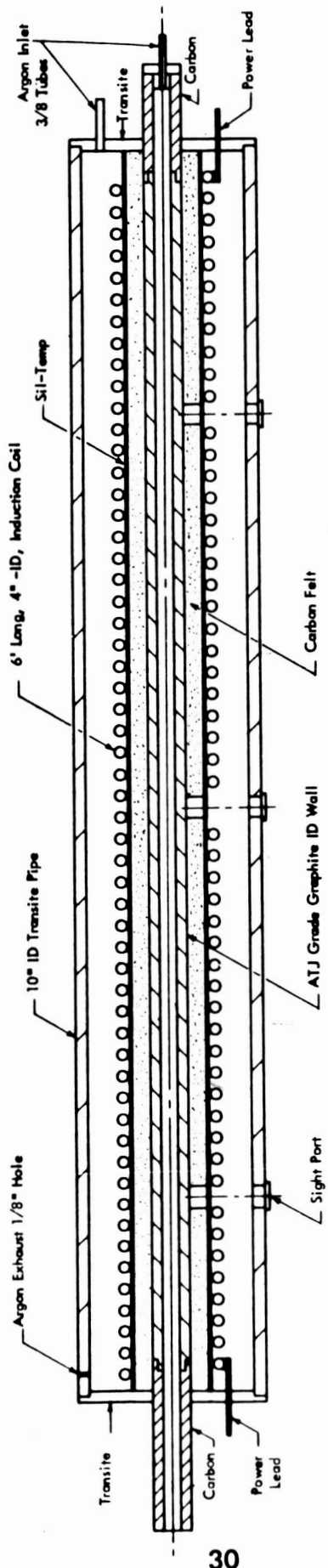


FIGURE 3 HEATED CATCH TUBE

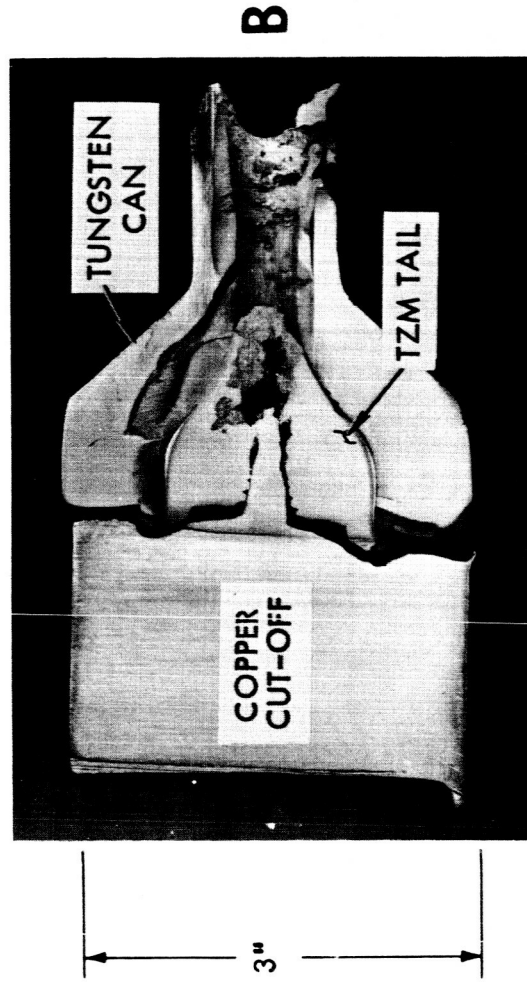
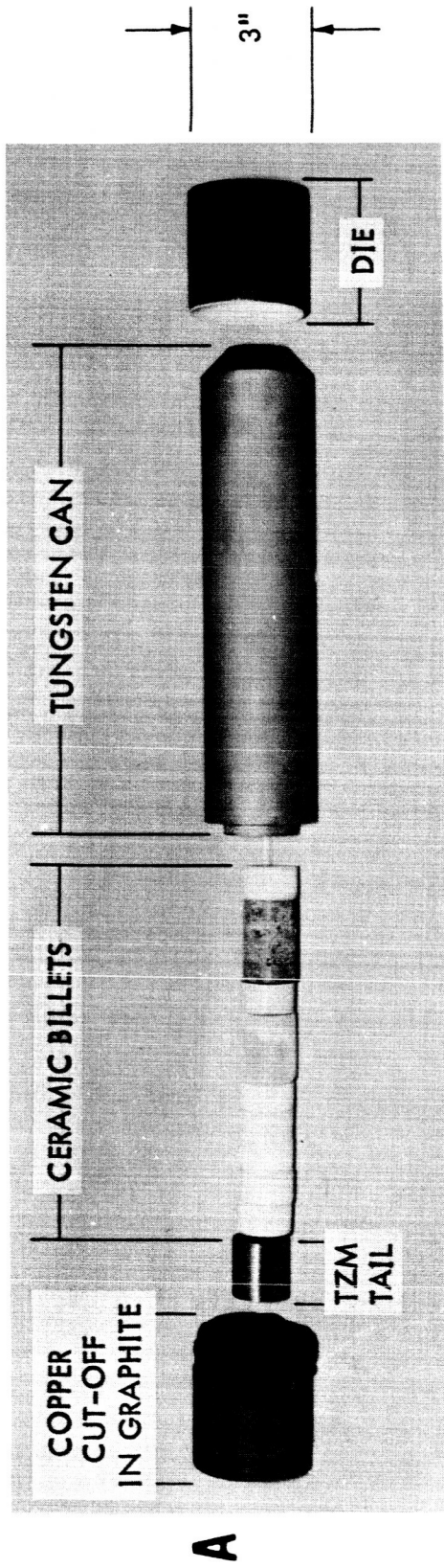
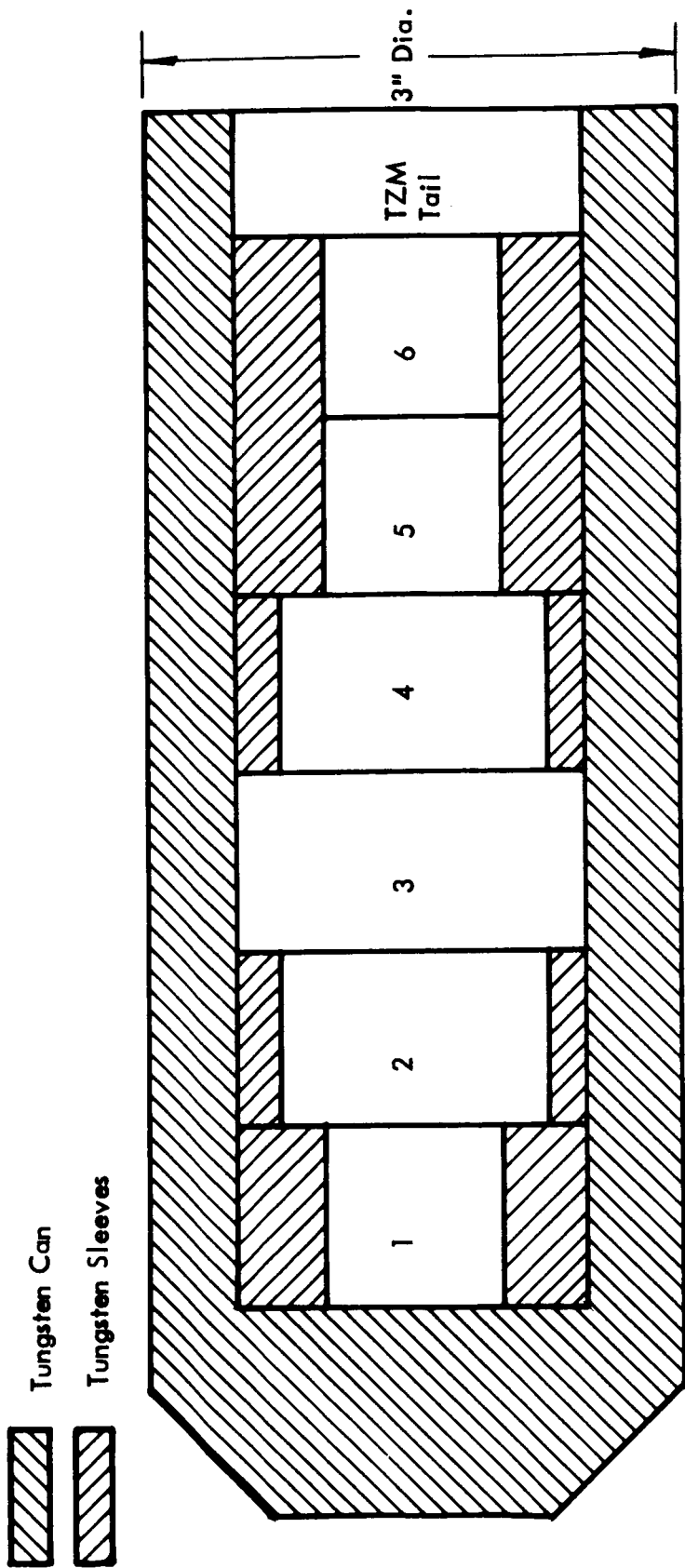


FIGURE 4 EXTRUSION BREAKDOWN AND REDUCTION. A) BREAKDOWN OF COMPOSITE BILLET B) STALLED TAIL OF EXTRUSION MgO-2



Not to scale

1. 1.0" diameter hot pressed billet
2. 1.5" diameter hot pressed billet
3. 2.0" diameter hot pressed billet
4. 1.5" diameter hot pressed billet
5. 1.0" diameter hot pressed billet
6. Dead burned "powder billet" (with penetrator used in extrusion to give the same diameter as billet 5).

FIGURE 5 MULTIDIAMETER CERAMIC EXTRUSION

→
EXTRUSION DIRECTION

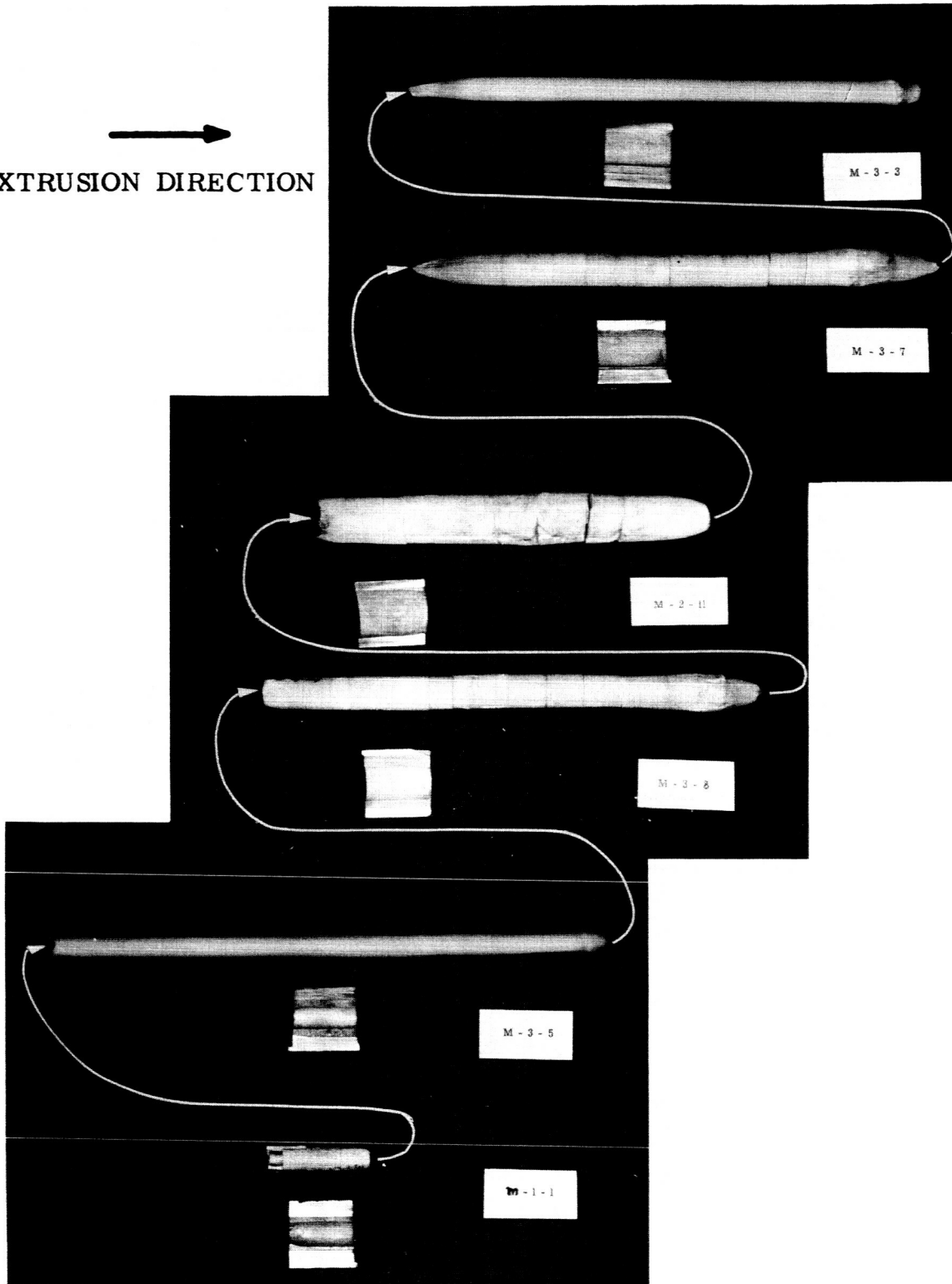


FIGURE 6 MULTIDIAMETER EXTRUSION MgO - 11

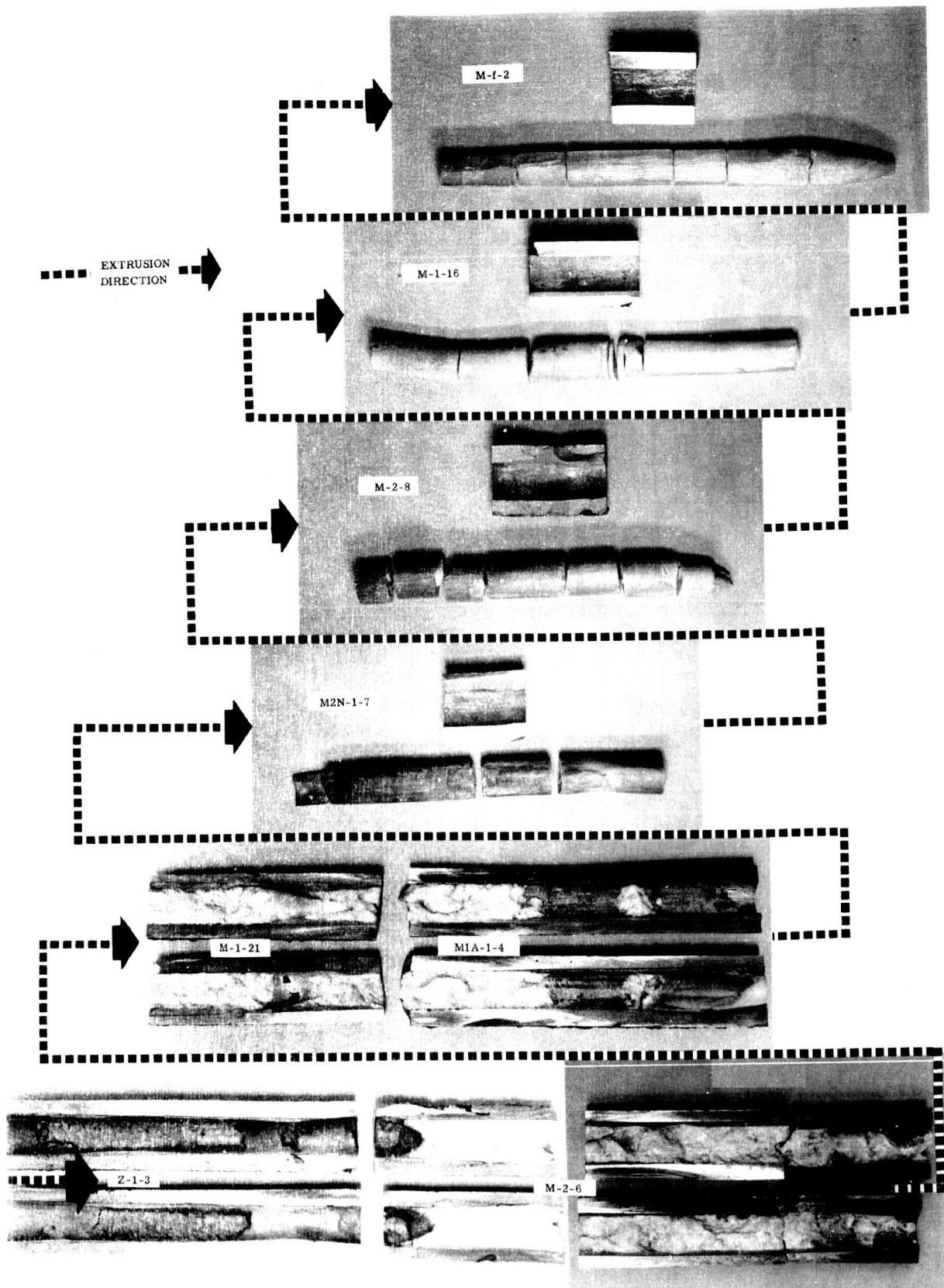


FIGURE 7 EXTRUSION MgO-12

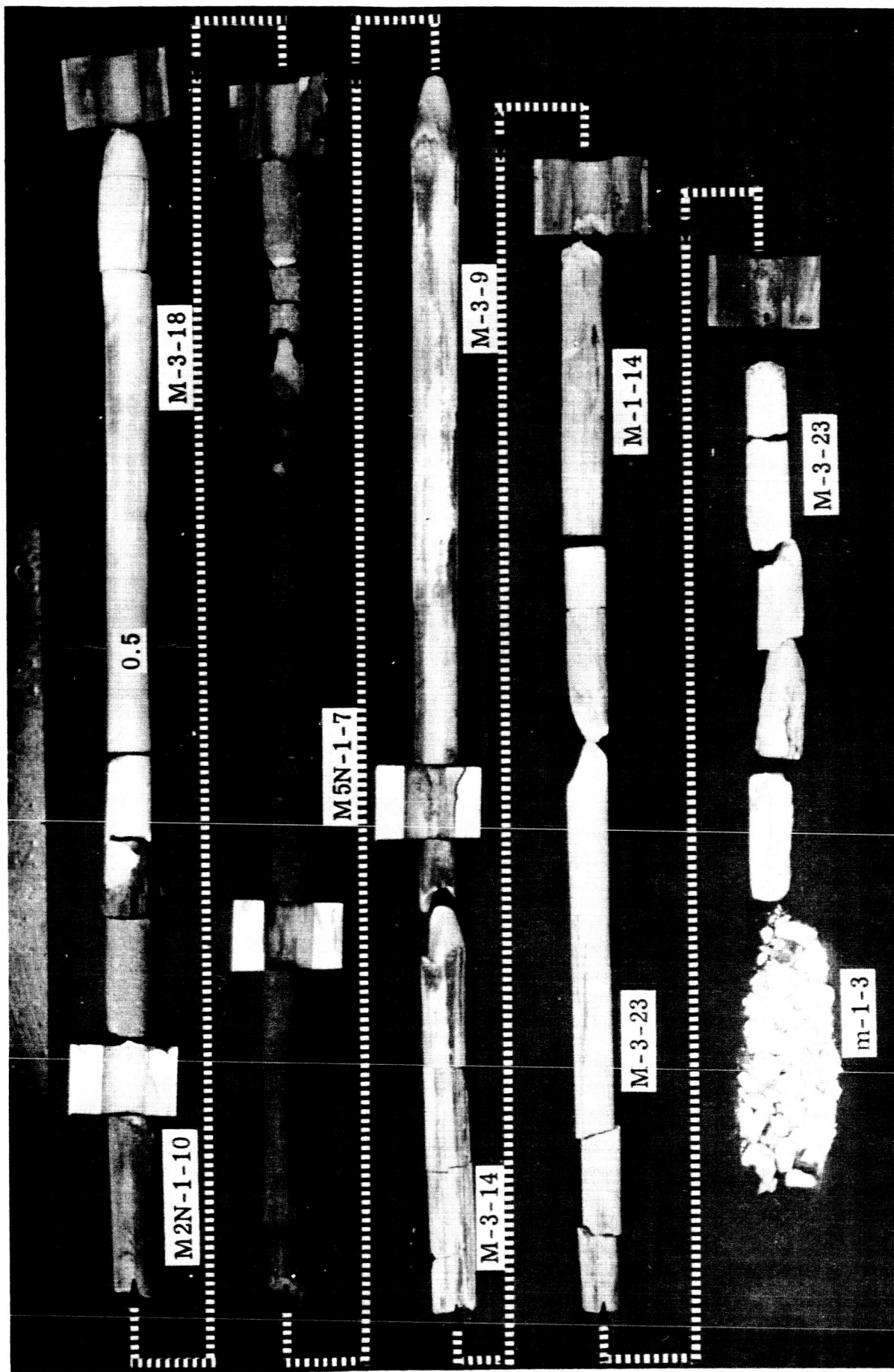


FIGURE 8 EXTRUSION MgO-14 (COOLED SUCCESSFULLY IN CATCH TUBE FROM 2000°C)

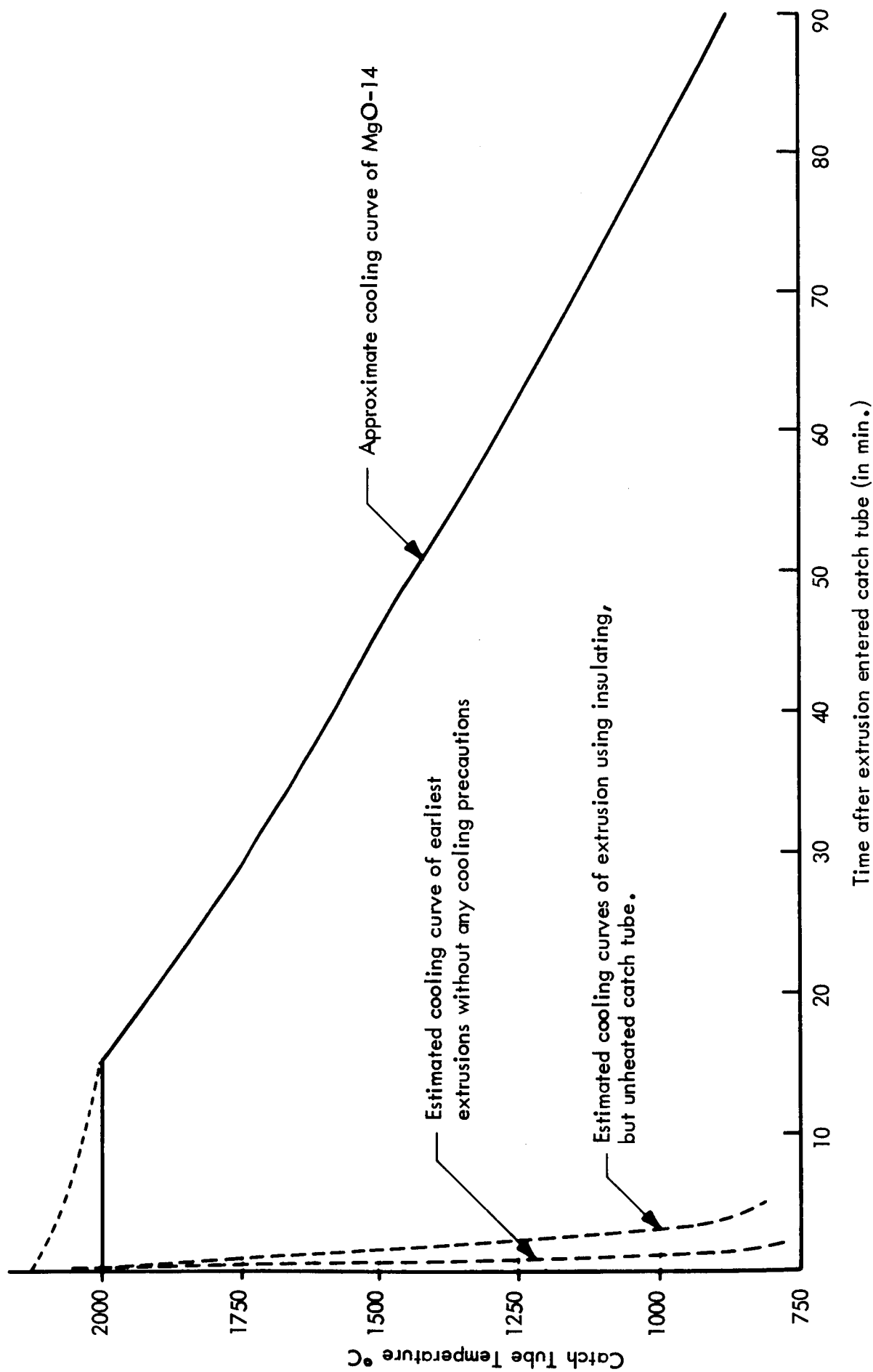


FIGURE 9 EXTRUSION MgO-14 COOLING

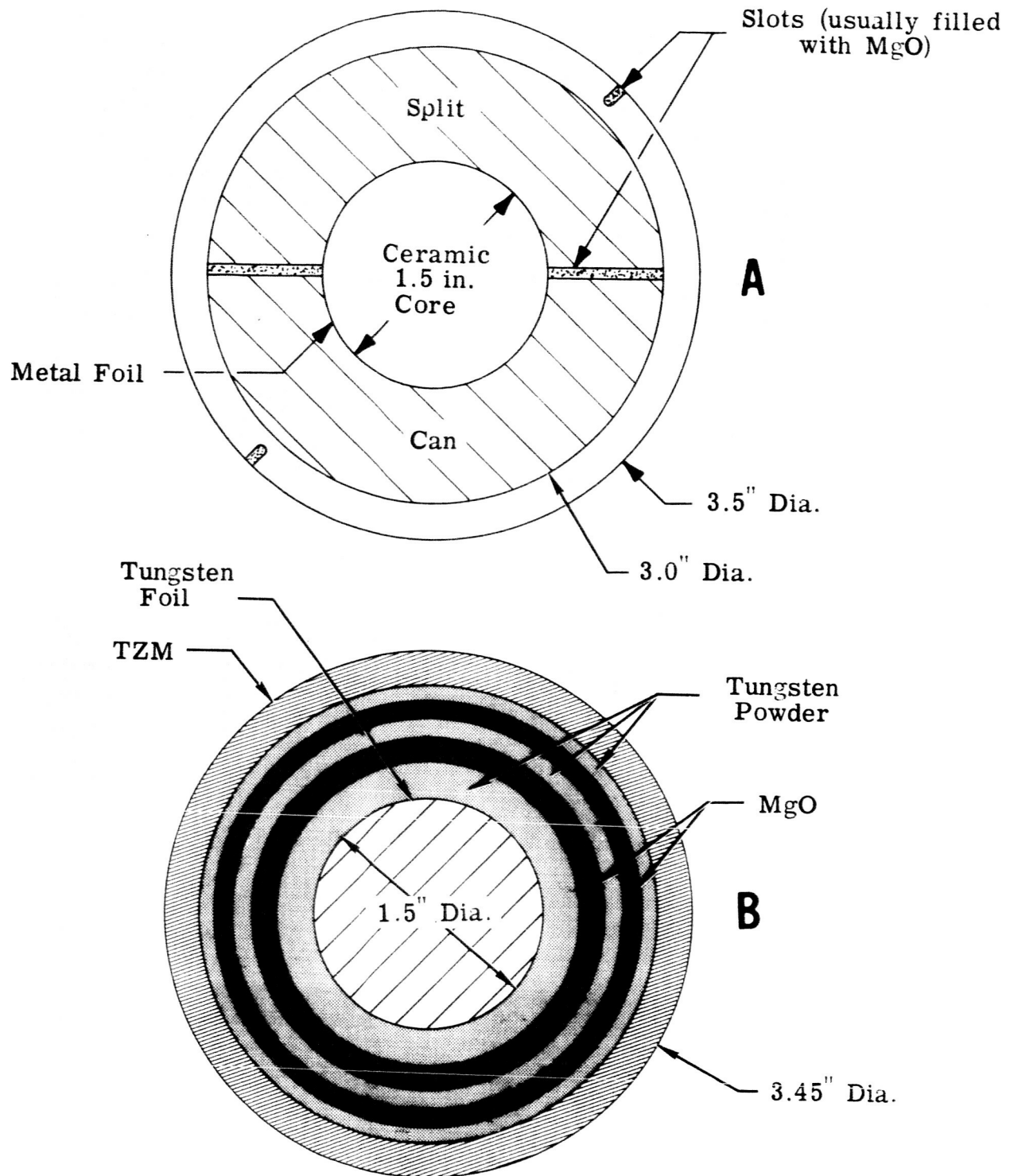
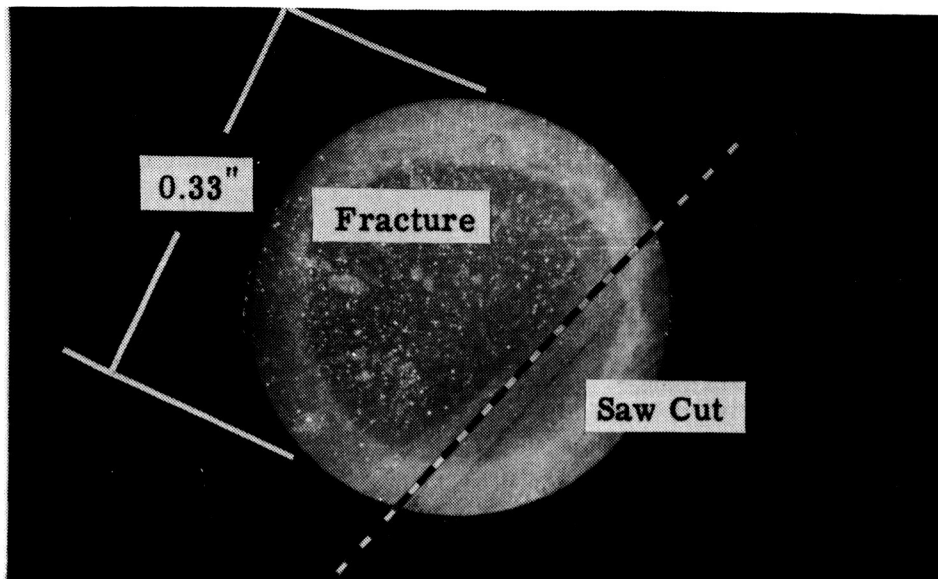
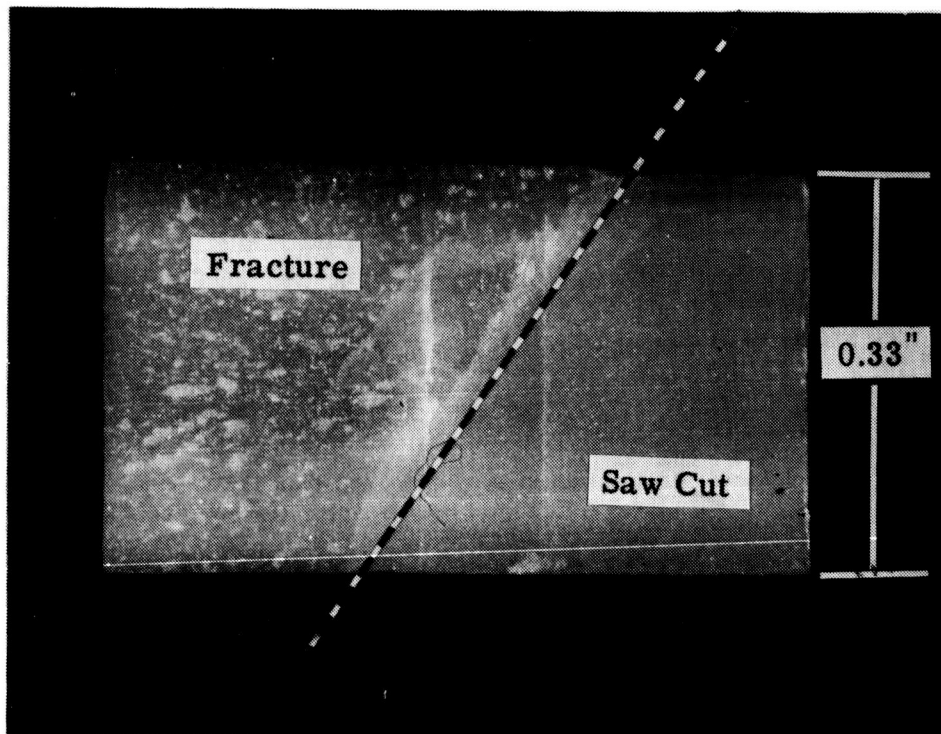


FIGURE 10 SPECIAL CAN CONFIGURATIONS (A) SPLIT CAN IN SLOTTED SHELL (B) SELF-INSULATING METAL-CERAMIC CAN.



A.



B.

Extrusion Direction 

FIGURE 11 FRACTURE IN CUTTING UNCRACKED EXTRUSIONS. Sections of M-3-5 (MgO-11). (A) Transverse Section, (B) Longitudinal Section Note Transverse Fractures

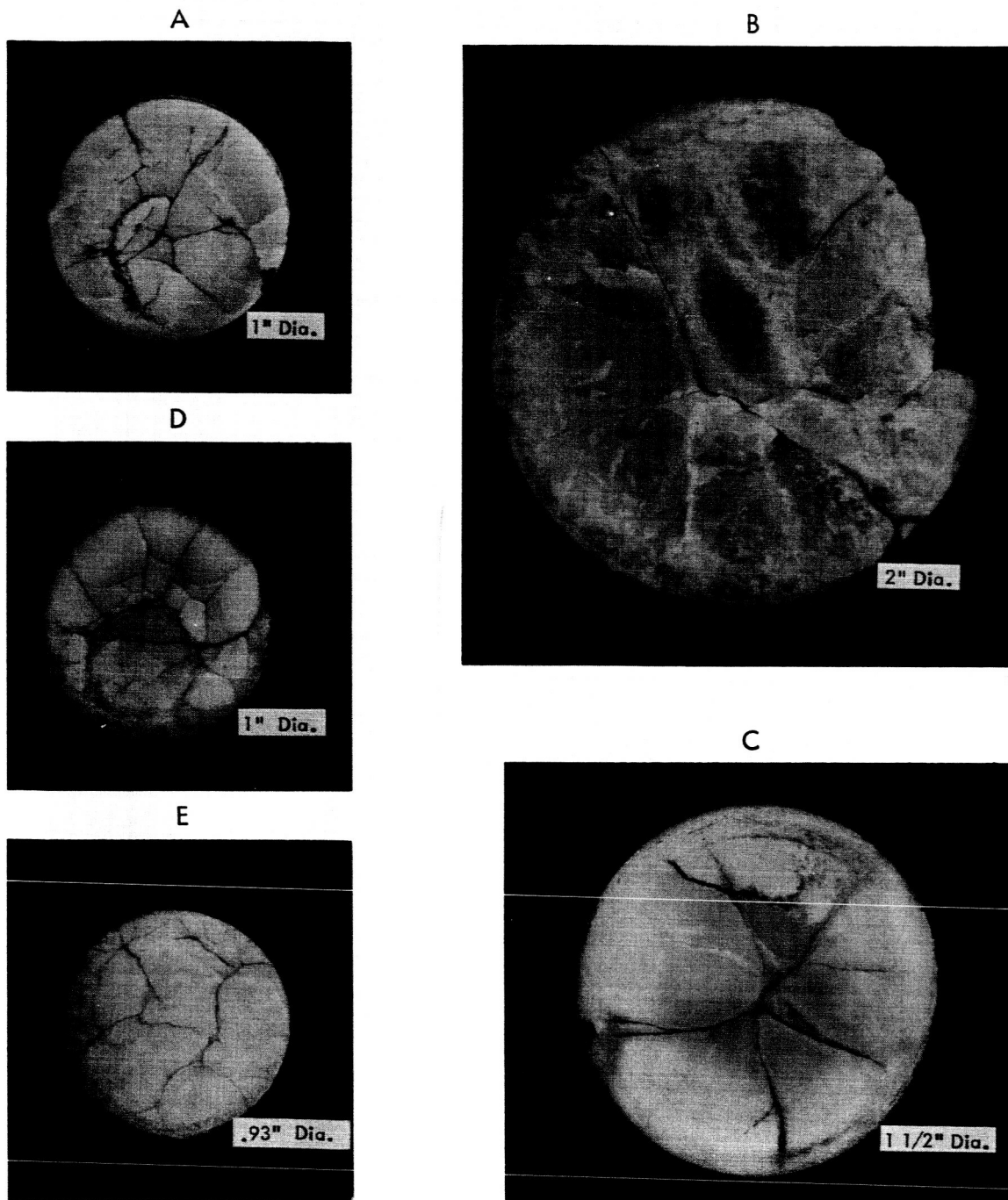
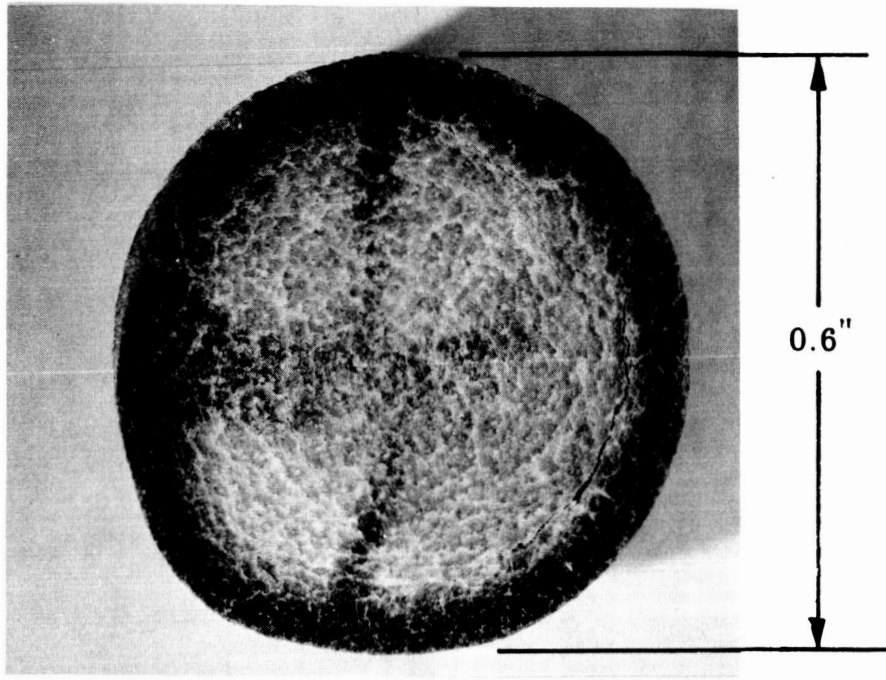
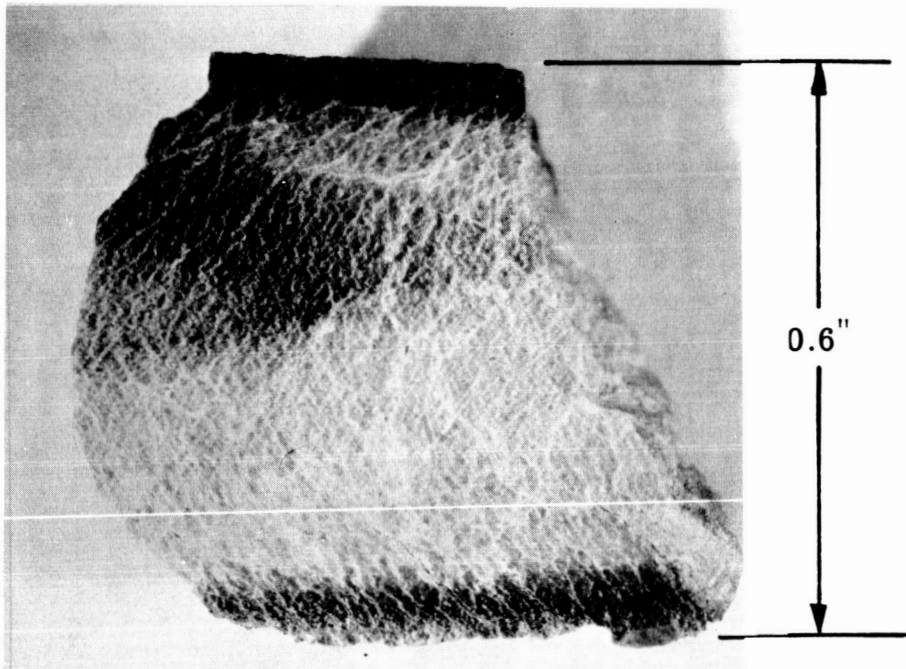


FIGURE 12 CRACKING IN EXTRUSION MgO-10 (UNEXTRUDED)
 A) M-2-20, B) M-3-2, C) M-2-7, D) M-2-21,
 E) m-1-1 (Note, billets listed in order: front to rear)



A.



B.


Extrusion Direction 

FIGURE 13 EXTRUDED ZrO_2 (Z-1-3) (A) Transverse Section,
(B) Longitudinal Section

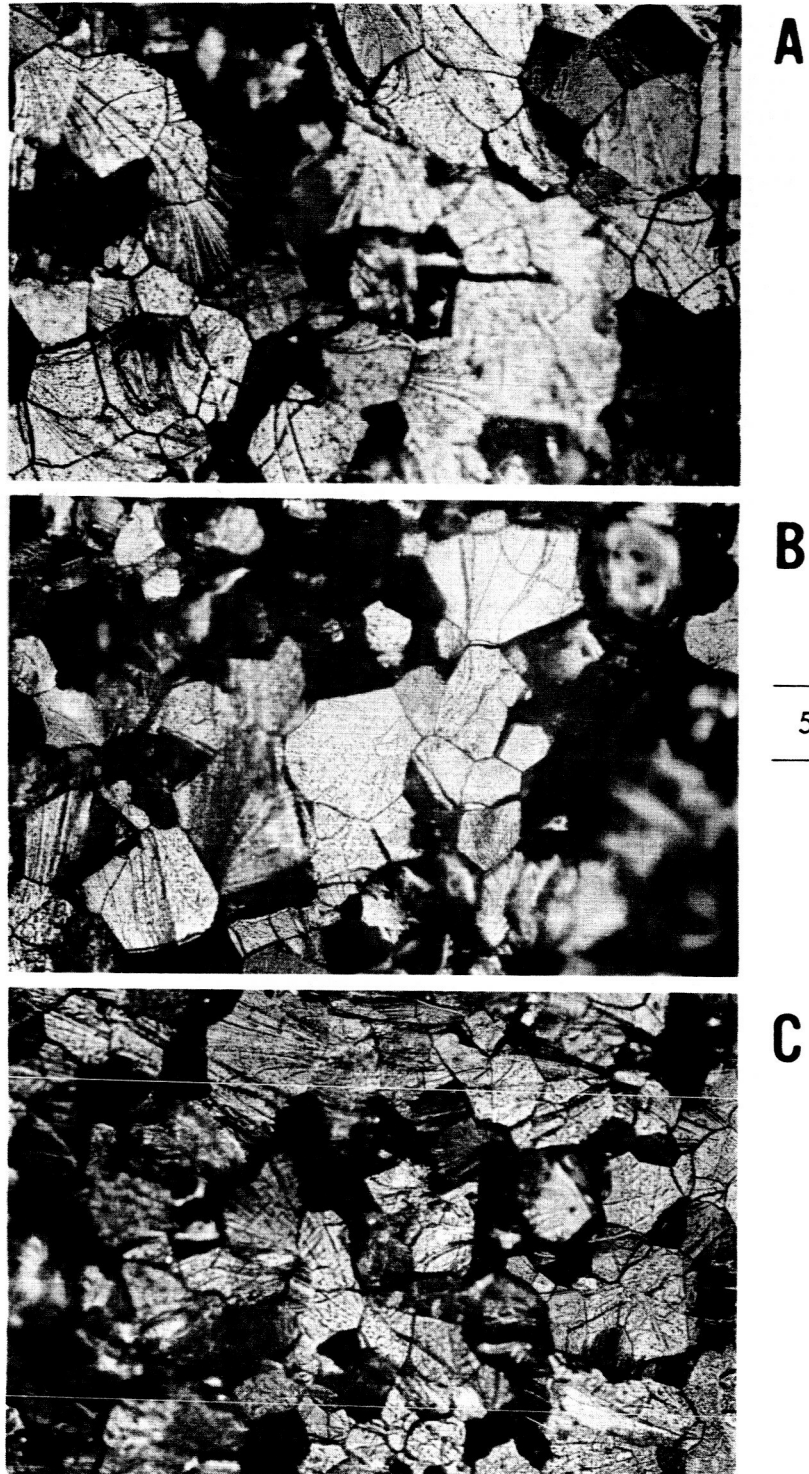
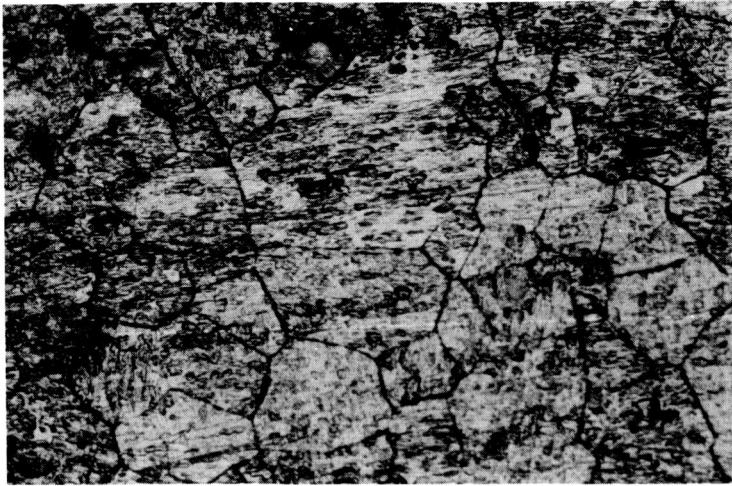
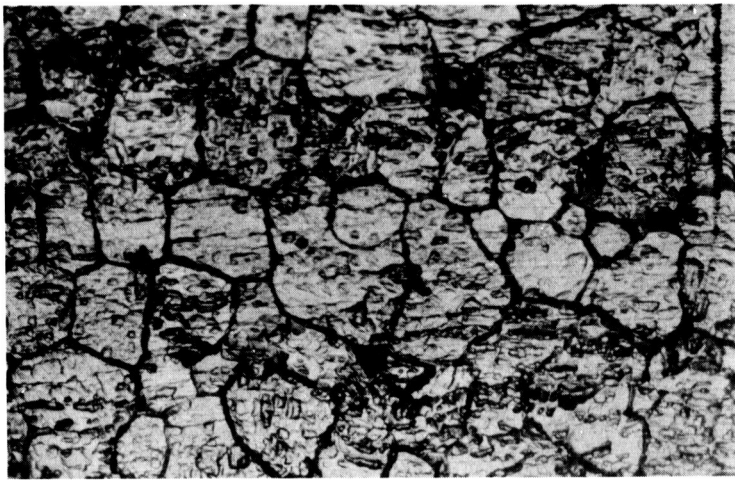


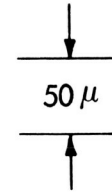
FIGURE 14 TYPICAL MICROSTRUCTURES, (A) (B) AND (C):
TRANSVERSE SECTIONS (FRACTURES) OF BILLETS
M2N-1-2 (MgO-3), M-1-4 (MgO-4), AND M-1-12 (MgO-5) RESPECTIVELY



D



E

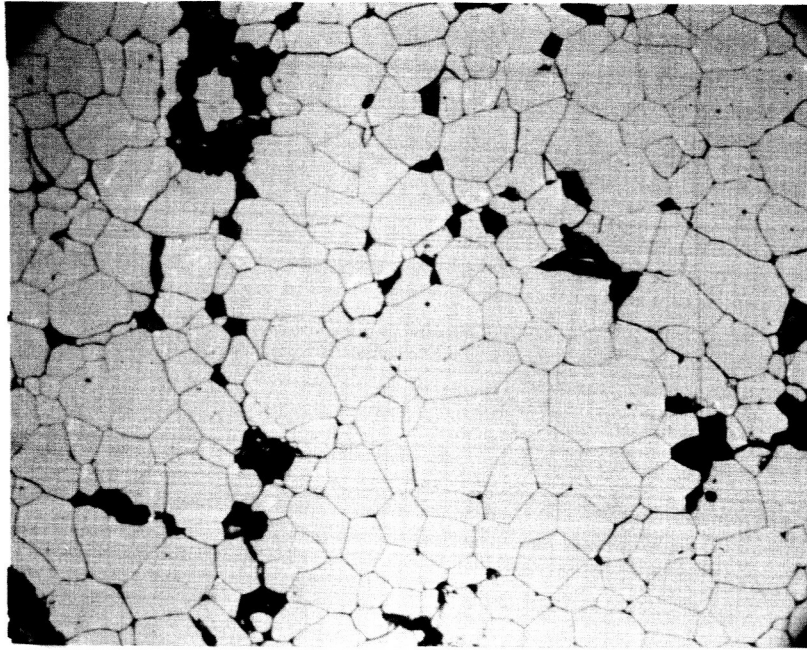


EXTRUSION
DIRECTION

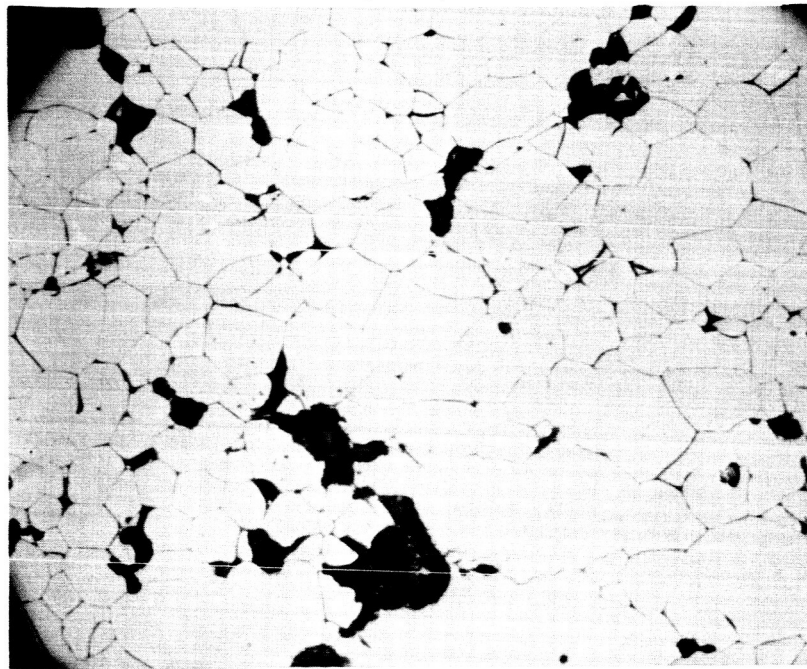
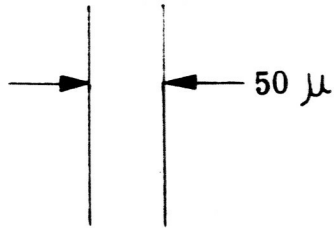


F

FIGURE 14 (CONT.) TYPICAL MICROSTRUCTURES. (D) (E) AND (F):
LONGITUDINAL SECTIONS OF BILLETS
M2N-1-2 (MgO-3), M-1-4 (MgO-4), AND M-1-12 (MgO-5) RESPECTIVELY



A.



B.


Extrusion Direction 

FIGURE 15 GRAIN STRUCTURE OF EXTRUDED ZrO_2 (Z-1-3)
(A) Transverse Section (B) Longitudinal Section

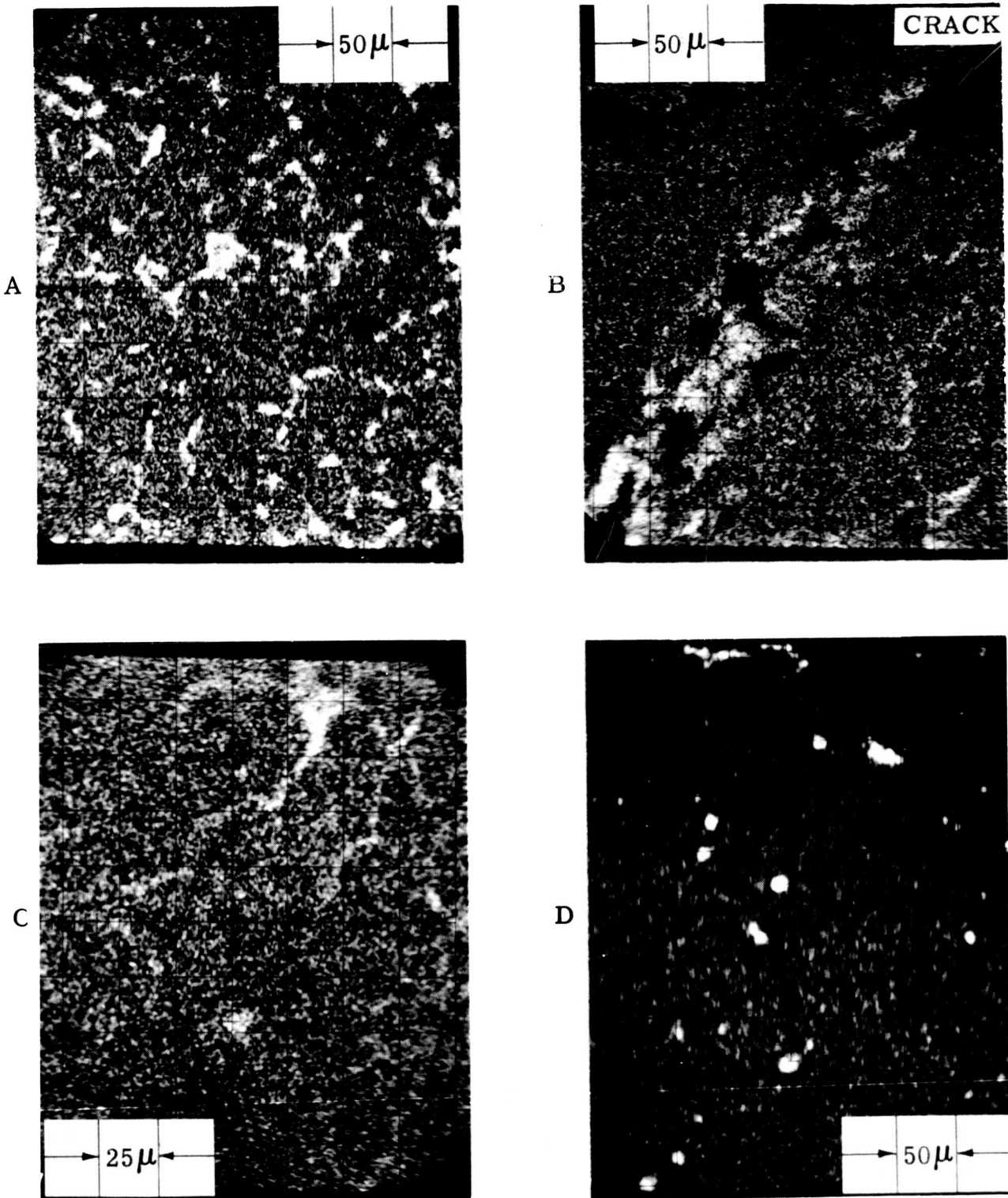
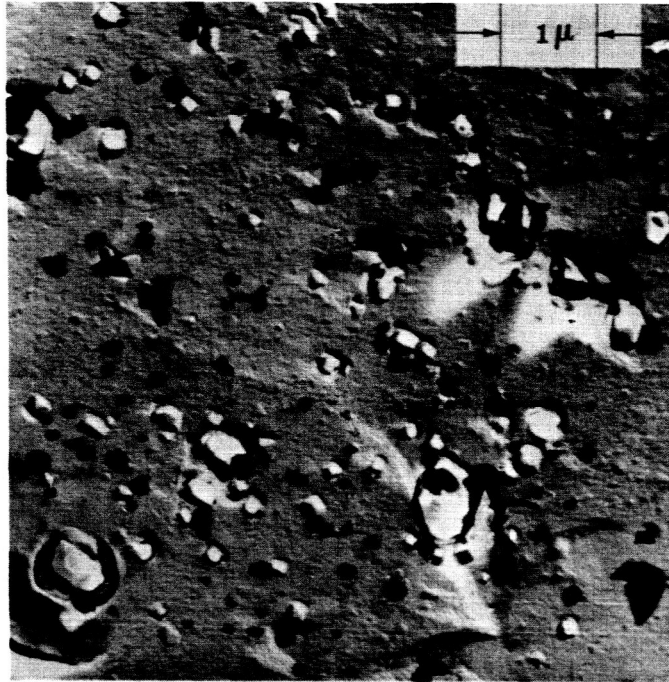
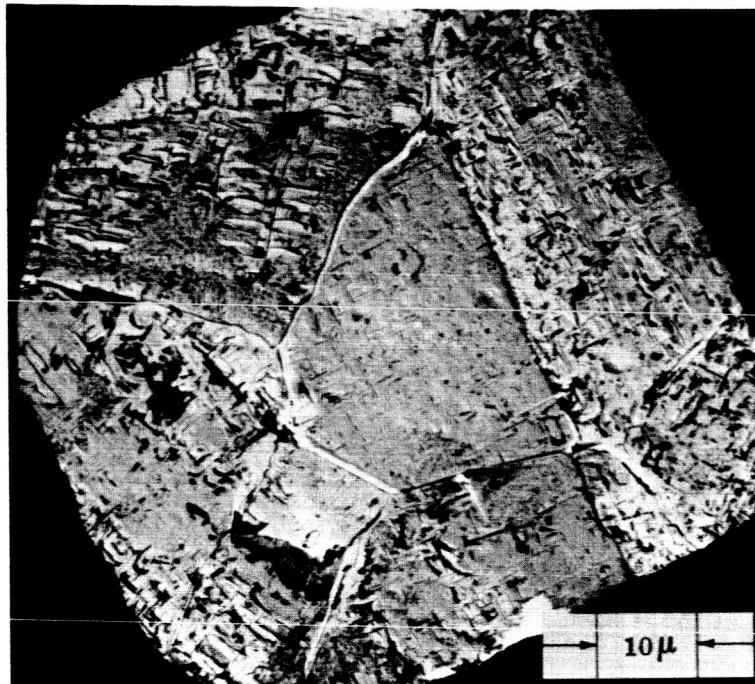


FIGURE 16 ZrO₂ ANALYSIS (A) AS RECEIVED BILLET-Ca FLUORESCENCE (B) LONGITUDINAL SECTION OF EXTRUDED ZrO₂ (Z-1-3)-Ca FLUORESCENCE (NOTE CRACK) (C) TRANSVERSE SECTION OF EXTRUDED ZrO₂ (Z-1-3)-Ca FLUORESCENCE (D) LONGITUDINAL SECTION EXTRUDED ZrO₂ (Z-1-3)-W FLUORESCENCE. (NOTE IN X-RAY FLUORESCENCE PHOTOS WHITE INDICATES PRESENCE OF THE FLUORESCENCING ELEMENT)

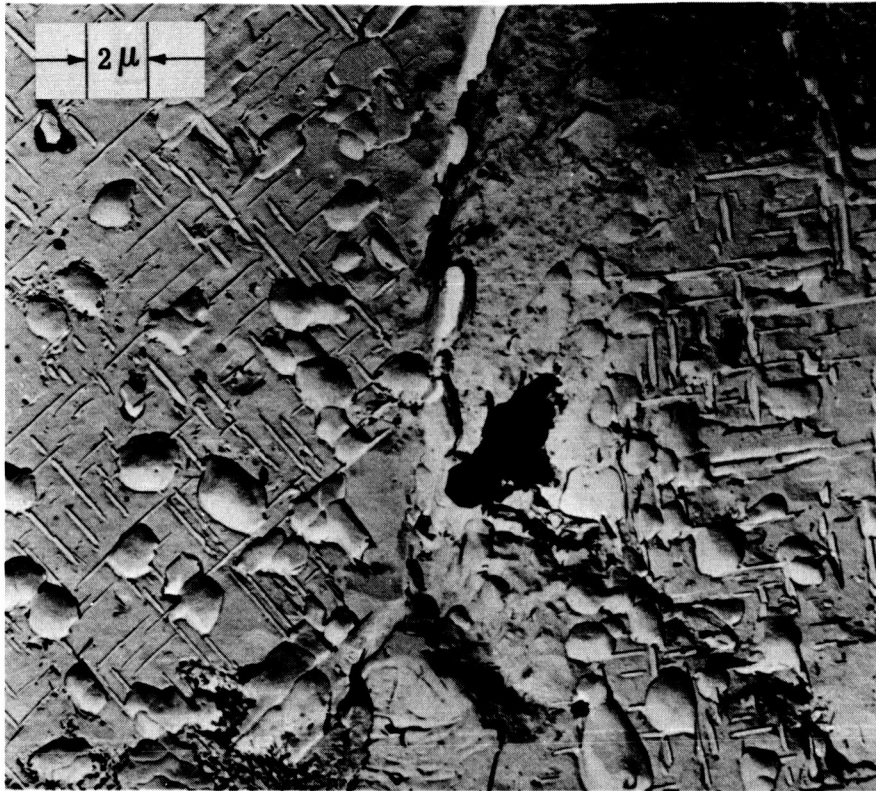


A

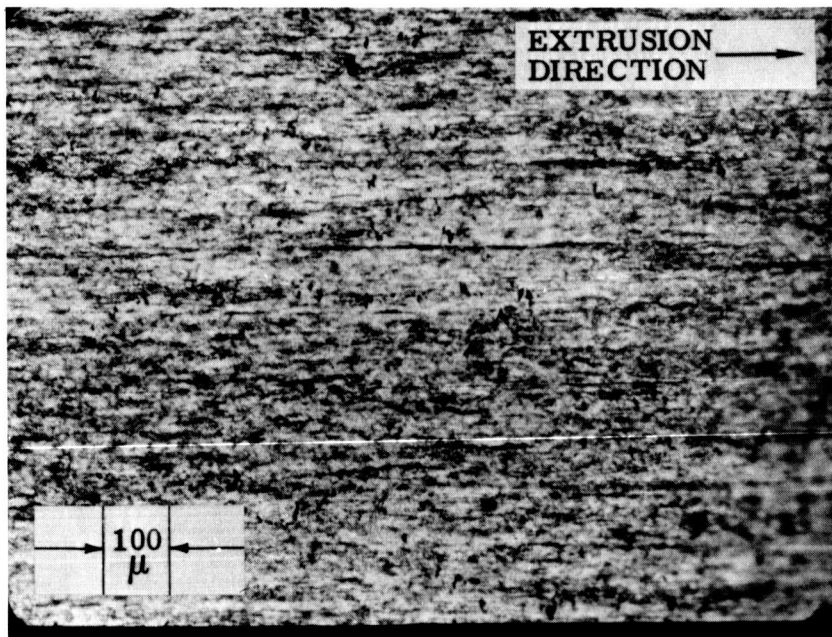


B

FIGURE 17 MgO-5 W/O Al₂O₃ ANALYSIS (A) HOT PRESSED AND FIRED (2600°F) BODY (B) HOT EXTRUDED BODY (M5A-1-2) RAPID COOLING)



C



D

FIGURE 17 (CONT.) MgO-5 W/O Al₂O₃ ANALYSIS (C) HOT EXTRUDED BODY (M5A-1-2, RAPID COOLING) (D) THIN SECTION OF HOT EXTRUDED BODY (M5A-1-5, COOLED IN CATCH TUBE)

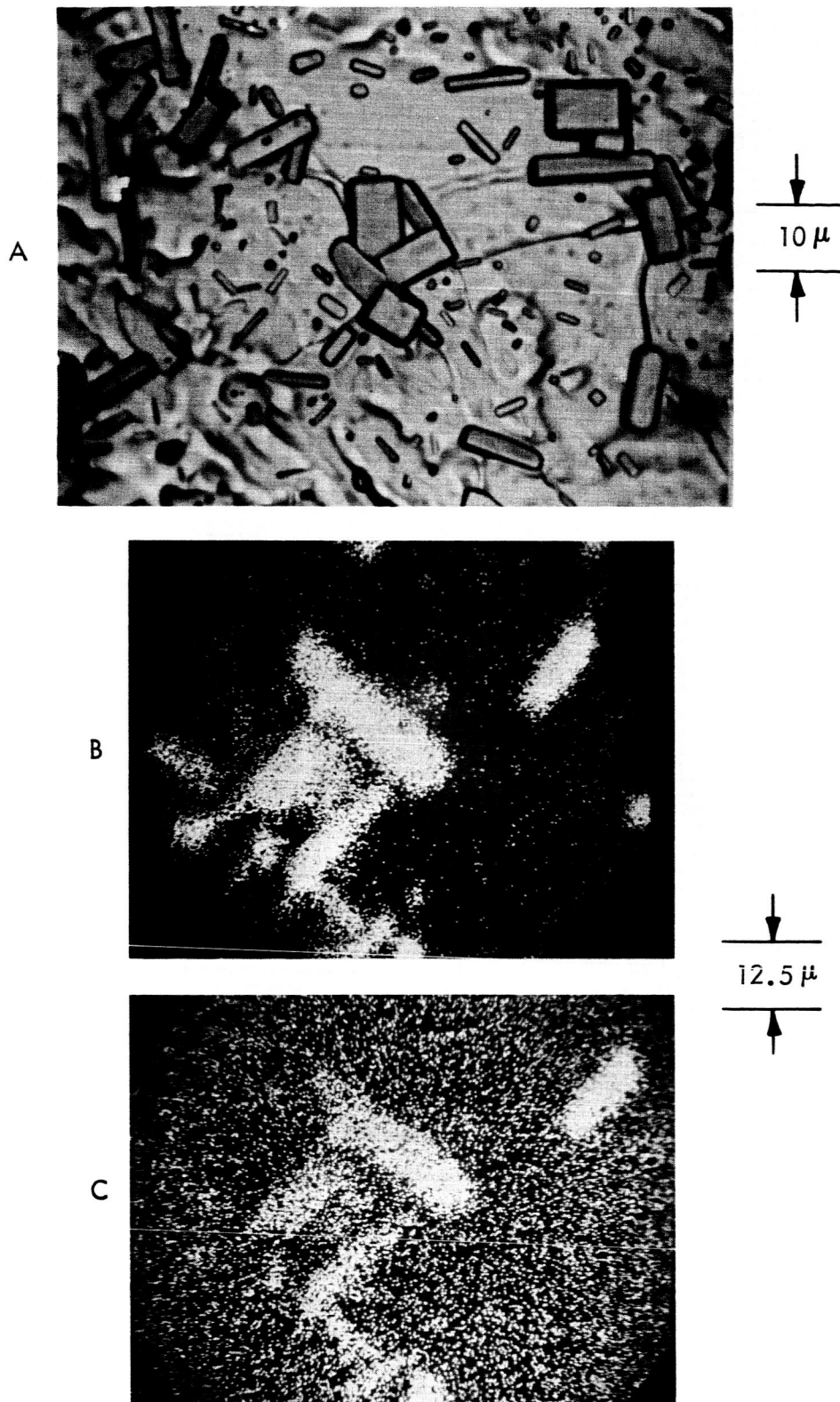
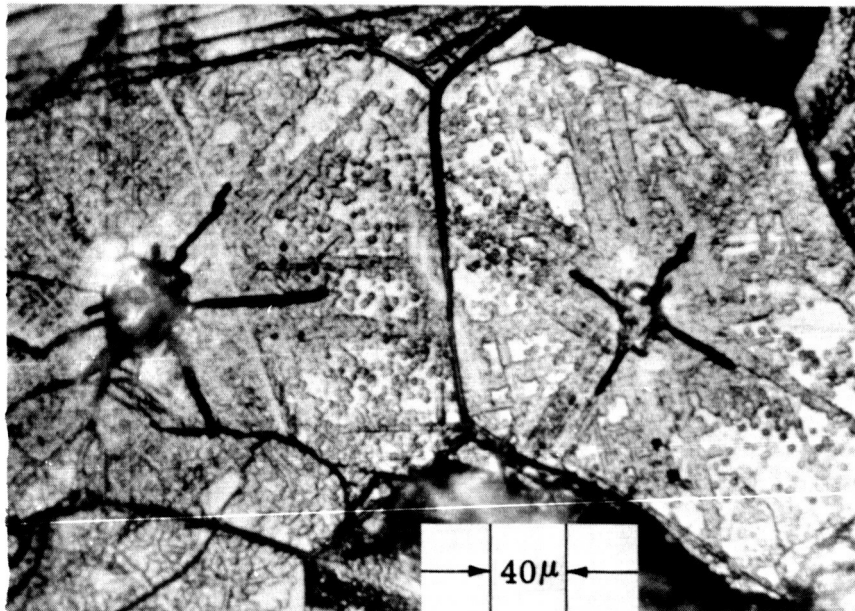
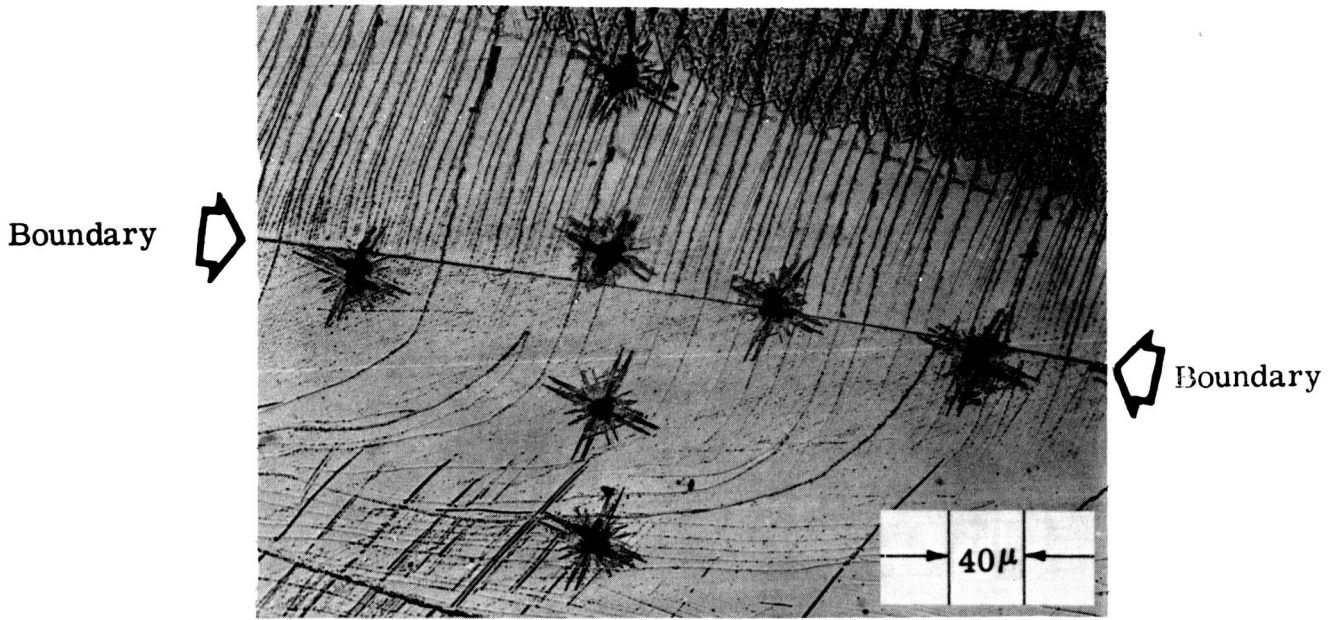
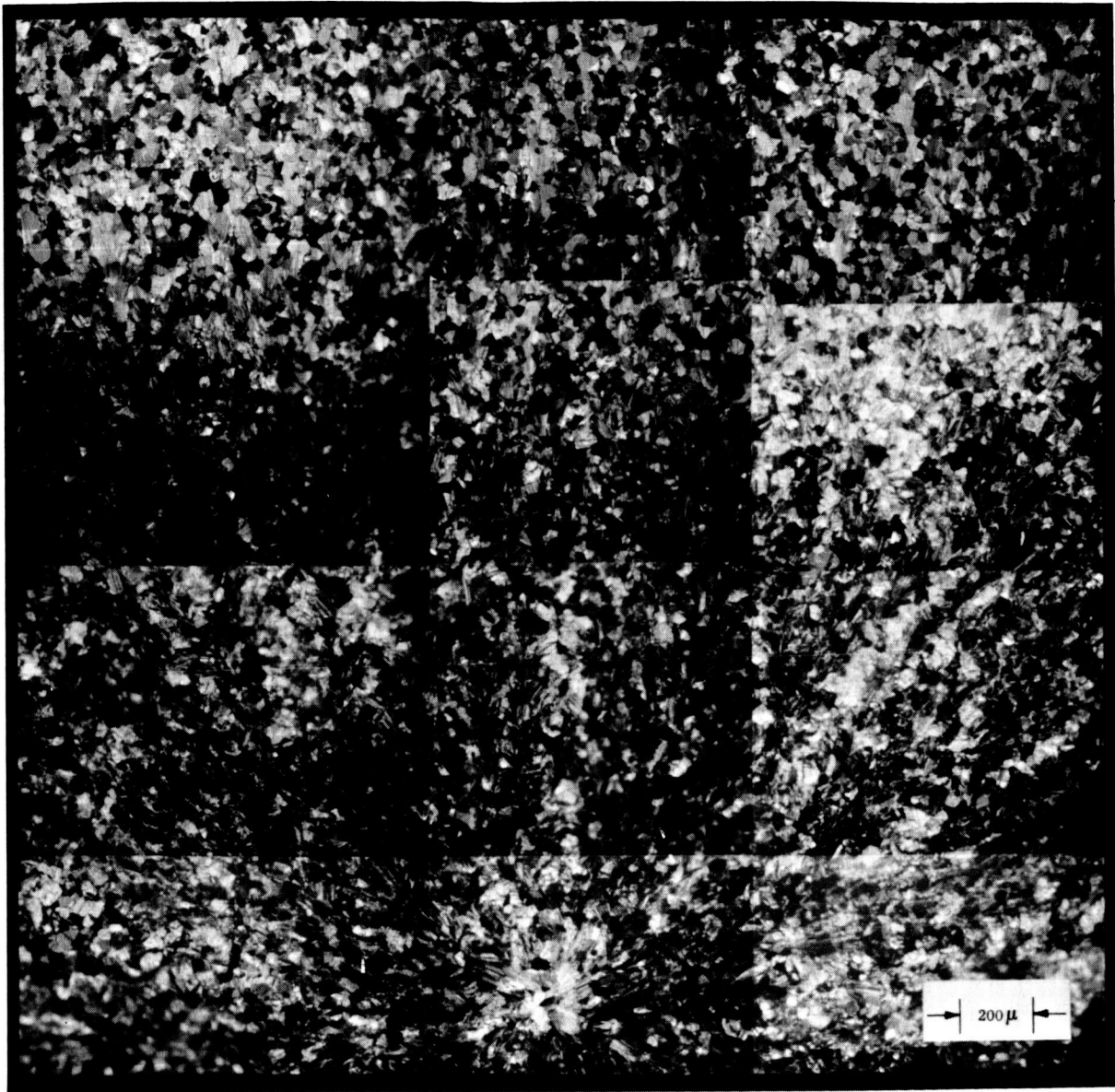


FIGURE 18 - ANALYSIS OF SURFACE PROTRUSIONS A) Protrusions on M2N-1-3 Surface After Approximately 4 hours at 1620°C, B) Si X-ray Fluorescence, C) Ca X-ray Fluorescence. NOTE: Random dots represent background noise.



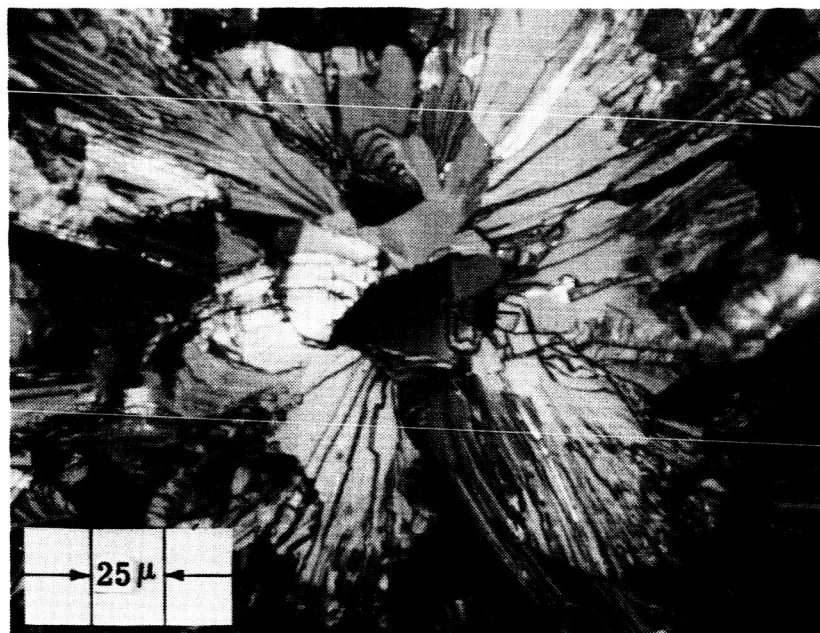
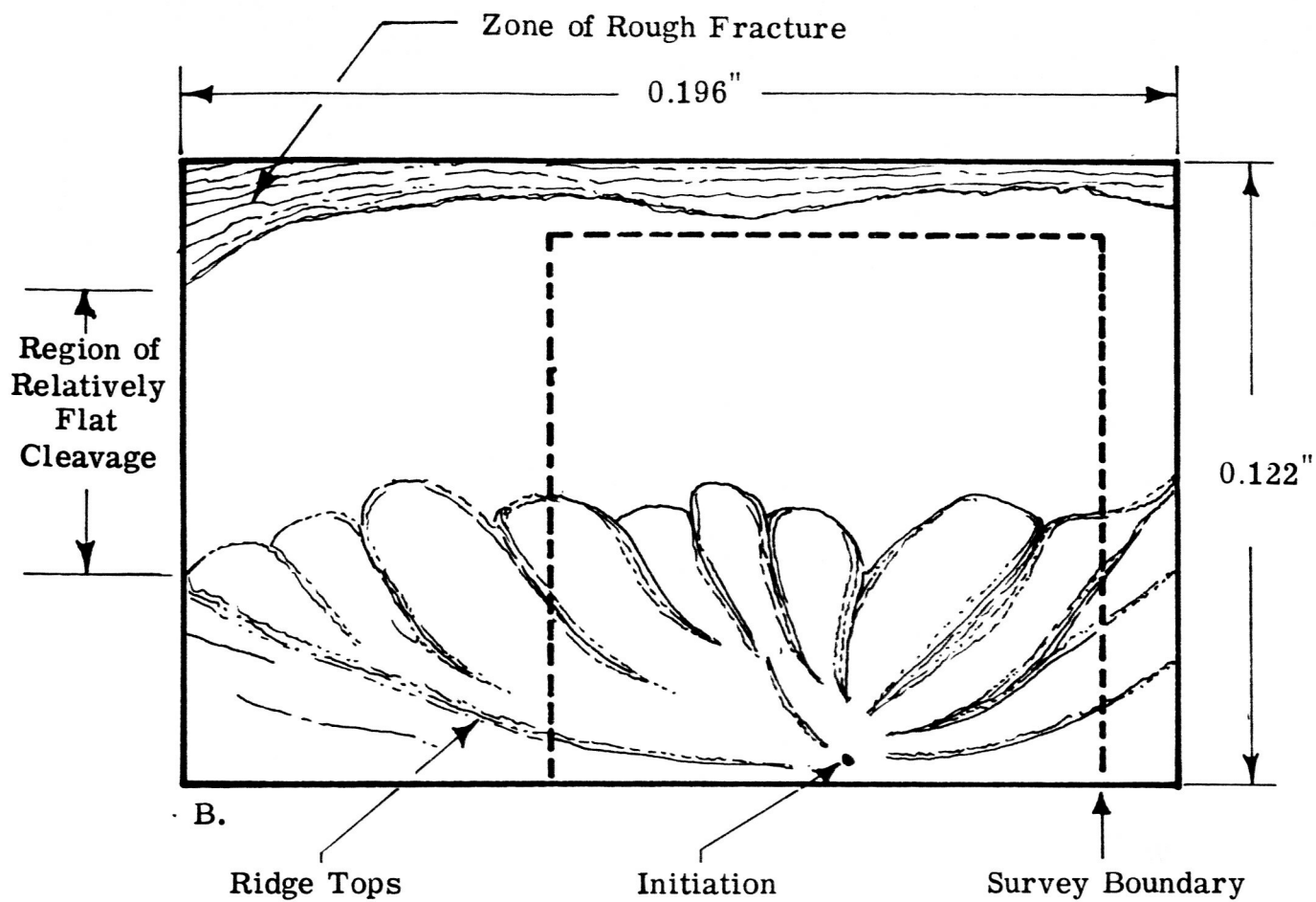
B.

FIGURE 19 MgO HARDNESS INDENTATIONS (10 Gm Load) ETCHED IN BOILING CHROMIC ACID. (A) $\{100\}$ Surfaces of a Bi-Crystal (B) $\{100\}$ Cleavage Surfaces of Extruded MgO (Polycrystalline).



A.

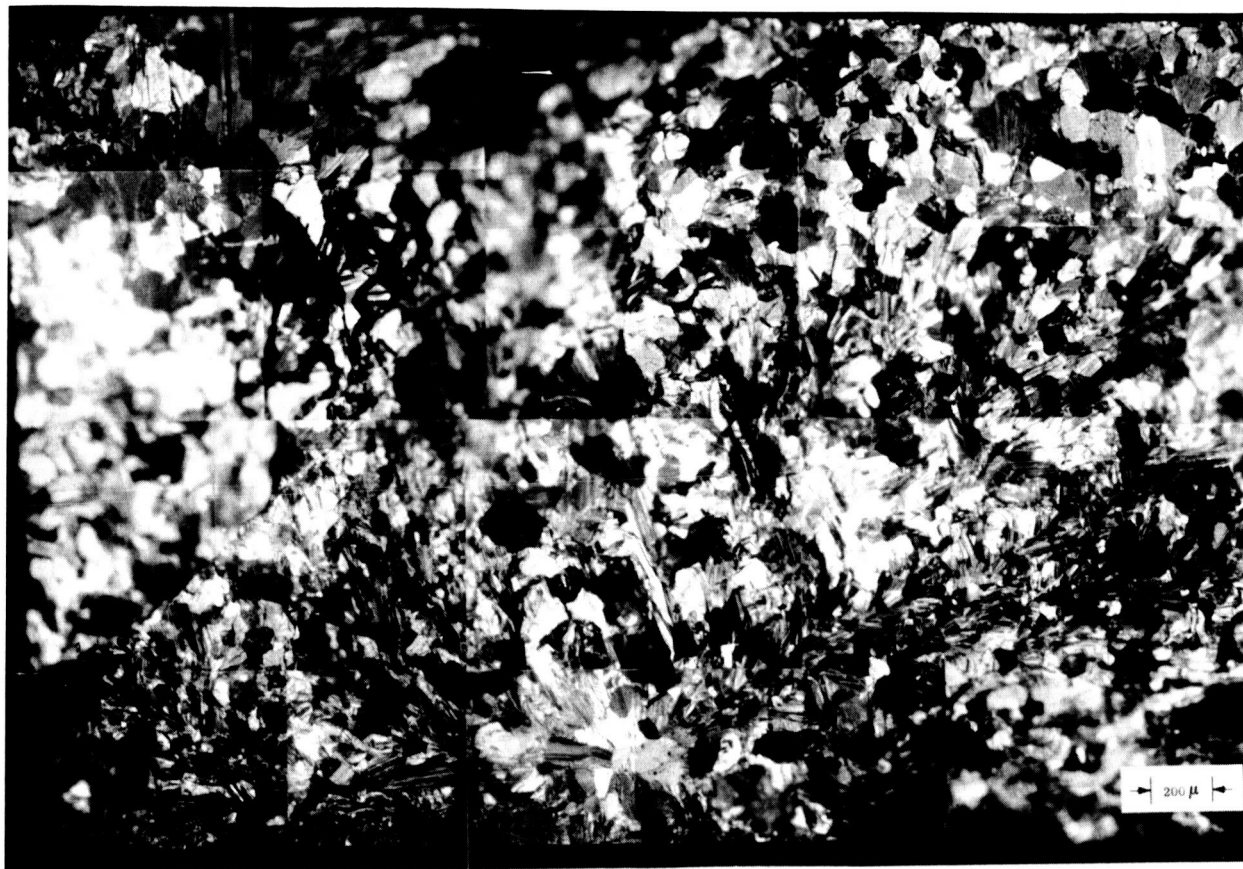
FIGURE 21 SAMPLE HOT PRESSED AND EXTRUDED MgO
FRACTURE (A) SURVEY OF FRACTURE ORIGIN
OF BEND TEST SPECIMEN FROM EXTRUDED
BILLET M-1-15



C.

Specimen M-1-15 1-3

FIGURE 21 (CONT.) SAMPLE HOT PRESSED AND EXTRUDED
MgO FRACTURE (B) SKETCH OF FRACTURE
SURFACE (C) PHOTO OF PROBABLE ORIGIN



A.

FIGURE 22 SAMPLE FUSED (CRYSTAL) AND EXTRUDED MgO
FRACTURE (A) SURVEY OF FRACTURE ORIGIN OF
BEND TEST SPECIMEN FROM EXTRUDED BILLET
M-f-4

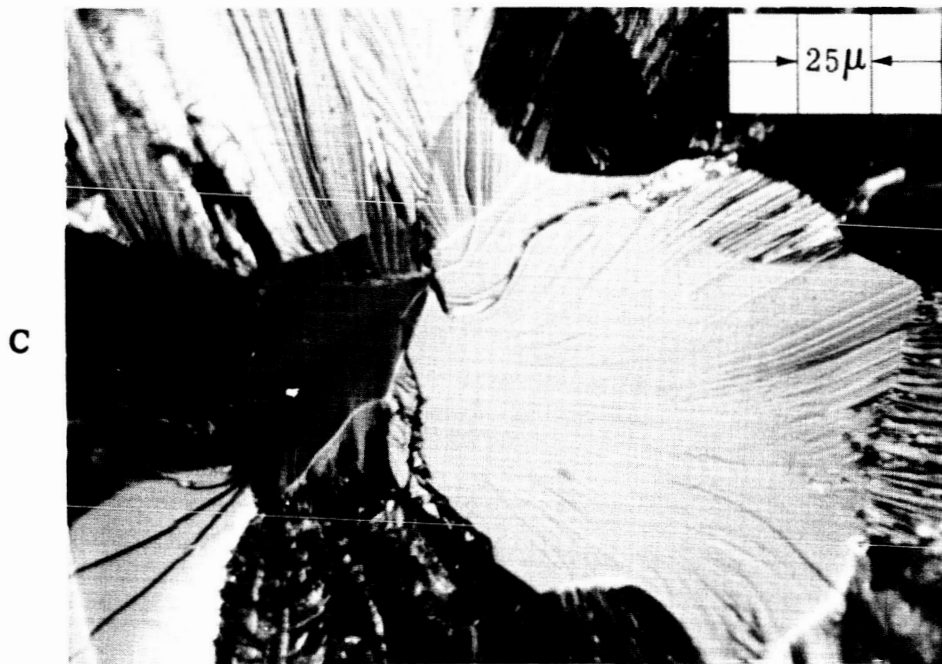
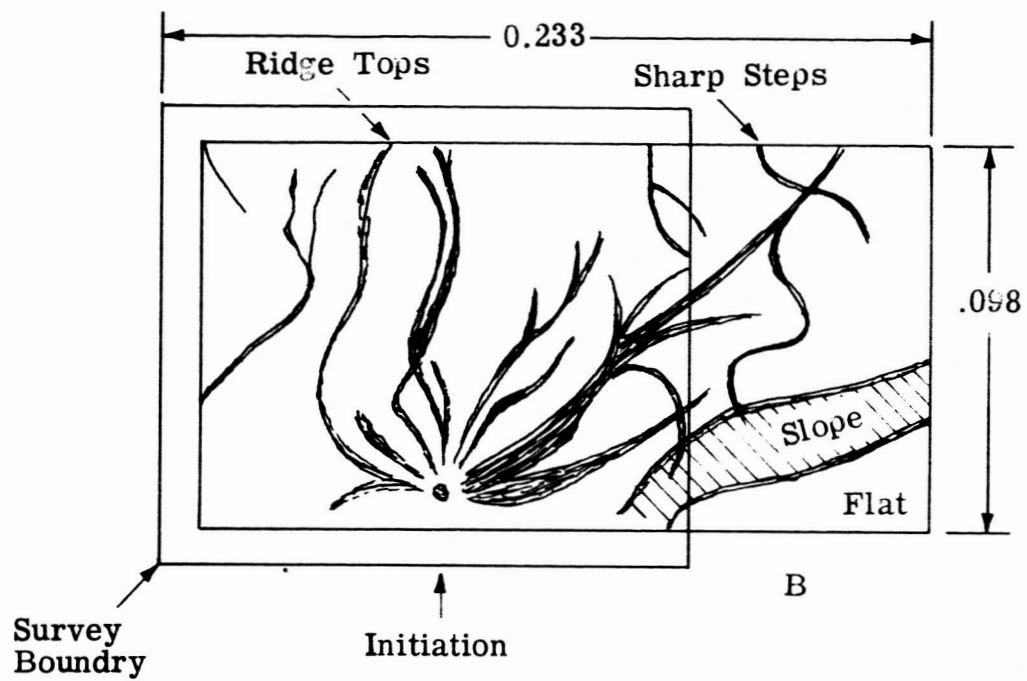


FIGURE 22 (CONT.) SAMPLE FUSED (CRYSTAL) AND EXTRUDED MgO FRACTURE (B) SKETCH OF FRACTURE SURFACE (C) PHOTO OF PROBABLE ORIGIN.

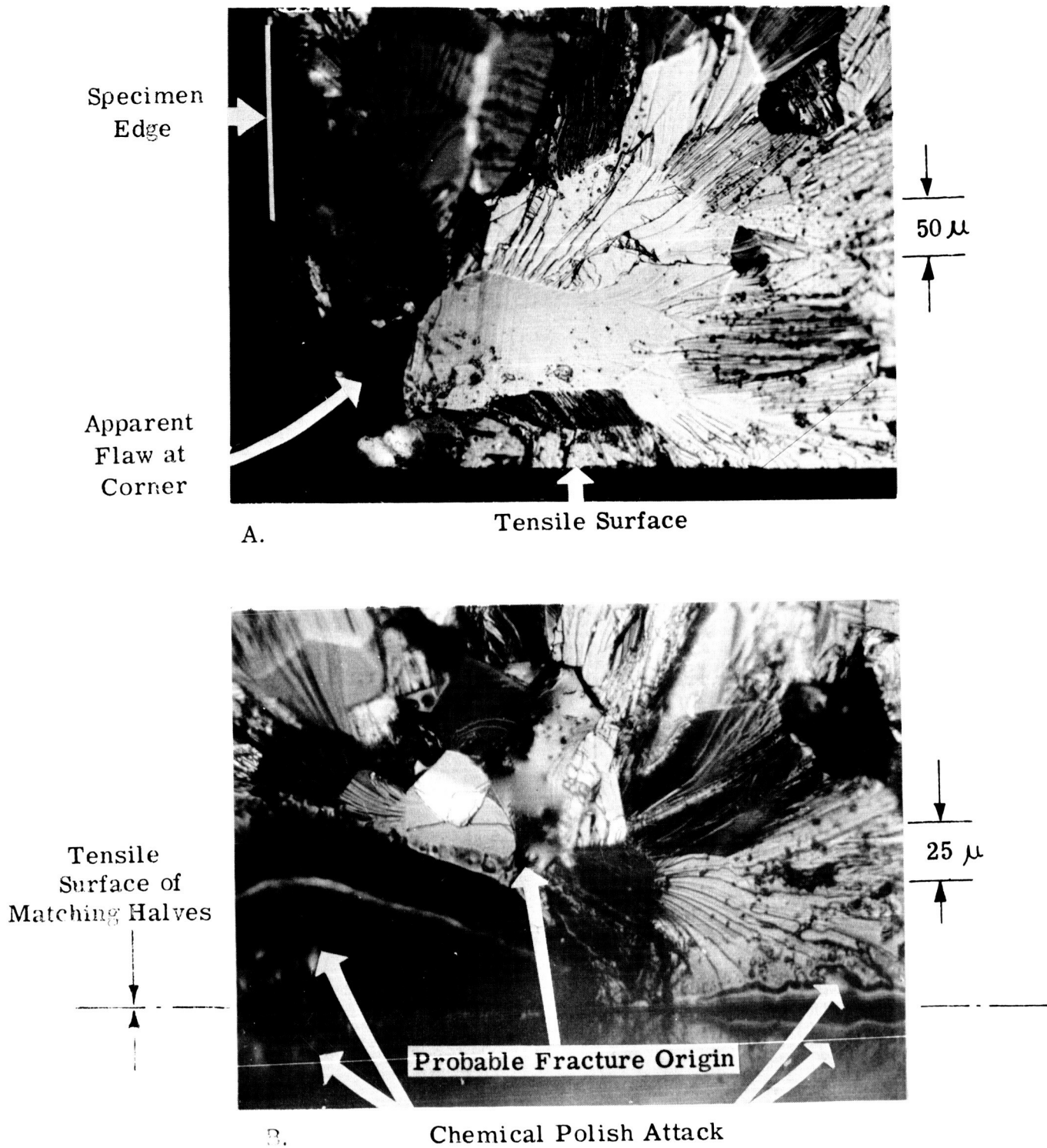


FIGURE 23

PROBABLE FLAW INDUCED FRACTURE IN EXTRUDED MgO. (A) Sample From Extruded Billet M-1-10, Tested As Sanded. Note Probable Flaw At Specimen Corner Where Fracture Originated. (B) Sample From Extruded Billet M2N-1-6 Tested After Chemical Polishing in Boiling H_3PO_4 Note Two Regions of Apparent Attack By H_3PO_4

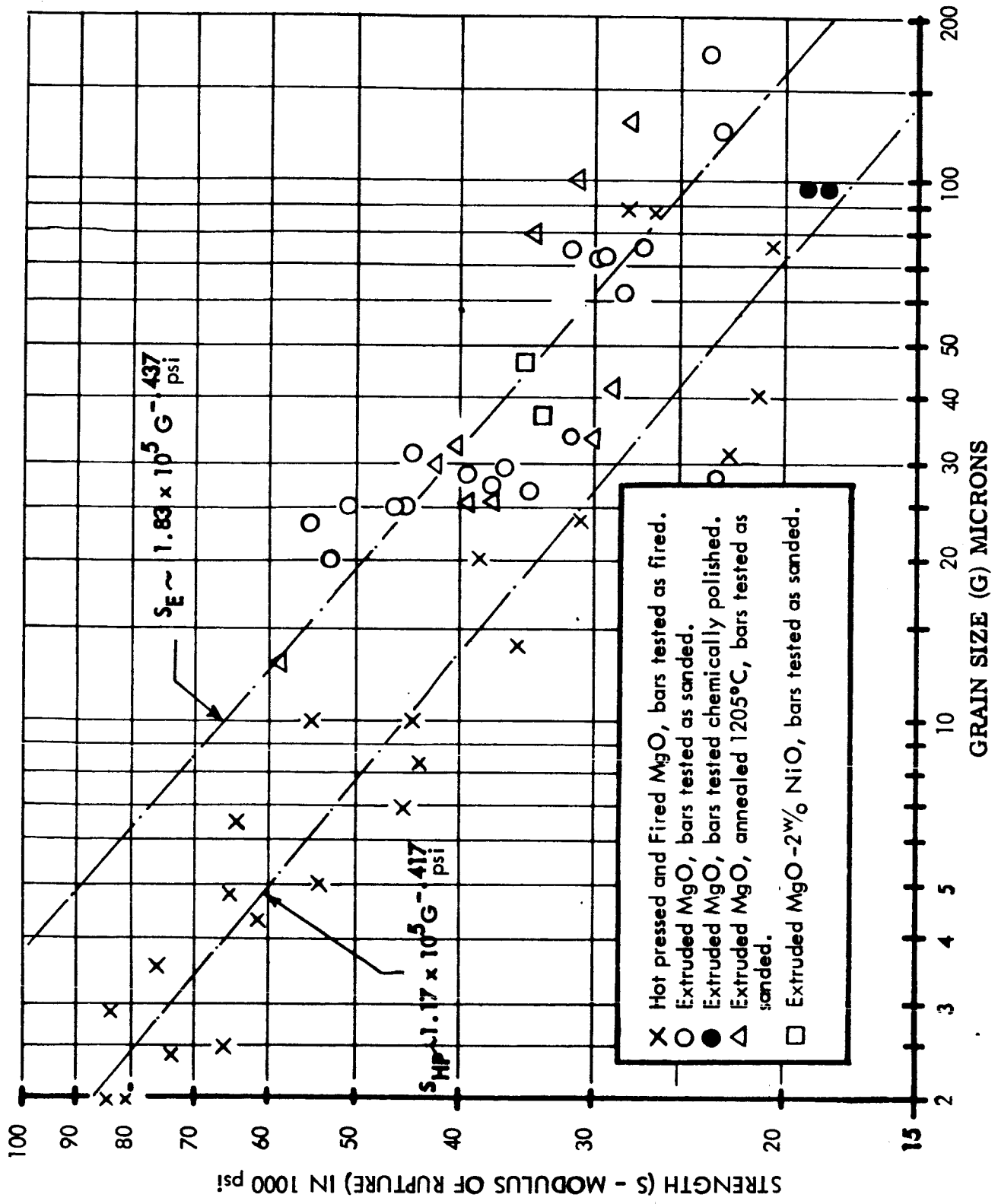


FIGURE 24 SELECTED EXTRUDED MgO STRENGTH - GRAIN SIZE DATA

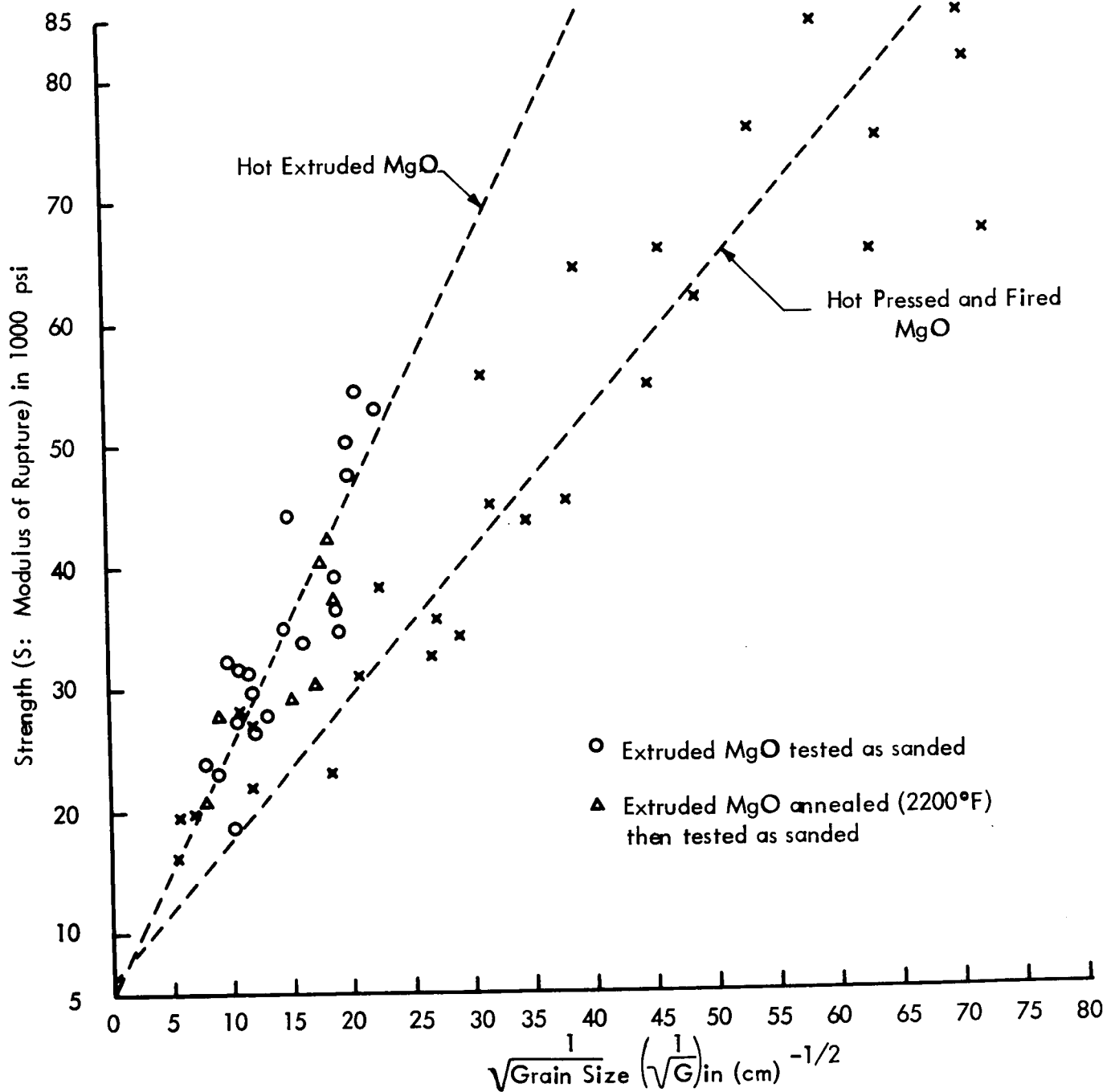


FIGURE 25 PETCH PLOT OF HOT PRESSED AND EXTRUDED MgO

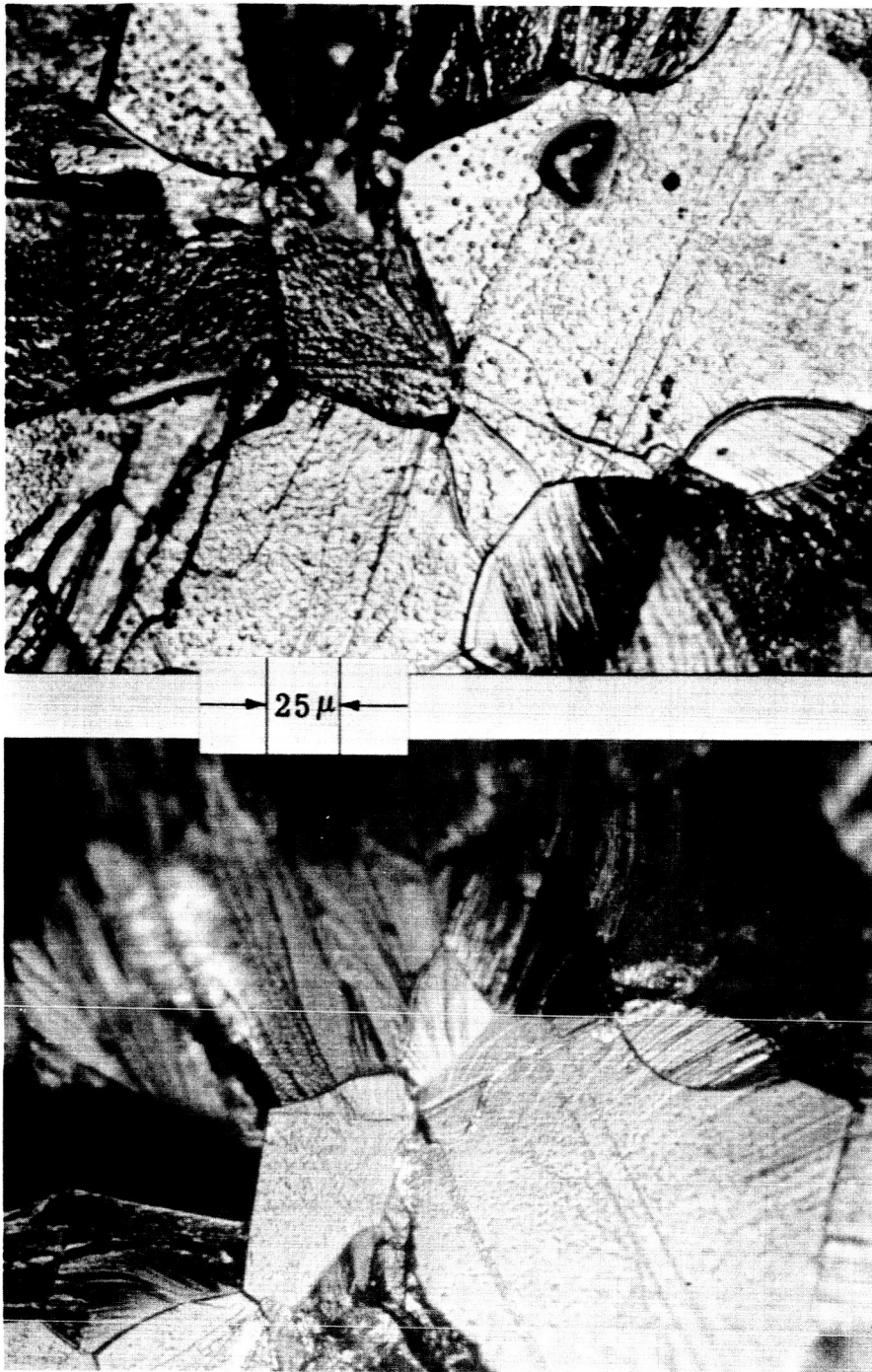
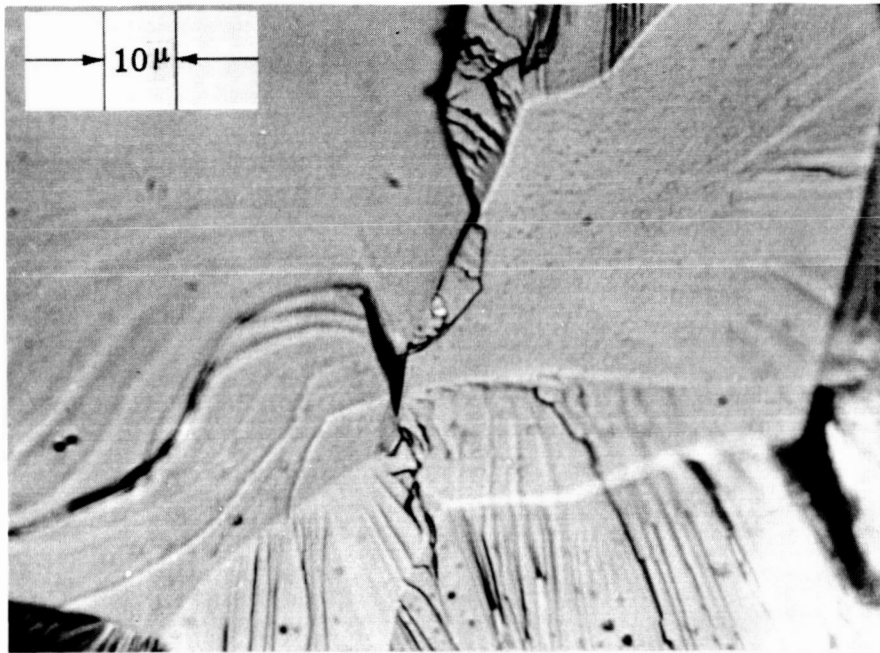
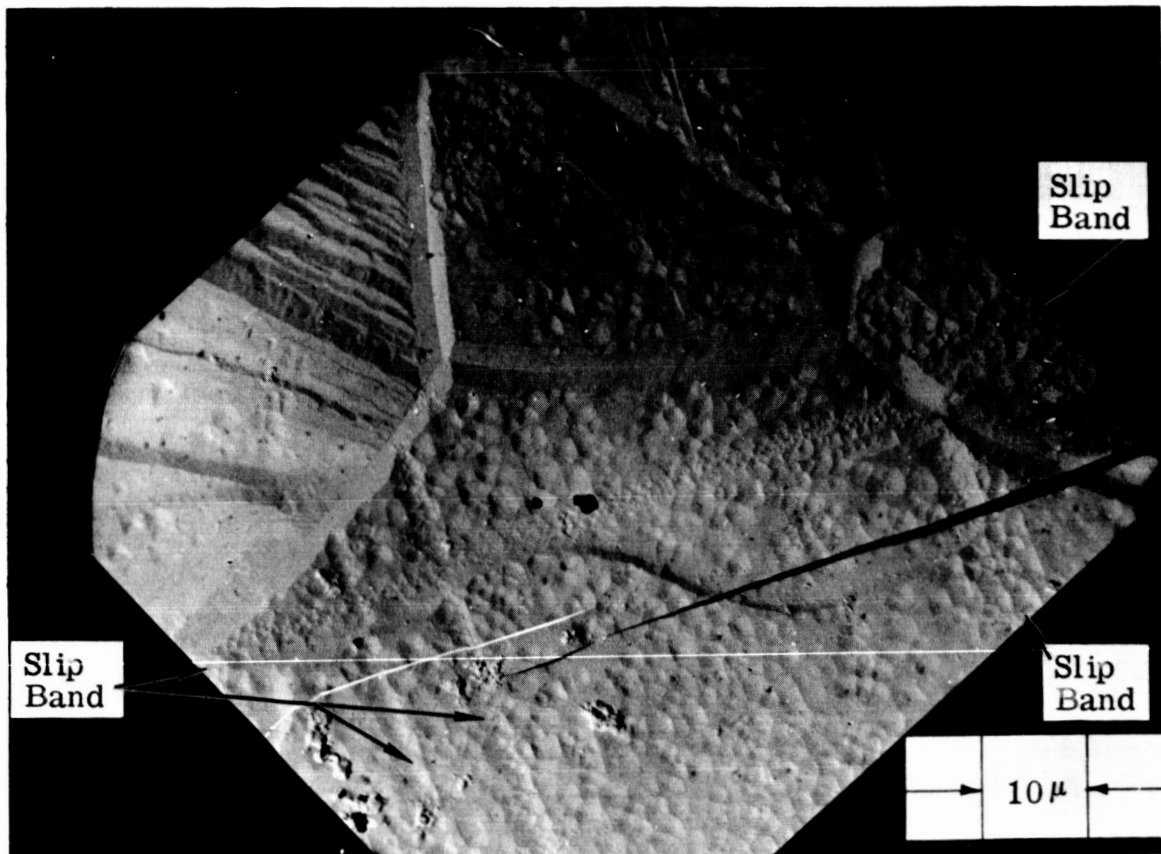


FIGURE 26 FRACTURE OF SPECIMEN FROM EXTRUDED BILLET M-f-4 (A) AND (B) MATCHING, ETCHED FRACTURE FACES.

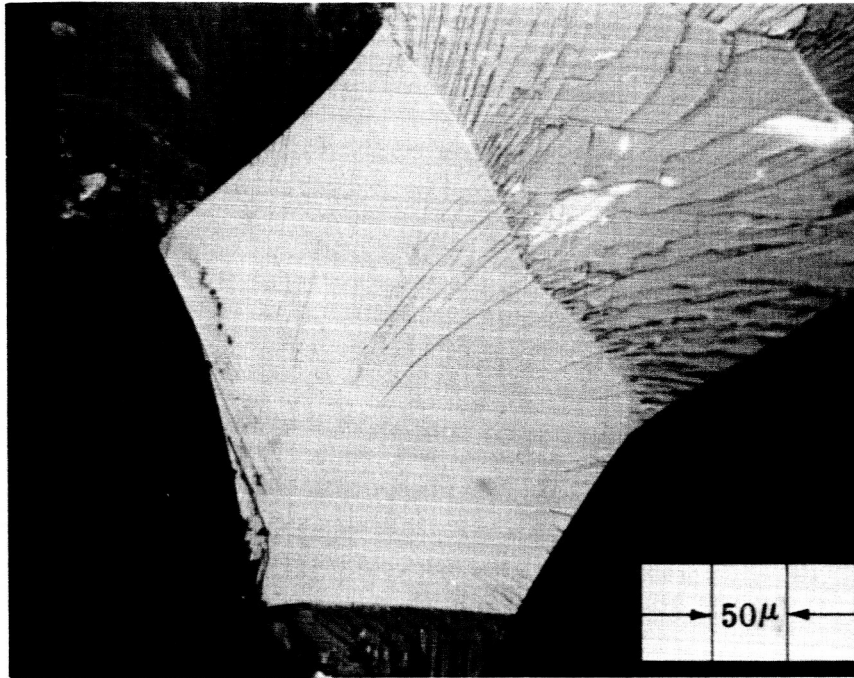


C

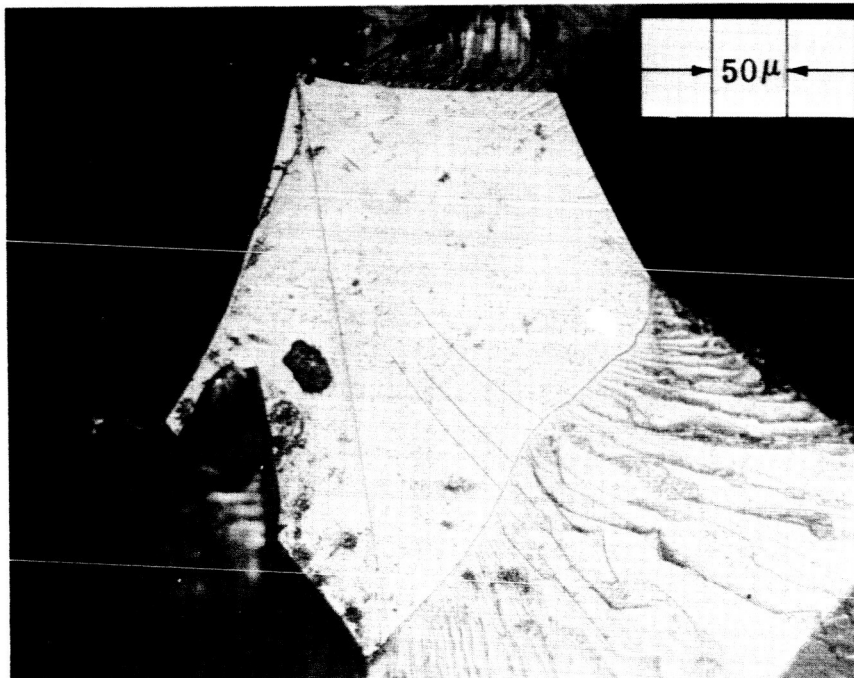


D

FIGURE 26 (CONT.) FRACTURE OF SPECIMEN FROM EXTRUDED BILLET M-f-4 (C) OPTICAL PHOTO OF AS FRACTURED SURFACE (D) ELECTRON MICROGRAPH OF MATCHING ETCHED FRACTURE SURFACE.



A



B

FIGURE 27 MATCHING FRACTURE HALVES OF SPECIMEN FROM EXTRUDED BILLET M-f-1 (A) UNETCHED (B) ETCHED

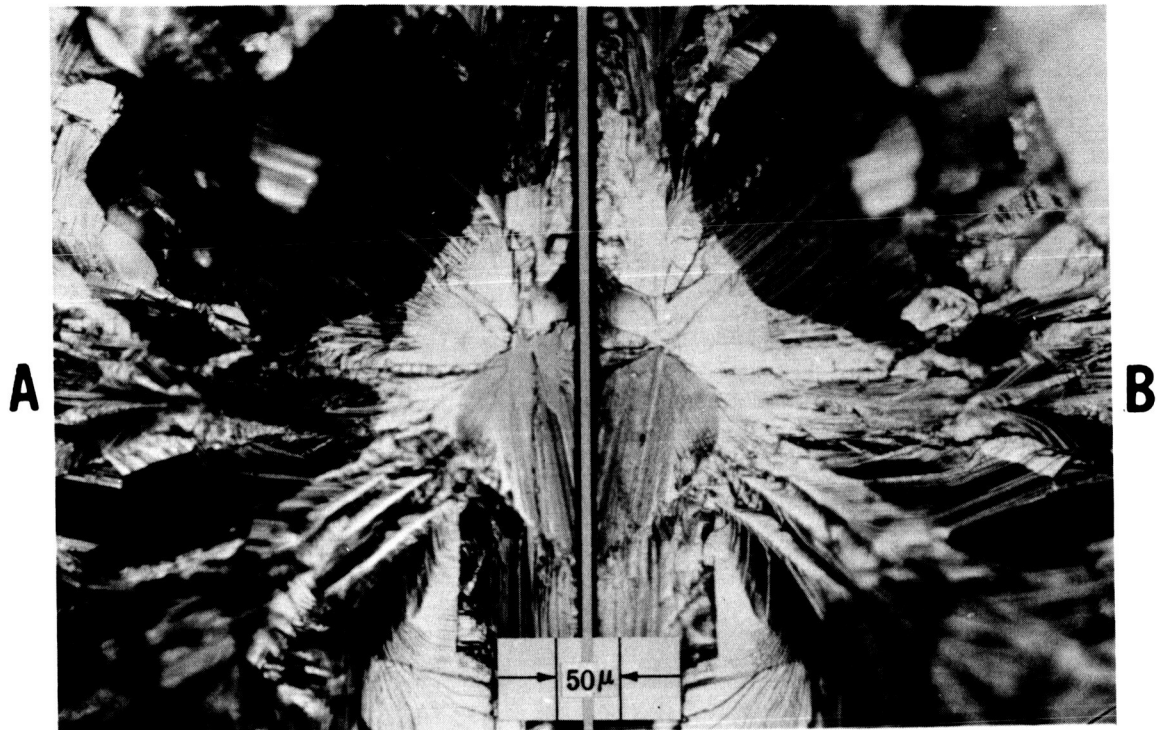


FIGURE 28 MATCHING FRACTURE HALVES OF SPECIMEN FROM EXTRUDED BILLET M-f-2 (A) AND (C) OPTICAL PHOTOS OF UNETCHED FRACTURE; (B) AND (D) OPTICAL PHOTOS OF ETCHED MATCHING FRACTURE HALVES

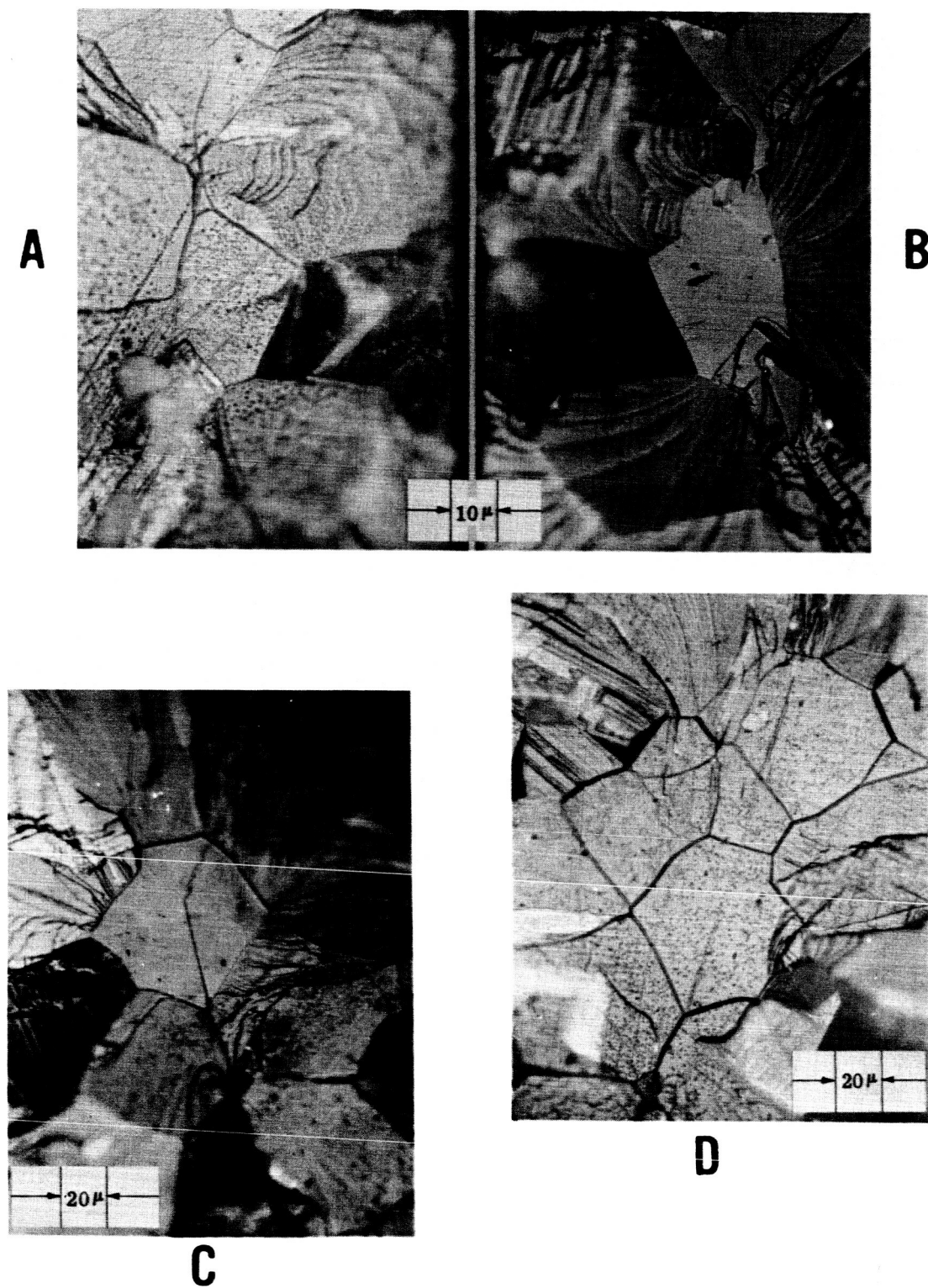


FIGURE 29 MATCHING FRACTURE HALVES OF SPECIMENS FROM EXTRUDED BILLETS M-f-2 AND M-1-11 (A) M-f-2 ETCHED (B) M-f-2 UNETCHED (C) M-1-11 UNETCHED (D) M-1-11 ETCHED

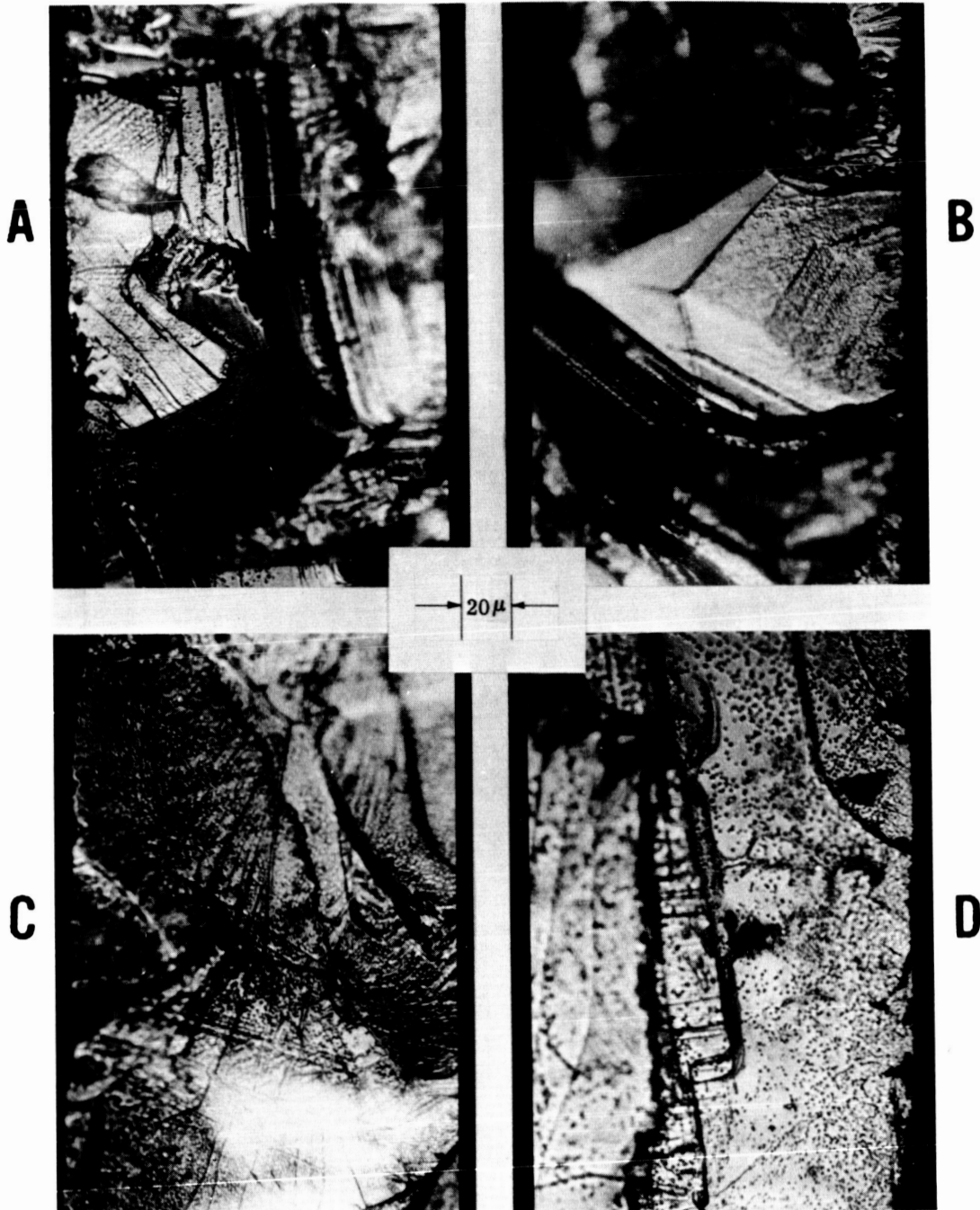


FIGURE 30 SAMPLE DISLOCATION DENSITY IN SURFACE GRAINS OF MgO TEST SPECIMEN. ALL PHOTOS ON FRACTURE SURFACE AWAY FROM FRACTURE ORIGIN. LOCATION OF PHOTOS AND BILLET SOURCE OF SPECIMENS ARE: (A) BOTTOM (TENSILE) SURFACE, M-f-4 (B) BOTTOM (TENSILE) SURFACE, M-f-2 (C) SIDE SURFACE, M-f-2 (D) SIDE SURFACE, M-f-1

TABLE I - BILLET FABRICATION

Number	Billet		Diameter (Inches)	Pressing			Fired to: (1)	Density (2) (gm/cc)
	Composition	Pressure Applied At:		Held At:	For (min.):			
M2C-1-1	MgO-2 w/o CaO	2400°F(1315°C)	2400°F(1315°C)	15	2400°F(1315°C)	3.57		
M2C-1-2	↓	↓	↓	15	↓	3.59		
M2C-1-3	↓	↓	↓	(15) Die broke	2400°F(1315°C)	3.58		
M5C-1-6	MgO-5 w/o CaO	2160°F(1170°C)	2280°F(1250°C)	15	2400°F(1315°C)	3.50		
M5C-1-7	↓	2300°F(1260°C)	2400°F(1315°C)	15	2400°F(1315°C)	3.54		
MZ/2-1-1	MgO-1/2 w/o ZrO ₂	2390°F(1305°C)	2400°F(1315°C)	15	2400°F(1315°C)	3.55		
MZ/2-1-2	↓	↓	↓	15	↓	3.59		
MZ/2-1-3	↓	↓	↓	15	2400°F(1315°C)	3.60		
M2Z-1-7	MgO-2 w/o ZrO ₂	2400°F(1315°C)	2450°F(1340°C)	15	2400°F(1315°C)	3.61		
M5Z-1-1	MgO-5 w/o ZrO ₂	2340°F(1270°C)	2400°F(1315°C)	15	2400°F(1315°C)	3.62		
M6Z-1-1	MgO-6 w/o ZrO ₂	2290°F(1255°C)	2400°F(1315°C)	15	2400°F(1315°C)	3.62		
A-1-1	Al ₂ O ₃ (Linde A)	2200°F(1205°C)	2600°F(1425°C)	60	2400°F(1315°C)	3.97		
A-1-2	↓	2200°F(1205°C)	2600°F(1425°C)	60	2400°F(1315°C)	3.97		
A-1-3	↓	2300°F(1260°C)	2500°F(1370°C)	45	2400°F(1315°C)	3.97		
AM/2-1-1	Al ₂ O ₃ -1/2 w/o MgO	2200°F(1205°C)	2600°F(1425°C)	70	2200°F(1315°C)	3.98		
AM/2-1-2	↓	2200°F(1205°C)	2600°F(1425°C)	60	2400°F(1315°C)	3.97		
AM/2-1-3	↓	2300°F(1260°C)	2500°F(1370°C)	30	2400°F(1315°C)	3.97		

(1) On Firing Schedule A (Appendix)

(2) After Firing. Nominal error ±0.01 gm/cc

(3) Obvious, macroscopic blisters formed due to outgassing.

(4) Ram broke, specimen repressed (density after repressing).

(5) Machined from body bulged out of broken 1.5" I.D. die.

(6) Rectangular cross section billets. Hot pressed samples cut from round billets, then fired.

(7) Isostatically pressed, machined, loaded in die then hot pressed.

TABLE I - (CONT'D)

Number	Billet		Pressing		Fired to: (1)	Density (2) (gm/cc)
	Composition	Diameter (inches)	Pressure Applied At:	Held At:		
M-3-22	MgO (Fisher)	1.0	2300°F(1260°C)	2330°F(1290°C)	2200°F(1205°C)	3.60
M-3-23	MgO (Mallinckrodt + 2 w/o LiF)	1.15	Cold pressed, 20,000 psi, broken and repressed		2250°F(1230°C)	3.38
M-3-24	MgO (Fisher + 2 w/o LiF)	1.45	Isostatically pressed 30,000 psi		2200°F(1205°C)	3.27
M-3-25	MgO (Mallinckrodt + 2 w/o LiF)	1.07	Cold pressed 3000 psi		2200°F(1205°C)	3.38
M-3-26	MgO (Mallinckrodt)	1.32	Cold pressed 5000 psi, broken and repressed		2250°F(1230°C)	2.34
M-3-27	MgO (Fisher)	1.20 (6)	Cold pressed 5000 psi, broken and repressed		2250°F(1230°C)	2.35
M-3-28	MgO (Fisher)	1 x 1 (6)	2380°F(1305°C)	2400°F(1315°C)	2200°F(1205°C)	3.59
M-3-29		1.4x1.4 (6)	2390°F(1310°C)			3.57
M-3-30		1.4x1.4 (6)	2400°F(1315°C) (7)			3.58
M-3-31		1.5	2340°F(1270°C)	2350°F(1285°C)		3.59
M-f-10	MgO (Norton)	.72x.90 (6)	Fused MgO Single Crystal			3.60
M1A-1-12	MgO-1 w/o Al ₂ O ₃	1 x 1 (6)	2400°F(1315°C)	2400°F(1315°C)	2200°F(1205°C)	3.58
M1A-1-13		1.5				3.59
M1A-1-14		1.5				-
M5A-1-4	MgO-5 w/o Al ₂ O ₃	1.5	2340°F(1270°C)	2400°F(1315°C)	2400°F(1315°C)	3.52
M5A-1-5		1.5	2340°F(1270°C)	2400°F(1315°C)	2400°F(1315°C)	3.49
M5A-1-6		1.0	2385°F(1305°C)	2400°F(1315°C)	2400°F(1315°C)	3.57
M5N-1-5	MgO-5 w/o NiO	1.5	2000°F(1095°C)	2000°F(1095°C)	2400°F(1315°C)	3.54
M5N-1-6		1.5	2000°F(1095°C)	2000°F(1095°C)	2400°F(1315°C)	3.54
M5N-1-7		1.5	2000°F(1095°C)	2000°F(1095°C)	2400°F(1315°C)	3.56
M5N-1-8		1.5 (6)	2015°F(1100°C)	2050°F(1120°C)		3.51
M5N-1-9		1 x 1 (6)	2000°F(1095°C)	2050°F(1120°C)	2200°F(1205°C)	3.54
M5N-1-10		1.5	2100°F(1145°C)	2100°F(1145°C)	-	3.22
M5N-1-11		1.5	2100°F(1145°C)	2185°F(1190°C)	-	3.67
M1C-1-1	MgO-1 w/o CaO	1.5	2400°F(1315°C)	2400°F(1315°C)	2400°F(1315°C)	3.58
M1C-1-2		1.5				3.59
M1C-1-3		1.0			2400°F(1315°C)	3.58

TABLE I - (CONT'D)

Number	Billet		Diameter (inches)	Pressing		For (min.):	Fired to: ⁽¹⁾	Density ⁽²⁾ (gm/cc)
	Composition	Pressure Applied At:		Held at:				
M-2-8	MgO (Fisher)	2150°F(1160°C)	2280°F(1250°C)	15	2400°F(1315°C)	3.45		
M-2-9		2040°F(1115°C)	2040°F(1115°C)	60		3.45		
M-2-10		2340°F(1270°C)	2400°F(1315°C)	15		3.56		
M-2-11			2380°F(1305°C)	20		3.53		
M-2-12			2400°F(1315°C)	Inadequate ram travel.		3.41		
M-2-13				15		3.56		
M-2-14				15		3.53		
M-2-15			2440°F(1335°C)	15		3.55		
M-2-16			2400°F(1315°C)	15		3.47		
M-2-17				Ram Broke		3.30		
M-2-18				15		3.58		
M-2-19						3.58		
M-2-20						3.59		
M-2-21						3.58		
M-3-1						(blis.) ⁽³⁾ 3.54		
M-3-2						3.56		
M-3-3						(blis.) ⁽³⁾ 3.50		
M-3-4			2340°F(1280°C)	15		2400°F(1315°C)	3.55	
M-3-5			2340°F(1280°C)	15		2200°F(1205°C)	3.57	
M-3-6			2340°F(1280°C)	15		2400°F(1315°C)	3.58	
M-3-7			2375°F(1300°C)	15		2200°F(1205°C)	3.50	
M-3-8		2265°F(1240°C)	Inadequate ram travel.	2200°F(1205°C)	3.50			
M-3-9		2340°F(1280°C)	20	2400°F(1315°C)	3.55			
M-3-10		2375°F(1300°C)	15	2400°F(1315°C)	3.57			
M-3-11		2375°F(1300°C)	15	2400°F(1315°C)	3.59			
M-3-12		2485°F(1360°C)	15	2400°F(1315°C)	3.58			
M-3-13		2475°F(1355°C)	20	2200°F(1205°C)	3.56			
M-3-14		2475°F(1355°C)	15	2400°F(1315°C)	3.59			
M-3-15		2275°F(1245°C)	20	2400°F(1315°C)	3.60			
M-3-16		2275°F(1245°C)	10 ⁽⁴⁾	2400°F(1315°C)	3.59			
M-3-17		2300°F(1260°C)	15 ⁽⁴⁾	2400°F(1315°C)	3.52			
M-3-18		2300°F(1260°C)	15	2400°F(1315°C)	3.49			
M-3-19		2300°F(1260°C)	15	2200°F(1205°C)	3.56			
M-3-20		2250°F(1230°C)	15	2400°F(1315°C)	3.58			
M-3-21		2300°F(1260°C)	Die Broke	2200°F(1205°C)	3.31			

TABLE II - RAW MATERIALS

Material	Type	Source
MgO	Fisher Electronic Grade	Fisher Scientific Co., Chicago, Illinois
MgO	Mallinckrodt A.R.	Mallinckrodt Chemical Works, St. Louis, Missouri
Al ₂ O ₃	Alon C- γ Al ₂ O ₃	Cabot Corporation, Boston, Mass.
Al ₂ O ₃	Linde A - α Al ₂ O ₃	Linde Division of Union Carbide, East Chicago, Indiana
NiO	Baker Reagent	J. T. Baker Chemical Co., Phillipsburgh, New Jersey
CaO	Calcined per Calcining Procedure A (Appendix) from Mallinckrodt Reagent Ca(OH) ₂	Mallinckrodt Chemical Works, St. Louis, Missouri
ZrO ₂	Colloidal (unstabilized)	Zirconium Corporation of America, Solon, Ohio
ZrO ₂	Fused CaO Stabilized	The Norton Company, Worcester, Mass.
LiF	Baker Reagent	J. T. Baker Chemical Co., Phillipsburgh, New Jersey

TABLE III - EXTRUSION PARAMETERS

Extrusion Number	Can O.D. (in)	Ceramic Billet Diameter (in)	Temperature ⁽¹⁾	Area Reduction Ratio	Speed in/sec	Force (tons)	
						Upset ⁽²⁾	Running
MgO-10	3.0	1.0-2.0	2200°C		Shelled		
MgO-11	3.0	1.0-2.0	2300°C	9 to 1	16	700	600-525
MgO-12	3.0	1.5	2200°C	6 to 1 ⁽³⁾	18	640	570-490
MgO-13	3.0	1.5	2200°C	9 to 1	13	650	600-520
MgO-14	3.0	1.0-1.5	2200°C	9 to 1	16	740	550
Al ₂ O ₃ -1	3.5	1.0-1.5	1950°C	9 to 1	15	825	550

(1) Temperature of composite can-ceramic billet on dropping from furnace.

(2) Force to extrude tungsten nose.

(3) A reduction of 9 to 1 was intended, but die enlarged.

TABLE IV - EXTRUDED BILLET DATA

Number (1)	Composition	Fabri- cation (2)	Density gm/cc		Area Reduction Ratio	Average Grain Size (microns)		Orientation	
			Before Extrusion (3)	After Extrusion (4)		Transverse	Longitudinal	High	Low
Extrusion: Number MgO-10, Temperature: 2200°C, Unextruded (Multidiameter Can)									
M-2-20	MgO	B	3.59	3.56(5)		76(5)	4.2	1.0	2.7
M-3-1	MgO	B	3.54	3.57(5)		65(5)	3.9	.9	2.2
M-3-2	MgO	B	3.56	3.56(5)		50(5)	4.5	.7	2.6
M-2-7	MgO	B	3.59	3.56(5)		90(5)	6.3	2.8	4.2
M-2-21	MgO	B	3.58	3.56(5)		64(5)	3.2	1.9	2.5
m-1-1	MgO	Powder	~1.5	3.54(5)		38(5)			
Extrusion: Number MgO-11, Temperature: 2300°C, Area Reduction Ratio: 9 to 1 (Multidiameter Can)									
M-3-3	MgO	B	3.50	3.58	9 to 1		79	68	76
M-3-7	MgO	B	3.50	3.57	4.5-9 to 1	25	63	49	57
M-2-11	MgO	B	3.53	3.57	6.3-7.1 to 1	30	44	35	40
M-3-8	MgO	B	3.50	3.55	9 to 1	30	90	71	79
M-3-5	MgO	B	3.57	3.60	9 to 1	25	25	11	17
m-1-2	MgO	Powder	~1.5		9 to 1	16			
Extrusion: Number MgO-12, Temperature 2200°C, Area Reduction Ratio: 6.2 to 1 (9 to 1 Intended, but die enlarged)									
M-f-2	MgO	Fusion	3.58	3.59	5.3-9 to 1	75	29	8	16
M-1-16	MgO	A	3.45	3.57	5.9-7.7 to 1	43	31	11	21
M-2-8	MgO	B	3.45	3.54	5.5-7.5 to 1	38	56	5	18
M2N-1-7	MgO-2 w/o NiO	A	3.36	3.57	6.3-7.7 to 1	38	48	7	19
M1A-1-4	MgO-1 w/o Al ₂ O ₃	A	3.57	3.55	4.6-6.3 to 1	47	31	7	16
M-1-21	MgO	B	less than 3.5	less than 3.5	6.3 to 1				
M-2-6	MgO	B	3.56	"	6.3 to 1				
Z-1-3	ZrO ₂	Sintered	5.40		4.6-8.4 to 1	32	39		

TABLE IV - (CONT'D)

Number (1)	Composition	Fabrication (2)	Density gm/cc		Area Reduction Ratio	Average Grain Size (microns)		Orientation	
			Before Extrusion (3)	After Extrusion (4)		Transverse	Longitudinal	High	Low
Extrusion: Number MgO-13, Temperature: 2200°C, Area Reduction Ratio: 9 to 1 (extruded into heated catch tube, but went through on to floor. Reloaded in catch tube (2000°C) at extrusion temperature of ~1300°C).									
M-f-9	MgO	Fusion		3.59	9-9.5 to 1	210	210		
M-2-9	MgO	B	3.45	3.58	7.5-9 to 1	33	48		
M-3-19	MgO	B	3.56	3.58	9-9.5 to 1	40	49		
M2N-1-5	MgO-2w/o NiO	A	3.36	3.60	9-10 to 1	43	56		
M-3-10	MgO	B	3.57	3.59	9-9.5 to 1	36	62		
M5N-1-5	MgO-5w/o NiO	B	3.54	3.66	9-9.5 to 1	29	37		
M1A-1-6	MgO-1w/o Al ₂ O ₃	A	3.56	3.58	8.5-9 to 1	46	47		
M5A-1-5	MgO-5w/o Al ₂ O ₃	B	3.49	3.53	7-9 to 1	25	31		
Extrusion: Number MgO-14, Temperature: 2200°C, Area Reduction Ratio: 9 to 1, (extruded into heated catch tube (2000°C) and cooled slowly).									
M-3-18	MgO	B	3.49	3.55	8-9 to 1	30			
M2N-1-10	MgO-2w/o NiO	A	3.40	3.58	9 to 1				
M5N-1-7	MgO-5w/o NiO	B	3.56	3.68	9 to 1				
M-3-9	MgO	B	3.55	3.60	8.5-9 to 1				
M-3-14	MgO	B	3.59	3.54-3.58	9 to 1	35			
M-3-23	MgO	Pressed & Fired	2.34	3.46	11-13 to 1				
m-1-3	MgO	Powder	1.5	3.44	10-12 to 1				
Extrusion: Number MgO-15, Temperature: 2400°C, Aborted due to reaction and melting of outer TZM shell.									
M2Z-1-2	MgO-2w/o ZrO ₂	Fusion							
M2Z-1-5	"	Hot pressed fused powder							
M2Z-1-6	"	B							
M4C-1-3	MgO-4w/o CaO	B							
M4C-1-5	"	B							
M5C-1-3	MgO-5w/o CaO	Fusion							

TABLE IV - (CONT'D)

Number (1)	Composition	Fabrication (2)	Density gm/cc		Area Reduction Ratio	Average Grain Size (microns)		Orientation	
			Before Extrusion (3)	After Extrusion (4)		Transverse	Longitudinal	High	Low

Extrusion: Number MgO-16, Temperature: 2200°C, Aborted due to reaction and melting of outer TZM shell.

M-3-25	MgO	Pressed & Fired	3.38						
M-3-17	MgO	B	3.52						
M-3-13	MgO	B	3.56						
M-3-21	MgO	B	3.31						
M-3-24	MgO	Pressed & Fired	3.27						
Z-1-5	ZrO ₂	See Text	5.30						

Extrusion: Al₂O₃-1, Temperature: 1950°C, Area Reduction Ratio: 9 to 1, extruded into heated catch tube (at 1875°C) soaked 20 min. at 1750°C then cooled at approximately 15°C/minute.

A-1-2	Al ₂ O ₃	See Text	3.88						
A-1-1		B	3.98						
AM/2-1-1	Al ₂ O ₃ -1/2 w/o MgO	B	3.98						
A45M _e -1-1	Al ₂ O ₃ -45w/o MgO	See Text	3.51						
" -2		"	3.48						
S _{ma} -1-4	MgAl ₂ O ₄	Fusion	3.05						

- (1) Billets listed from front to rear.
- (2) A and B refer respectively to Hot Pressing Procedures A and B.
- (3) Nominal density error ±0.01 gm/cc.
- (4) Nominal density error ±0.02 gm/cc (cracking can reduce apparent density).
- (5) Data after billet heated for extrusion.

TABLE V - EXTRUSION ANNEALING

Spec. No.	Orientation: As-Extruded (1)			Orientation: After Annealing at 2400°F (1315°C) for 1 Hour (1)		
	High	Low	Average	High	Low	Average
M2N-1-1	44	35	40	39	7	19
M1A-1-1	40	30	35	59	44	52
M-f-4	64	33	45	54	34	42
M2N-1-3	63	55	59	108	85	95
M-1-10	62	52	59	122.5	70	92.5
M10N-1-1	21	9	14	75	37.5	52.5
M1A-1-2	35	17	34	60	15	39
M-1-4	35	30	32	59	47	52
M4C-1-4	6.5	4.5	6.0	24.5	22	23.5
M-1-14	62	42	53	315	225	145
MG-1	7	3	5	42	4	25
mg-1	46	38	40	51	39	44

(1) Values are the ratio of the diffracted x-ray intensity from the $\{200\}$ plane of a transverse section of an extrusion to the diffracted intensity from a randomly oriented sample.

TABLE VI - COMPARISON OF EXTRUDED MgO STRENGTHS ON DIFFERENT SPANS

Specimen No.	Modulus of Rupture (in 1000 psi) on Spans of:				
	2.0"	1.5"	1.0"	0.75"	0.50"
M-3-5 ₂₋₁	33.88 (Broke ~.05" off center)		27.5 (Broke ~.05" off center)		39.6
M-3-3 ₂₋₁	18.7 (Broke ~.1" off center)			39.1	37.3
M-1-15 ₁₋₁	20.8		21.6		21.3
M-f-5 ₂₋₁		23.0			24.0 23.2
M-3-7 _{1c}				30.1	32.0
*M-f-5 ₁				18.5	18.9
*M-f-5 ₂				20.7	20.4

*Chemically polished, all other specimens tested as-sanded.

TABLE VII - FRACTURE STATISTICS

	<u>Specimens Fracturing Inside Body</u>	<u>Specimens Fracturing at Surface or Corner</u>	<u>Number of Chemically Polished Bodies</u>
As Extruded Bodies - Tested as-sanded or chemically polished.	28	16	14
As Extruded Bodies - Tested as--sanded.	26	4	0
Annealed (2200°F) Extruded Bodies - Tested as-sanded.	10	4	0
Annealed (2200-2800°F) Extruded Bodies - Tested as--annealed.	8	3	0

TABLE VIII - INTERNAL FRACTURE DATA

Billet No.	Modulus of Rupture (KSI)	Average Grain Size (microns)	Origin in From Surface	
			Grains ⁽¹⁾	Microns ⁽²⁾
M-3-7	54.5	23	2-6	75
	50.4	25	2-4	75
	39.2	28	4-7	90
	34.8	27	2	40
M-3-8	44.9	24	2-3	70
	47.9	25	3	70
M-3-3	18.7	26	2-3	40
	39.1	20	2-3	30
	37.3	26	2	30
M-3-5	28.3		4	210
	33.8	27	2	40
	39.6	26	2	30
M-1-11	27.7	61	4-5	400
	27.5	70	2-3	130
	29.8	73	2-3	100
M-1-10	29.0	42	1-2	40
M-1-15	42.2	30	5-8	170
M-2-11	36.6	29	2	60
	45.0	25	4-6	70
M-f-2	32.5		1	20
	35.1	79	1	40
	27.1	70	3	120
	31.1	87	2	110
	32.4	110	2	90
M-f-4	29.3	73	5	300
M-f-5	18.5	97	1	75
	18.9	97		
	21.3	151	2-5	
	20.7	130	2-3	400
	31.5	75	2-3	
	24.0	173	6	
	23.2	125	3-5	
M2N-1-3	35.3	24	2	30
M2N-1-6	33.8	37	1-2	60
	35.0	47	1-2	60
	44.4	31	3	80

(1) Number indicates the grain in which fracture origin is located - either within that grain or at its boundary away from the tensile surface.

(2) Approximate distance of origin from tensile surface.

APPENDIX 1

BILLET VACUUM HOT PRESSING PROCEDURE A (WITH LiF)

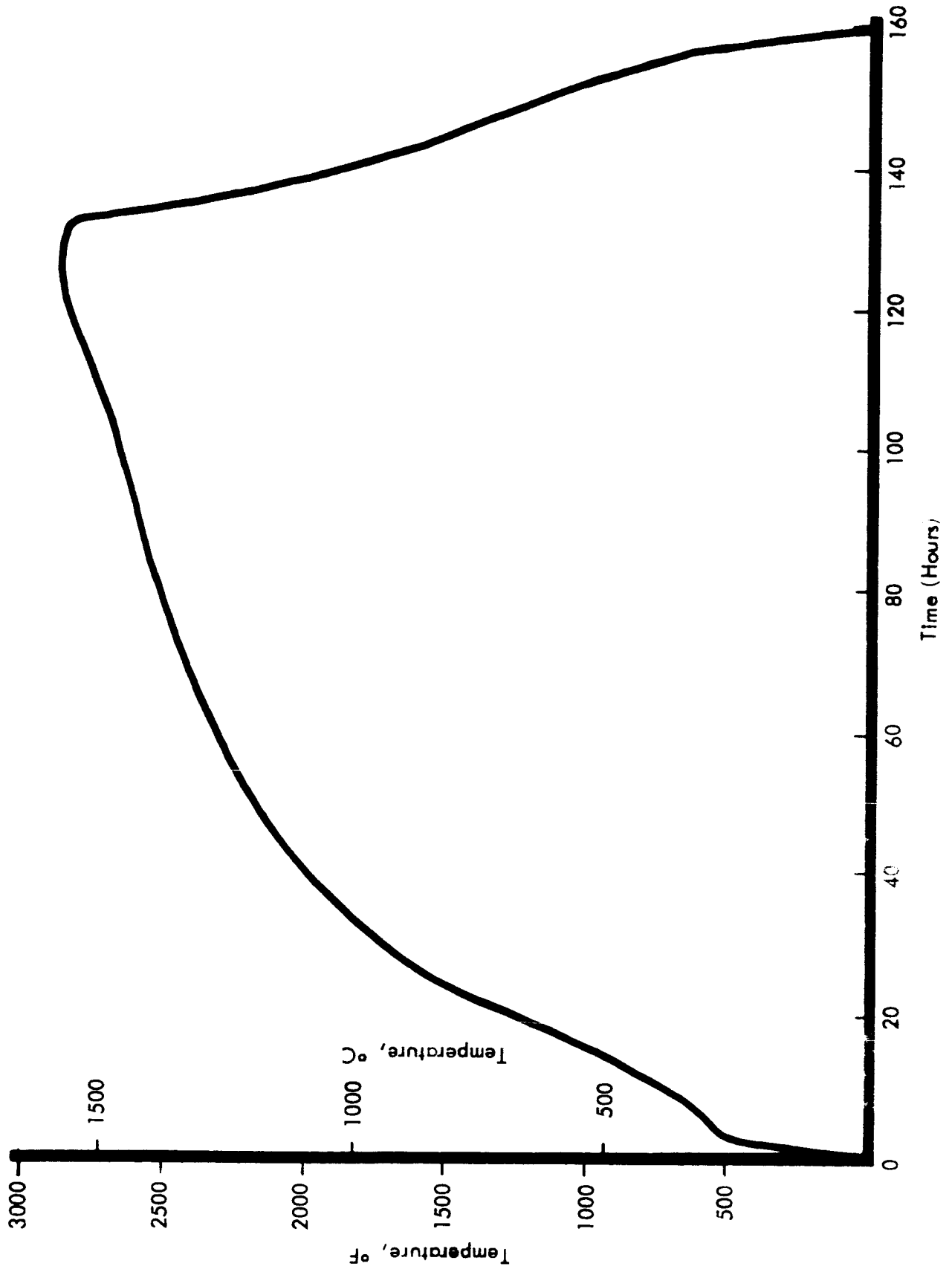
1. Two weight percent reagent grade LiF is added to the ceramic powder by milling for 2 hours in an organic fluid, normally benzene.
2. The milled slurry is dried, screened through a number 28 screen, and stored in sealed jars. The time of storage in sealed jars is normally less than one week prior to complete usage of the powder.
3. Powder is loaded in the die by cold pressing at 1000-2000 psi. Pyrolytic graphite spacers are placed between the rams and the powder when graphite dies are used.
4. The die is placed in the vacuum hot press which is pumped down to a chamber pressure of 10^{-4} - 10^{-5} torr in about 1 hour.
5. After at least 4 hours at 10^{-4} - 10^{-5} torr, the die is heated at an approximately linear rate to 650°C (1200°F) in about 0.5 hour. Temperatures are measured by a thermocouple in the die wall approximately 0.75" from the inside die surface and about 1" above the specimen.
6. Between 650°C and 700°C (1295°F) the ram pressure is built up to approximately 3500 psi.
7. Heating, while maintaining this ram pressure, is continued at a slightly slower rate until a temperature of 980°C (1800°F) is reached after a total heating time of 50 to 60 minutes.
8. Pressing conditions of 980°C and 3500 psi are held for 15 minutes with vacuum chamber pressure averaging 2 to 4×10^{-3} torr.
9. The heating power is shut off and the ram pressure released over a period of about 1 minute.
10. The die is removed from the vacuum hot press after 2 to 4 hours of cooling.
11. The specimen is ejected from the die at temperatures of 400°C (750°F) or less.

APPENDIX 2

BILLET VACUUM HOT PRESSING PROCEDURE B (WITHOUT LiF)

1. Powder is directly loaded into the die from sealed bottles, without any prior milling unless milling was previously used to mix alloy agents. Pyrolytic graphite spacers are used between the rams and the specimen when graphite dies are used.
2. The powder is cold pressed at 1000-2000 psi.
3. The die is placed in the vacuum hot press which is pumped down to a chamber pressure of 10^{-4} - 10^{-5} torr in about one hour.
4. After at least 2 hours at 10^{-4} - 10^{-5} torr the die is heated to 1650°F(900°C) in about 30 minutes. Temperatures are measured by a thermocouple located in the die wall about 0.75" from the inside die surface and about 1" above the specimen.
5. Starting at 1750°F(950°C) the ram pressure is built up to 5000 psi over a period of about 2 minutes.
6. A temperature of 2400°F(1315°C) is then reached in about 20 minutes, while maintaining the ram pressure at 5000 psi.
7. Pressing conditions of 2400°F and 5000 psi are held for 15 minutes with vacuum chamber pressure averaging about 10^{-2} torr.
8. The induction heating power is shut off and the ram pressure released over a period of about 1 minute.
9. The die is removed from the vacuum hot press after cooling for two to four hours.
10. The specimen is ejected from the die at a temperature of 750°F(400°C) or less.

APPENDIX 3



FIRING SCHEDULE A

APPENDIX 4

BILLET HEAT LOSS ESTIMATE

A rough estimate of billet heat losses can be made by assuming the billet has infinite thermal conductivity, and loses heat only by radiation into an infinite space or perfectly absorbing media (i. e., no reflection or re-radiation back to the billet).

A typical billet weighs about 17 killograms and has about 580 cm^2 surface. Assume the billet has temperature of 2400°K and emittance (ϵ) of .7, then

$$\dot{q} = \epsilon \sigma (T_1^4 - T_2^4) = \text{rate of heat lost by radiation per unit area}$$

$$\dot{q} = (.7)(5.7 \times 10^{-5}) \left[(2400)^4 - (300)^4 \right] \approx 133 \times 10^7 \text{ ergs/cm}^2\text{-sec.}$$

$$\dot{Q} = (133 \times 10^7)(580) = 7.72 \times 10^{11} \text{ ergs/sec}$$

$$\dot{Q} = (7.72 \times 10^{11})(2.39 \times 10^{-8}) = 1.85 \times 10^4 \text{ cal/sec.}$$

In 10 seconds, the total heat loss (Q) is:

$$Q = (10)(1.85 \times 10^4) \approx 2 \times 10^5 \text{ cal}$$

$$Q = (\text{heat capacity})(\text{mass})(\text{change in temperature})$$

$$Q = (3.8 \times 10^{-2})(1.7 \times 10^4) \Delta T = 2 \times 10^5$$

$$T \approx 300^\circ\text{C}$$

The limited thermal conductivity of the billet will certainly reduce this figure, as may the glass lubricant (as insulation); however, conduction losses by the billet contacting press parts would counteract some of this reduction.

APPENDIX 5

STRENGTH OF HOT PRESSED MgO

It has generally been recognized that strengths of ceramics decrease as either porosity or grain sizes increase. Knudsen⁽¹⁾ suggested the equation:

$$\text{Strength (S)} = k G^{-a} e^{-bP}$$

to numerically express these relationships, where k, a and b are empirical constants, G the grain size, P the volume fraction porosity, and e the Napierian Log base (2.718....).

Spriggs and Visilos⁽²⁾ showed the above equation held for MgO, giving strengths (in 4 point bending supported on a 1.50" span with bars 1.75" x .25" x .15") of:

$$S = 75,000 G^{-1/2} e^{-bP} \text{ psi (b = 6 to 9) for hot pressed and carefully machined MgO, and}$$

$$S = 75,000 G^{-1/3} e^{-bP} \text{ psi for MgO fired after hot pressing and machining.}$$

These authors subsequently published more data⁽³⁾ in which the equations (for zero porosity) were modified as follows:

$$S = 75,000 G^{-1/2} \text{ psi for hot pressed and carefully machined MgO}$$

$$S = 50,000 G^{-1/6} \text{ for MgO fired after hot pressing and machining.}$$

The authors could not explain the difference between fired and unfired hot pressed MgO.

In order to eliminate questions of this variation and to check materials being developed, an investigation was carried out at Boeing. The same raw material, Fisher Electronic grade MgO was used and fabrication conditions were similar to those of the reference work (graphite dies, temperatures of 2300°F(1260°C) ±200°F, and pressures of 5000 psi), except hot pressing was carried out in vacuum. However, the most significant difference was in the use and evaluation of firing treatment.

Extensive evidence⁽⁴⁾ shows that volatile-producing impurities can be readily trapped in hot pressed bodies made from highly active materials such as the above Fisher MgO. The most common one in MgO is Mg(CO₃) as shown by IR transmission of translucent as-hot-pressed specimens. Decomposition of this trapped carbonate explains much of the clouding and bloating observed upon annealing hot pressed MgO by many investigators, including the referenced work. Recognizing this, precautions (mainly vacuum hot pressing) to minimize these contaminants were taken; however, these did not eliminate this problem. Therefore, firing cycles were adapted to subsequently fire the hot pressed specimens in order to slowly break down and diffuse out these gaseous impurities, and obtain some sintering to heal the voids left by the decomposed compounds. This could generally be done by slowly raising the temperature to about 2200°F(1205°C). Rice⁽⁵⁾ has shown that this results in substantial increases in strength up to some optimum temperature (usually approximately 2200°F) as shown in Figure A1. Comparison of as-sanded, fired, and chemically polished specimens

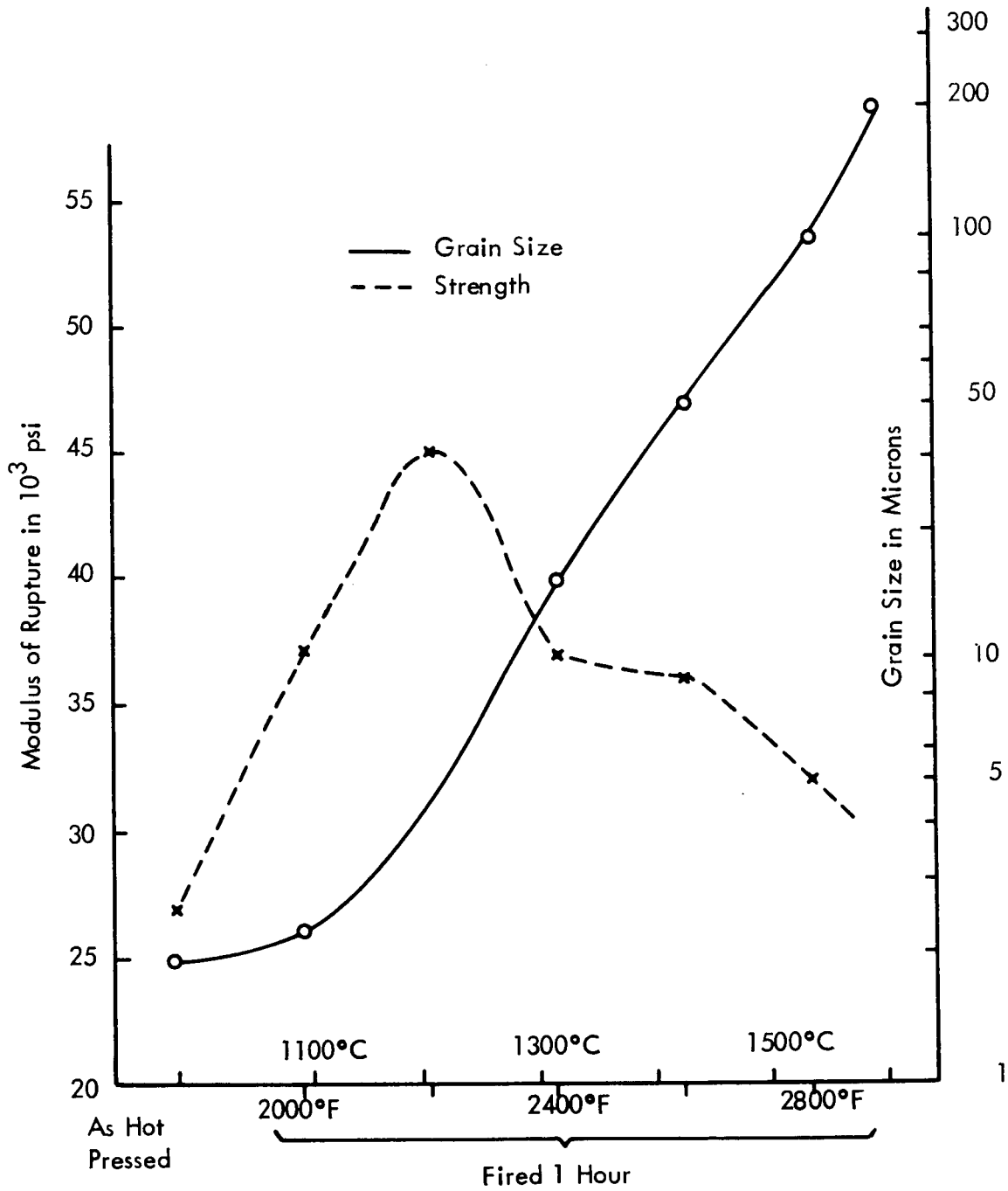


FIGURE 1A MgO STRENGTH AND GRAIN SIZE vs. FIRING TEMPERATURE. ALL STRENGTH POINTS REPRESENT AT LEAST 5 SPECIMENS TESTED IN 3 POINT FLEXURE ON A 0.78" SPAN. FIRING TO 1050°C WAS OVER A PERIOD OF 3 DAYS. ALL SPECIMENS WERE HOT PRESSED AT 1205°C (Courtesy of Plenum Press)

shows that surface finish plays only a secondary role (e.g., chemically polishing increased strengths of bars fired to 2100°F about 15% and 600 grit sanding reduced fired strengths about 15%). Thus, this maximum in strength is a true effect of firing. The location of this peak for a particular fabrication may vary 100°F, and sometimes nearly 200°F, and the peak increase in strength may only be about 50% rather than nearly 100%. (These variations appear to be the reason for the plateau in Figure A1 since this averages specimens from several fabrications.)

After firing to temperatures near those giving maximum strength, the carbonate IR absorption bands are gone. Therefore, it was concluded that below the optimum firing temperature, MgO strengths were controlled by the presence of such volatile producing impurities, while firing at or past the optimum temperature eliminates this control.

Thus, the following procedure was used. Disks of 1.5 and 2.0" diameters and about 0.25" thick were vacuum hot pressed, wet ground and dry sanded (600 grit finish) to give bars with cross sections of about 0.25" x 0.12". These were then fired to various temperatures on the developed firing cycles, and only those specimens near or past the optimum firing for each disk were accepted. This procedure also gives a range of grain sizes from each original disk.

All specimens were tested at ambient conditions in 3 point bending using 0.75" span and 0.125" diameter steel loading points. Cross head speed was 0.05 in/min. Tests cover a wide range of time and hence average effects of set-up variation, weather, etc. Grain sizes were measured by counting grain boundary intersections with straight lines near the tensile surface.

Results are shown in Figure A2 along with data from References 2 and 3. The latter also shows higher strengths as a result of firing, and their fired strengths though somewhat lower, generally have the same slope as the work herein presented. The lower strengths from the reference works may be due to differences in specimen factors such as porosity and test factors such as specimen size and type of tests (4 point versus 3 point testing). In the present work no bodies were completely pore free, though most were fairly translucent, especially at larger grain sizes. The smallest grain size specimens generally had 0.1 to 1% porosity which is the same or greater than the larger specimens. In the 50 to 100 micron grain size range, both sets of data show a deviation from the slope for grain sizes. There are numerous factors which could cause this deviation toward higher strengths as large grain sizes are obtained by progressively higher temperature firing.

- (1) Grain growth may cause orientation (through preferential elimination of grains of high misorientation) and thus change fracture mechanisms or strengths.
- (2) Larger grains may reduce the probability of having a grain oriented for easiest fracture nucleation at the region of maximum stress.
- (3) There may be some further elimination of impurities which are no longer controlling, but may be limiting strength.

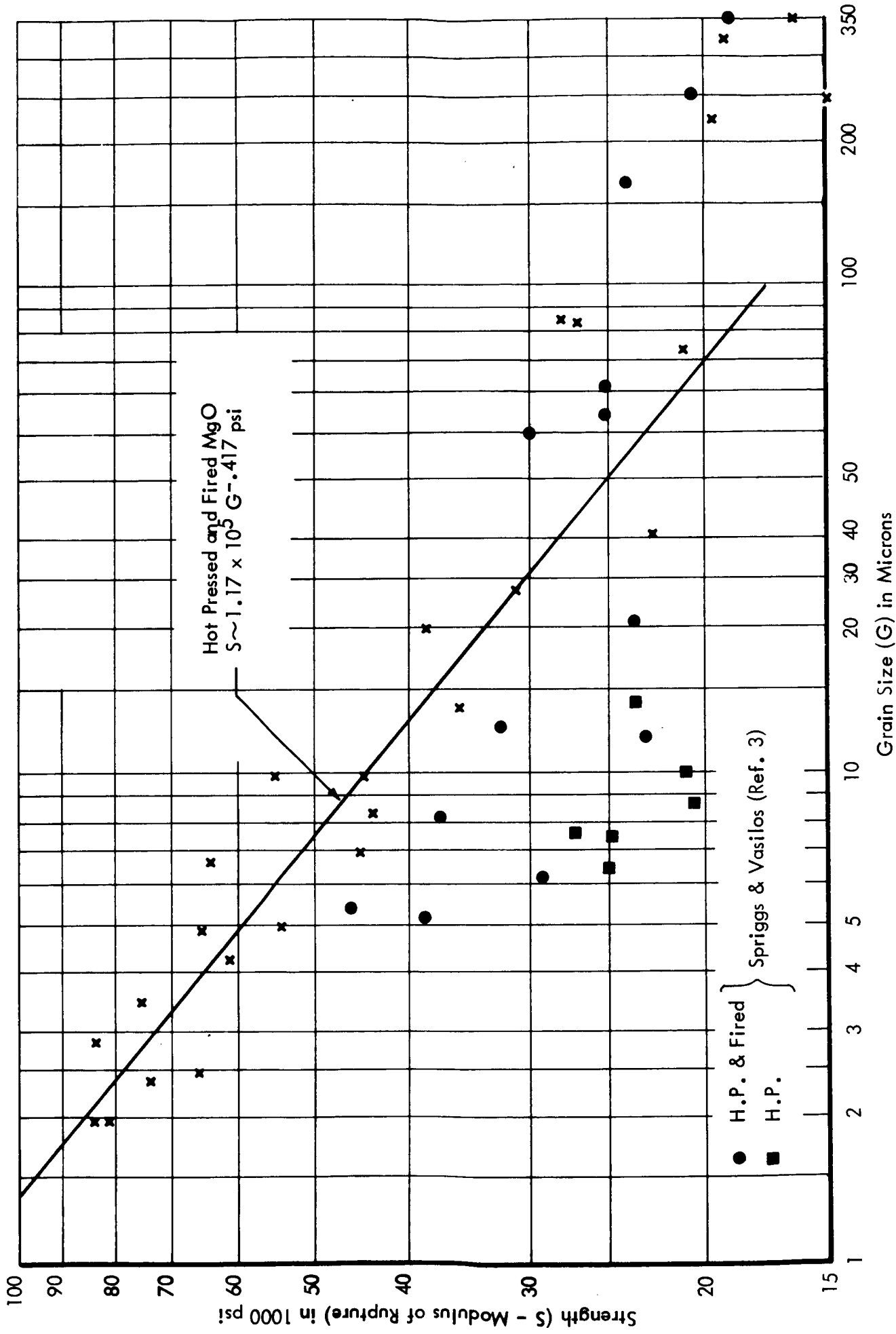


FIGURE 2A STRENGTH vs. GRAIN SIZE FOR HOT-PRESSED AND FIRED MgO

- (4) Stable impurities which may initially be inhomogeneously distributed may become more homogeneously distributed, which could result in strengthening.
- (5) Annealing and pinning of dislocations may occur to strengthen bodies.
- (6) Surface grains may be smaller than the rest of the grains because they cannot grow in one direction. Thus fracture initiation in a smaller surface grain would require more stress, so the mean grain size would not be representative. (There is evidence to suggest this in some cases).
- (7) Larger grains may have more dislocation sources such as impurities or pores⁽⁵⁾ inside the grain that would effectively reduce the grain size if grain boundaries are the normal sources of dislocation ions in smaller grains. (This may be the case since Passmore, et al⁽⁶⁾ showed there are few or no mobile dislocations in polycrystalline MgO grains, while Copley⁽⁷⁾ reports sub-boundaries in MgO crystals appear to act as dislocation sources.)
- (8) Pores in the body will be trapped in the grains by grain growth which may result in strengthening, possibly due to impurity accumulation at pores⁽⁵⁾. Recent experiments indicate this may be the most important of the above factors.

From Figure A2 it is seen that the strength varies as $G^{-.4}$ to $-.5$. The above discussion shows that the presented data is probably somewhat low for small grain sizes and high for large grain sizes, thus indicating the relationship actually should be $G^{-.5}$ or very close to this.

Another technique of fabricating dense MgO is by hot pressing with LiF⁽⁸⁾ or NaF. An optimum strength with firing is also found in these systems as shown in Figure A3, though not as pronounced as in the Fisher MgO without additives. Again the height and temperature of this peak varies some from fabrication to fabrication; however, it is nominally around 2400°F (1315°C). Data from these systems was therefore accepted only if it was near or higher than the optimum temperature. Results for both Mallinckrodt AR and Fisher Electronic Grade MgO with 2 w/o LiF and for Mallinckrodt MgO with 1 and 2 w/o NaF are shown in Figure A4. This shows that MgO from either source made with either additive generally has the same strength versus grain size variation as MgO without additives. Grain sizes smaller than 15-10 microns cannot be achieved because of the higher firing temperature with (2400°F) than without (2200°F) LiF, and due to effects of the additives on grain growth. The latter appears to be the greatest factor, probably due to a liquid phase from the additive during firing. (Typical pressing conditions with NaF or LiF at about 1800°F and 3000-5000 psi for 15 minutes result in grain sizes of 0.5 to 3.0 microns from Mallinckrodt MgO.) After firing, no Li is detectable in specimens, but a few hundred to a few thousand parts per million F (probably as MgF₂) remain in these bodies. This may explain the apparently slightly higher strengths of the fluoride processed bodies.

Testing: Room Temperature, 3 Point Loading
1.0" Span, 0.05 inches/minute Head Travel

Specimens: As ground, 600 grit finish

*Subsequent to 10 hours at 1150°C (2100°F)

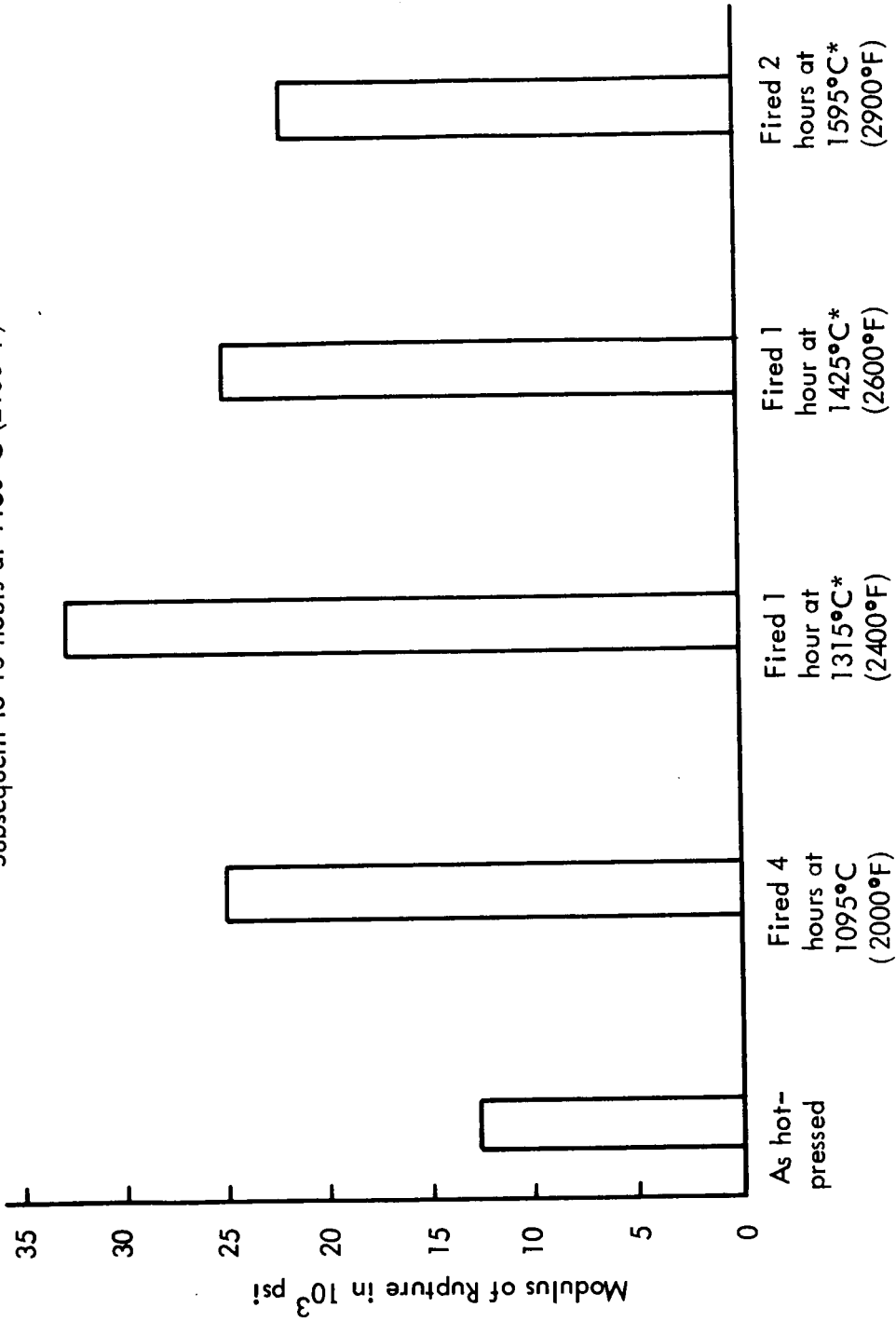


FIGURE 3A FLEXURAL MODULUS OF RUPTURE FOR MgO FABRICATED WITH 0.5% LiF

APPENDIX 5

REFERENCES

1. F.P. Knudsen, "Dependence of Mechanical Strength of Brittle Polycrystalline Specimens on Porosity and Grain Size", J. Am. Ceram. Soc. 42 (8), p. 376-387 (1959).
2. R.M. Spriggs, T. Vasilos, "Effect of Grain Size and Porosity on the Transverse Bend Strength and Elastic Modulus of Hot Pressed Alumina and Magnesia", presented at the 63rd Annual American Ceramic Society Meeting in Toronto, Canada, April, 1961. (Abstract: Am. Ceram. Soc. Bul. 40 (4), p. 187, 1961)
3. R.M. Spriggs, T. Vasilos, "Effect of Grain Size on Transverse Bend Strength of Al_2O_3 and MgO", J. Am. Ceram. Soc. 46 (5), p. 224-26 (1963).
4. R.W. Rice, "Microstructure, Strength, and Fracture of Dense MgO, CaO and Al_2O_3 ", to be published.
5. R.W. Rice, "Internal Surfaces in MgO", presented at the Conference on Surfaces and Grain Boundaries in Ceramics at Raleigh, N.C., in November, 1964 (Proceedings being published by Plenum Press).
6. E.M. Passmore, R. Duff, T. Vasilos, "Mechanisms of Deformation in Polycrystalline Magnesium Oxide", Technical Report AFML-TR-65-122, June, 1965.
7. S.M. Copley, Ph.D Thesis - see S.M. Copley, J.A. Pask, "Deformation of Polycrystalline MgO at Elevated Temperatures", J. Am. Ceram. Soc. 48 (12), p. 636-42 (December, 1965).
8. R.W. Rice, "Production of Transparent MgO at Moderate Temperatures and Pressures", presented at the 64th Annual Meeting of the American Ceramic Society in New York, New York, May, 1962. (Abstract: Am. Ceram. Soc. Bul. 41 (4), p. 271, 1962).

APPENDIX 6

CALCINING PROCEDURE A

1. Powder is loaded in 99% pure MgO crucibles approximately 3" in diameter x 4" high with 0.1" wall thickness by using the crucible to scoop powder from the container.
2. The crucibles are placed in a metal retort with half of them inverted on top of the remainder. The top crucibles are slotted on the side near their base to allow ready gas escape and good flushing while acting as lids to prevent excess spillage of powder, and possible contamination from the retort metal lid.
3. A thin metal lid is welded on the retort to seal it.
4. Lines are attached to fittings to introduce argon at the bottom in front, and a vacuum system to the top of the retort in the back.
5. The retort is loaded in the furnace and the vacuum and argon valves are set to establish an argon flush at about 10" absolute pressure.
6. The retort is heated at a linear rate to reach 600°C(1110°F) in approximately 5.5 hours. Temperatures are measured by a thermocouple near the center of the retort.
7. After 1 hour at 600°C, the retort is cooled in approximately 1.5 hours, initially in the furnace, then out of the furnace.
8. When the retort is less than 100°C(212°F) the vacuum valve is closed, when the retort is near atmosphere pressure, the argon valve is closed, and the retort is flooded with benzene through a third fitting.
9. The thin retort lid is then removed and the powder, covered with benzene, is transferred to jars which are closed for storage.